NAS CR-54188
EOS Report 4971-Final

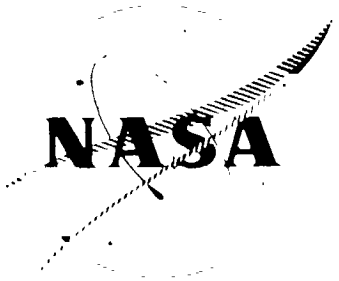

DEVELOPMENT OF COMPOSITE IONIZER MATERIALS

by

M. LaChance, B. Thompson,
H. Todd and G. Kuskevics

prepared for

NATIONAL AERONAUTICS AND SPACE ADMINISTRATION

CONTRACT NAS3-5248

EOS ELECTRO-OPTICAL SYSTEMS, INC., PASADENA, CALIFORNIA
A Subsidiary of Xerox Corporation

NASA CR-54188
EOS Report 4971-Final

FINAL REPORT

DEVELOPMENT OF COMPOSITE IONIZER MATERIALS

by

M. LaChance, B. Thompson,
H. Todd and G. Kuskevics

prepared for

NATIONAL AERONAUTICS AND SPACE ADMINISTRATION

8 April 1965

CONTRACT NAS3-5248

Technical Management
NASA Lewis Research Center
Cleveland, Ohio 44135
Spacecraft Technology Procurement Section
A. E. Anglin

ELECTRO-OPTICAL SYSTEMS, INC.
300 No. Halstead Street
Pasadena, California

ABSTRACT

20487

Research to improve the pore structure, thermal stability, and performance of tungsten ionizers was conducted. The approach used was to add secondary elements to tungsten microspheres by three different methods: metal particle addition, vapor deposition of metal films, and hydrogen-reduction of inorganic compounds. It was indicated that a composite powder mixture can exhibit very good dimensional stability during sintering at 2000°C, yet can result in an ionizer having a very coarse sintered pore structure, and markedly reduced ionization performance. Therefore, the diffusion mechanisms during sintering have a direct and important influence on ionizer pore structures and subsequent performance. Although pure tungsten with a fine pore structure exhibited good ionization performance, a very short operating lifetime was indicated. Precoating tungsten with about 100Å of tantalum resulted in the finest pore structure, the best ionization performance, and an appreciably longer life expectancy than pure tungsten. Addition of 10 atom percent of tantalum particles resulted in pore structures slightly less fine than that of pure tungsten, of somewhat lower ionization performance, but with greatly extended life expectancy. Based on total consideration of characteristics, W-7A.%Ta (fabricated for metal particle mixture) is recommended as the best ionizer composition for long-time operation.

CONTENTS

CONTENTS (contd)

CONTENTS (contd)

ILLUSTRATIONS

ILLUSTRATIONS (contd)

ILLUSTRATIONS (contd)

ILLUSTRATIONS (contd)

ILLUSTRATIONS (contd)

TABLES

TABLES (contd)

SUMMARY

Objectives of this research were improvement of the pore structure, structural and dimensional stabilities, and performance of contact-type ionizers by addition of secondary elements. With fine presized microspheres used as a base, secondary elements were added as discrete particles, as vapor-deposited precoatings, and as hydrogen-reduced inorganic compounds.

The powders were fabricated to ionizer form by blending, hydrostatic pressing, vacuum sintering to equivalent densities, infiltration, machining to buttons, and vacuum distillation of infiltrant.

The composite ionizers were evaluated by determining (1) densification rates at 2000°C; (2) sintered densities, permeability coefficien pore volumes, and pore structures; (3) ionization performance; and (4) useful operating lifetimes (by means of accelerated tests in vacuum, without cesium).

The results of this research provide a better understanding of the effects of secondary additions to tungsten powder on sintering mechanisms, sintered pore structures, and stability of pore structures in subsequent heating. They also provide a good correlation between sintered pore structures and ionization performance.

1. INTRODUCTION

The objectives of this research were to develop contact-type ionizer material having improved (1) pore characteristics, (2) stability of pore structure and external dimensions at ionizer service temperatures, and (3) engine performance.

1.1 Review of Previous Research

This NASA contract is the third of a series having the improvement of ionizers as a common objective. Pertinent results obtained under the first contract, NAS8-2547 (Ref. 1), and under the second, NAS3-2519 (Ref. 2,3), are summarized in sections 1.1.1 and 1.1.2.

1.1.1 Contract NAS8-2547

A special method for compacting tungsten microspheres, used for the experimental ionizers, was developed initially since conventional methods proved inadequate. Comparative evaluations of experimental and commercial ionizers were based on structure, nitrogen permeability variance, and engine performance. As a substitute for hydrogen-reduced tungsten powder, the spherical particles proved to be more stable thermally for the building of ionizer structures. Variance of nitrogen permeability within large lots of ionizer buttons was markedly lower for those made from microspheres than from hydrogen-reduced powder. The highest ion-current density of about 30 mA/cm^2 was reached only with a spherical powder ionizer, as compared to about 15-20 mA/cm^2 for commercial ionizers. Neutral fractions and critical temperatures were similar to, or sometimes better than, those for the commercial type.

Another means of increasing the thermal stability of ionizer structures was demonstrated. This was based on retarding the rate of high-temperature diffusion and grain growth through tantalum inoculation of tungsten powder, prior to its compaction. Thus, it was indicated

that use of tantalum-inoculated microspheres in a narrow size range, with diameters less than 5μ, should provide improved ionizer structures.

1.1.2 Contract NAS3-2519

Extensive fabrication and performance testing of spherical tungsten powder ionizers was performed. With all fabrication parameters, except powder size distribution held constant, an ionizer series of increasingly fine porosity was prepared. Thus, it was possible to determine the effect of pore refinement on ionizer performance at essentially constant levels of ionizer density and purity. The program comprised the spectrum of powder metallurgy, from powder classification through characterization of ionizer structures.

Ionization performance testing was conducted on classified spherical powder ionizers at three levels of pore refinement. Performance of this series was compared to that of course-structured hydrogen-reduced powder ionizers (available commercially in large size). Data indicated that successive refinement of pore structure led to progressively improved ionization performance. Use of the finest classified microspheres (1-4μ) increased the number of pores per unit area by a factor greater than 5, and reduced mean pore size by a factor of about 0.4 (based on comparison with ionizers made from coarse unclassified microspheres). Thus, the greatly improved ionization performance of the finer pore structures appeared associated more closely with increased pores per unit area than with reduced pore size.

Since fine pore structures have inherently lower thermal stability than coarse structures, stabilizing effects of tantalum and chromium particles on tungsten were studied. No stabilization of spherical powder compacts by the use of chromium additive was detected. On the other hand, sintering rates of tungsten-tantalum mixtures were reduced markedly, indicating improved stability of external dimensions. However, addition of tantalum particles to tungsten microspheres decreased uniformity of ionizer pore size.

1.2 Goals, Approach and Scope of Present Contract

This contract was directed toward achievement of the following specific goals:

1. Pore Size: 1μ or less, uniformly distributed.
2. Pore Density: more than 10^7 pores per cm^2.
3. Lifetime: capable of 10,000 hours of operation under ionization (1100 - 1300°C with cesium) and with no change in structural characteristics such as pore size, volume or density, and gas permeability.
4. Emissivity: 0.3 or less for total emissivity of the surface.
5. Critical Temperature: lowest critical temperature consistent with high current density.
6. Neutral Fraction: lowest neutral fraction consistent with high current density.

The general approach used in this program has been as follows:

1. To a base of fine, presized tungsten microspheres, addition of secondary metallic elements as fine metal particles, as vapor-deposited coatings, and as inorganic compounds, subsequently reduced by hydrogen.
2. Evaluation and comparison of effects of alloying on sintering rates, nitrogen permeabilities, pore structures, ionization performance, and useful lifetimes at ionizer operating temperatures.

For performance and reporting purposes, the research program has been divided into phases as follows:

Phase		Reference, Report Section
I	Ionizers from tungsten microspheres, and tantalum particles	3
II	Ionizers from tungsten microspheres, precoated by vacuum deposition with Ta, Re and Os.	4

III	Ionizers from tungsten microspheres with secondary additions by chemical method (oxidation-reduction)	5
IV	Performance testing of selected ionizers	7
V	Simulated life testing at 1600°C and 1800°C	6
VI (Change No.2)	Machining and brazing of LOS and Philips Mod. E ionizers	2

Additional work included the fabrication of selected ionizer samples for NASA Lewis.

2. EXPERIMENTAL MATERIALS, EQUIPMENT, AND PROCEDURES

This section describes materials, equipment, and standard procedures used for fabricating and evaluating the experimental ionizers. Equipment and procedures pertaining to evaluation of ionization performance are described in Section 7.

2.1 Test Materials

2.1.1 Tungsten and Tantalum Powders

Spherical tungsten powder, designated as Lot L, was purchased from the Linde Division of Union Carbide. It was used as the common base powder for fabricating all experimental ionizers.

Spectrographic analysis of Lot L powder indicated less than 373 ppm total impurities. This corresponds to a spectrographic purity (by difference) of greater than 99.96%. Carbon content was not determined. However, conductometric analyses of other powder lots from the same supplier indicated that carbon varied from 2 to 60 ppm. Gaseous impurities (O, N, and H) are considered negligible because of the high temperatures at which the ionizers are subsequently sintered. Results of this analysis are compared, in Table 2-I, with analyses of spherical powder lots used in previous programs. The differences in impurity levels are considered insignificant.

Two size fractions of National Research Corporation SGH Grade tantalum were selected for preparation of W-Ta mixed-powder compacts of Phase I. Spectrographic impurity content of this tantalum was less than 200 ppm, with 1800 ppm O, 20 ppm N and 44 ppm C. This powder was the purest obtainable in fine particle size.

Particle size distribution of Lot L tungsten powder is given in Table II, together with distribution of Lots E3 and E4, used in the previous program. Size distribution of Lot L lies between Lots E3 and E4 and shows 92.0%, by number of particles in the 1.7-5μ range. This is a significantly narrower distribution than the contractual specification: 80% of particles in the 1.5-5.5μ range.

TABLE 2-I

COMPARISON OF SPECTROGRAPHIC PURITIES

OF SPHERICAL TUNGSTEN POWDER LOTS

Impurity Element	Impurities in Powder Lot**, ppm C	E	L
Al	< 3	< 3	10
B	< 10*	< 10*	20
Be	< 1*	< 1*	< 5*
Ca	< 1	1	10
Co	< 100*	< 100*	< 10
Cr	< 10*	< 10*	< 50
Cu	< 3*	20	20
Fe	< 30	< 30	< 8*
Mn	< 1*	< 1*	< 10
Mo	30	30	< 10*
Ni	< 30*	< 30*	< 10
Zr	< 100*	< 100*	10
Others	< 200	< 200	< 200
	< 519	< 536	< 373
Tungsten Purity	>99.94%	>99.94%	>99.96%

* Not Detected

** Lot C - coarse unsized microspheres used for NAS8-2547

Lot E - fine unsized microspheres used for NAS3-2519

Lot L - fine sized microspheres used for NAS3-5248

TABLE 2-II

PARTICLE SIZE DISTRIBUTION OF SPHERICAL TUNGSTEN POWDER AND TANTALUM POWDER FRACTIONS

(Determined by micromerograph)

	Spherical Tungsten Powder					
Particle Diam.	Lot E3		Lot L		Lot E4	
Range, μ	% by Wt	% by No	% by Wt	% by No	% by Wt	% by No
0-1	nil	nil	nil	nil	nil	nil
1-2	2.8	25.2	1.2	9.2*	nil	nil
2-3	22.4	43.6	14.4	44.7	9.4	34.5
3-4	28.0	19.9	20.0	22.6	27.4	36.7
4-5	23.3	7.8	29.1	15.5	31.8	20.0
5-6	14.0	2.6	19.1	5.6	18.3	6.3
6-7	7.7	0.9	9.4	1.7	8.9	1.9
7-8	1.8	0.1	4.3	0.5	4.2	0.6
8-9	nil	nil	1.9	0.1	nil	nil
9-10	nil	nil	0.6	<0.1	nil	nil
10-11	nil	nil	nil	nil	nil	nil

* 92.0%, by No., of particles in 1.7-5μ range

	Tantalum Powder Fraction			
Particle Diam.	BF		CF	
Range, μ	% by Wt	% by No	% by Wt	% by No
0-1	nil	nil	nil	nil
1-2	27.5	73.1*	3.5	39.9**
2-3	36.3	20.9	9.5	23.4
3-4	23.5	4.9	20.7	18.6
4-5	9.0	0.9	26.4	11.1
5-6	3.7	0.2	21.0	4.9
6-7	nil	nil	10.1	1.4
7-8	nil	nil	5.3	0.5
8-9	nil	nil	2.7	0.2
9-10	nil	nil	0.8	<0.1
10-11	nil	nil	nil	nil

* 94%, by No., of particles in 1-3μ range
** 93%, by No., of particles in 1-5μ range

Particle size distribution of tantalum powder Lots BF and CF, used for W-Ta mixed-powder ionizers of Phase I, are also given in Table 2-II. Distribution of the BF tantalum, with 94% by number, of particles in the 1-3μ range, is narrower than the Lot L tungsten base powder; distribution of the CF tantalum, with 93% in the 1-5μ range is closely comparable to the Lot L base.

2.1.2 Vapor-Coated Tungsten Microspheres

Lot L spherical tungsten powder was coated by vacuum deposition at the National Research Corporation for use in Phase II of this program. Three coating elements, Ta, Re, and Os, were applied in two thicknesses each. The spherical tungsten powder was contained in a stainless steel drum (mounted on a horizontal axis) within a vacuum chamber. As the drum was rotated, the powder was raised by internal vanes and allowed to fall freely, exposing it to the coating vapor. The coating metals (100-400 gm) were contained in a water-cooled copper crucible and melted with an electron beam, focused on the metal surface.

Initial coating runs, described in Table 2-IIIa, provided coatings on the tungsten of 102Å Ta (1.51 W/o)*, 45Å Re (0.86 W/o), and 17Å Os (0.35 W/o); these materials were used to make ionizers. In addition, thicker coatings were applied to similar quantities of powder, as shown in Table 2-IIIb. Here it is seen that the tantalum coating thickness was increased appreciably from 102Å, of the initial run, to 837Å. However, the coating thicknesses of rhenium and osmium were increased only to 150Å and 133Å, respectively. Since the goal was a thickness of 1000Å, it is therefore obvious that this coating technique is not advanced enough to apply such thick coatings in a practical length of time. Further, control of coating thickness would require considerably more experience with the specific coating elements.

---

* Symbols W/o and A/o are used throughout to designate weight and atom percentages, respectively.

TABLE 2-III

CONDITIONS USED TO APPLY VAPOR-COATINGS

TO TUNGSTEN MICROSPHERES OF LOT L

2-IIIa Thin Coatings

NRC* Run No.	Coating Metal	Coating Time, Min.	Ambient Pressure, torr	Beam Power, kW	Coating Metal Analysis, W/o Laboratory*				Value Used
					MTL	NRC	L&C	EOS	
304	Tantalum	45	2×10^{-5}	14	1.51	4.47	--	--	1.51 (102Å)
306	Rhenium	180	2×10^{-5}	7	0.76 0.84 0.92	---	0.37	--	0.86 (45Å)
---	Osmium	--**	---**	--**	---	---	0.35	--	0.35 (17Å)

2-IIIb Thicker Coatings

NRC* Run No.	Coating Metal	Coating Time, min	Ambient Pressure, torr	Beam Power, kW	Coating Metal Analysis, W/o Laboratory*				Value Used
					MTL	NRC	L&C	EOS	
307	Tantalum	180	2×10^{-5}	6					
308	Tantalum	60	1×10^{-5}	10					
316	Tantalum	$\pm\frac{50}{290}$	5×10^{-6}	14	11.99	11.30	--	--	11.6 (837
311	Rhenium	60	1×10^{-5}	11					
317	Rhenium	$\pm\frac{50}{110}$	8×10^{-6}	14	1.25	---	2.70	2.90	2.80 2.80 (150Å)
310	Osmium	60	1×10^{-5}	9	---	---	2.66	--	2.66 (133Å)

*MTL - Materials Testing Laboratory of Magniflux Corporation
NRC - Contract Research Division of NRC
L&C - Ledoux and Company
EOS - Electro-Optical Systems, Inc.
** - Data not supplied

2.1.3 Miscellaneous Materials

The purities of tantalum, rhenium, and osmium used by the National Research Corporation to vapor-coat tungsten microspheres were not reported to EOS. However, since these metals were electron-beam melted under high vacuum, it may be assumed that all relatively volatile impurities were eliminated early in the coating process.

Three compounds were used for the chemical addition of secondary elements to tungsten microspheres, as follows:

Osmium tetroxide of 99.8+% purity was purchased from Matheson, Coleman, and Bell.

Tantalum pentoxide was prepared by heating 99.79+% purity tantalum powder (NRC-Grade SGH) in air.

Ammonium perrhenate was prepared by dissolving 99.9+% purity rhenium powder in nitric acid, evaporating to dryness, and precipitating with ammonium hydroxide.

Copper for infiltration of the compacts was of 99.999+% purity and was purchased from the American Smelting and Refining Company.

Reagent grade iron, used for preparing the Cu-2Fe infiltrant alloy, was purchased from the J. T. Baker Chemical Company.

2.2 Equipment and Standard Procedures

2.2.1 Classification and Size Analyses of Metal Powders

Metal powders for this research were sized in a Sharples K8 cyclonic classifier and analyzed in a Sharples micromerograph analyzer. Descriptions of these devices were given previously (Ref. 2,pp 2-6 through 2-9).

2.2.2 Blending and Loading of Powders

Prior to compaction, all powders and powder mixtures were dried thoroughly and tumbled for at least 2 hours in glass jars. Rotation speed was adjusted to induce maximum lapover action of the powders. Stainless steel bearings (1/4-inch in diameter) were placed in the jars to

minimize agglomeration and to promote homogeneity. Loading of the powders into the rubber molds was done (in dry air) within a dry box. The powders were packed by tamping lightly with a 1/8-inch-diameter steel rod.

2.2.3 Compaction of Metal Powders

The powder compacts were pressed hydrostatically under 59,000 psi in the die shown in Figure 2-1. Mechanical pressure was applied to the steel ram by means of a conventional hydraulic press. Uniaxial ram pressure was translated into hydrostatic pressure by the rubber insert mold. Selected samples, submitted to NASA, were compacted in the same rubber mold, sealed in a prophylactic, and pressed under glycerine at 59,000 psi. Powder samples containing chemical compound additives were compacted in rubber laboratory tubing, the ends of which were sealed with rubber stoppers and Pliobond cement. They were then pressed under glycerine, pressurized to 60,000 psi.

2.2.4 Vacuum Sintering and Simulated Life Testing

Heating for sintering and life testing was done in the 10^{-5} torr pressure range in the furnace of Figure 2-2, described previously (Ref. 2). Sample temperature was monitored closely with an optical pyrometer, calibrated at regular intervals by sighting on pure metals of known melting point. Heating to 1600°C was done at the maximum rate which would still permit a pressure of less than 1×10^{-4} torr. This required an average time of 20 minutes. Heating from 1600°C to sintering temperature was done as rapidly as possible (in approximately 5 minutes) regardless of pressure increase from outgassing. This increased the timing accuracy of cumulative sintering cycles.

2.2.5 Infiltration, Machining and Infiltrant Removal

All samples requiring machining were infiltrated with Cu-2A/o Fe alloy. This was performed by heating the infiltrant in quartz boats to 1175°C under hydrogen, and then immersing the porous samples for 30 minutes. Machining was done on a standard lathe and the samples were surfaced by wet grinding to a 6 RMS finish. None of the samples were etched after the grinding operation. The infiltrant was removed by

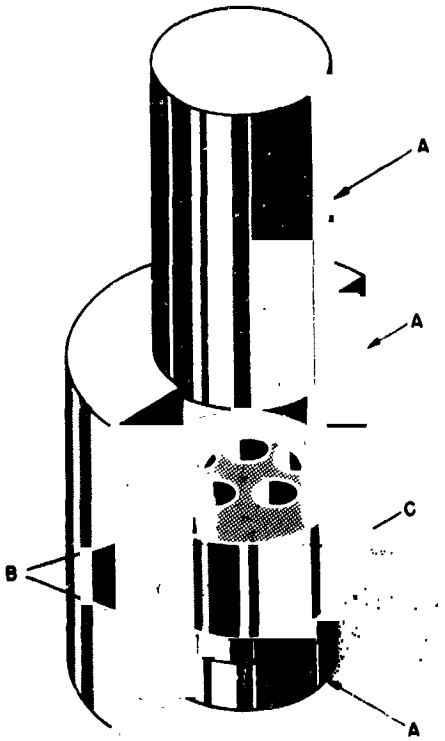

A - STEEL DIE COMPONENTS
B - RUBBER DISCS
C - MULTI-CHAMBERED RUBBER CYLINDER

FIG. 2-1a

DIE ASSEMBLY USED TO COMPACT TUNGSTEN MICROSPHERES UNDER HYDROSTATIC PRESSURE

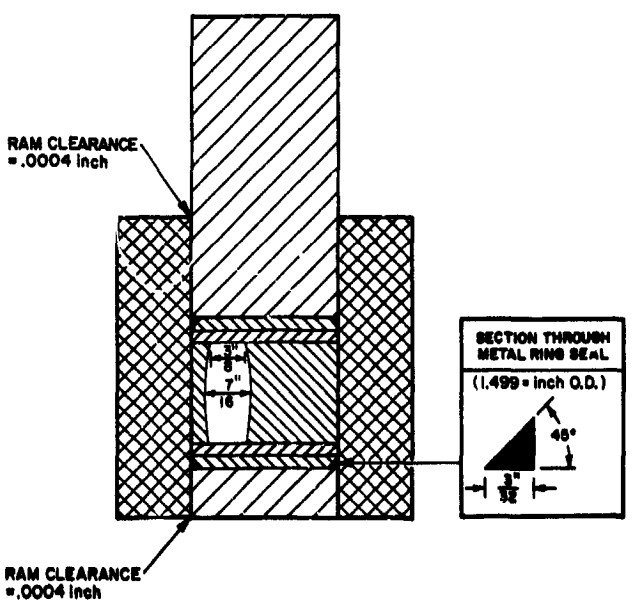

FIG. 2-1b

CROSS SECTION VIEW OF CYLINDRICAL POWDER-PRESSING DIE SHOWING STEEL RAM, BASE INSERT, AND FEMALE SECTION WITH SILASTIC RUBBER MOLD, NEOPRENE DISCS, AND LEADED BRONZE PRESSURE SEALS IN SITU (Drawing scale 1/2X)

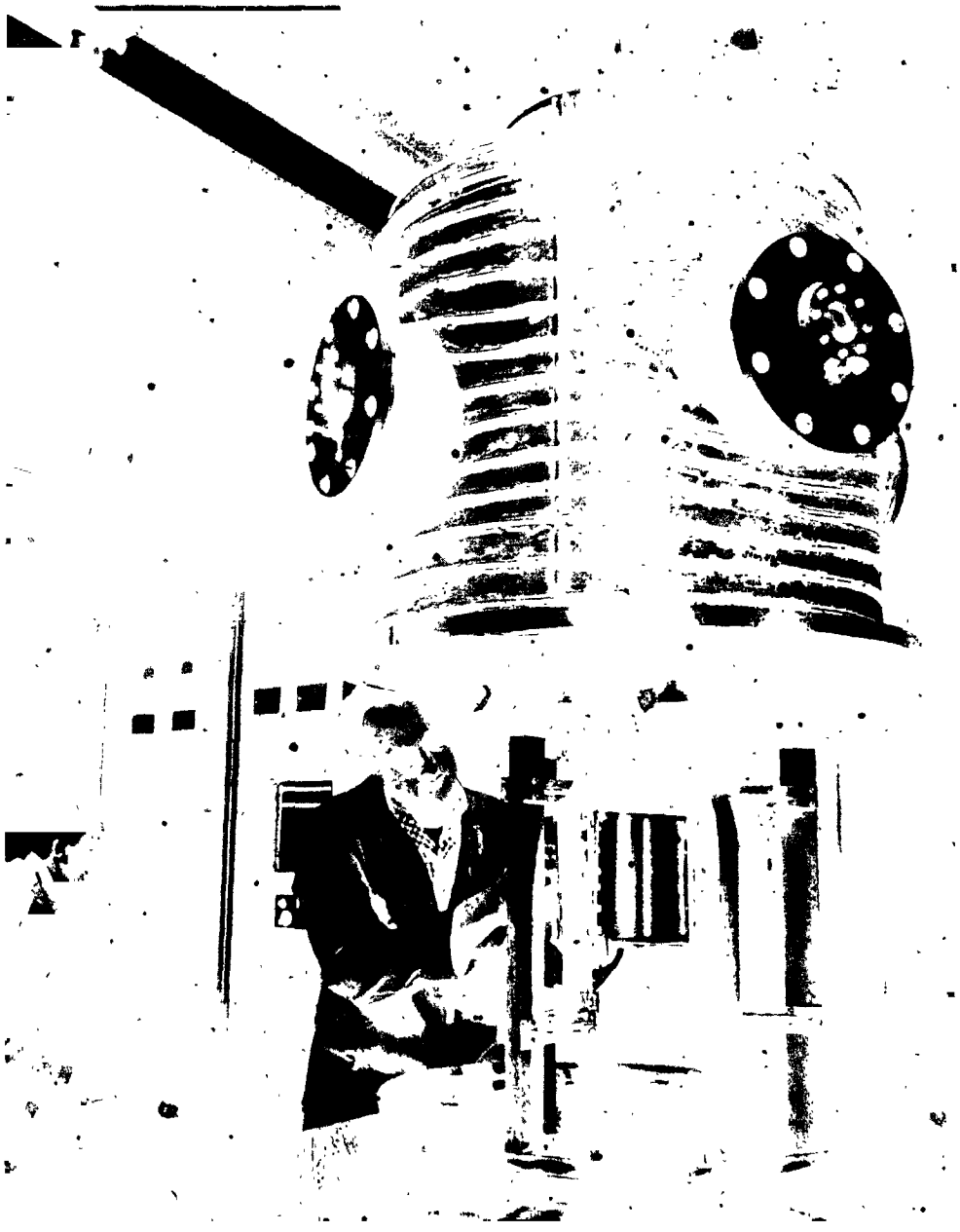

FIG. 2-2 VACUUM SINTERING FURNACE WITH TANTALUM SHEET-RESISTOR HEATING ELEMENTS

vacuum distillation at 1400°C for 15 minutes, and at 1750°C for 45 minutes. The latter temperature was intentionally selected as 50°C lower than the 1800°C minimum temperature used in sintering. This minimized the risk of further densification during the distillation process. Spectrographic analysis of W-10A/o Ta ionizers, after distillation of infiltrant, indicated an impurity content of less than 810 ppm or a purity greater than 99.92%. Iron at 110 ppm and molybdenum at 150 ppm were the residuals large enough to indicate significance. Source of the residual iron is the Cu-2Fe infiltrant. The iron pickup has varied from 80 to 170 ppm, dependent mainly on the temperature of final distillation. The higher this temperature, the lower the residual iron content. Literal interpretation of the spectrographic results also indicates a pickup of 120 ppm (from 30 to 150 ppm) of molybdenum. This may or may not be real, since the lower limit of Mo detection has been reported by the Materials Testing Laboratory as both 10 and 200 ppm. This casts doubt on Mo values below 200 ppm, and emphasizes a specific technical limitation.

2.2.6 Determination of Density

Densities of regular geometric samples, such as discs and cylinders, were determined from their direct weight-to-volume ratios. Densities of the irregular barrel-shape compacts were determined by the pycnometer method (using Hg as the immersion fluid) according to the following formula:

$$\rho = 13.546\ S/(M_1 - M_2)$$

where S is the weight of the sample in air, M_1 is the maximum weight of Hg which can be held by the pycnometer bottle, and M_2 is the weight of Hg in the pycnometer after immersion of the sample. Then, if P is the weight of the empty pycnometer bottle, the collective weight of pycnometer, residual Hg, and immersed sample is given by $(P + M_2 + S)$, and

$$M_1 - M_2 = P + M_1 + S - (P + M_2 + S),$$

which is equal to the weight of Hg displaced by the sample.

2.2.7 Determination of Nitrogen Permeability

The term "nitrogen permeability" is used, throughout this report, synonymously with mass permeability coefficient. This is done as a simplification and to distinguish it from "cesium permeability". Determination of the mass permeability coefficient of porous bodies, with respect to a diffusing gas, is a reliable and simple way of determining fluid-transmitting efficiency. Permeability coefficients, in contrast to density values, are extremely sensitive to slight changes in pore structure. Therefore, permeability coefficients have been determined for all ionizer buttons produced under this and previous contracts.

A sketch of the apparatus used to measure permeability coefficient K, as well as the derivation of this coefficient, was given previously in Section 4.8.2 of Ref. 2. Here and in Ref. 2 this coefficient is expressed in units of gm/cm·sec·torr, the natural units of measurement. However, the physical dimension of K is time, and by converting the pressure from torr to dynes/cm^2 (i.e., multiplying by 7.5×10^{-4}) K will be in seconds. The product of K (in sec) and the coefficient of kinematic viscosity (in cm^2/sec) is the specific permeability, K_S (in cm^2).

2.2.8 Determination of Pore Volumes

Pore volumes are expressed herein as percentages of sample volumes. They are of two types, open and occluded. Open pore volumes were determined by measuring the volumes of Hg which could be intruded at pressures up to $\approx$ 5000 psi. This was done in an Aminco-Winslow Porosimeter device, described in Section 4.8.4 of Ref. 2. Percent total pore volumes were determined from

$$100\ (1 - \rho/\rho_{\text{theor.}})$$

Occluded pore volumes were then calculated by subtracting percent open pore volumes from percent total pore volumes.

2.2.9 Metallographic Preparation

A continuing effort has been underway at EOS to delineate the true pore structures of tungsten ionizers. The importance of

true structures for high-magnification photography is emphasized as being directly pertinent to the accuracy of optical pore counts, pore density values, and average pore diameters.

Figure 2-3 illustrates the effect of metallographic preparation on the appearance of two tungsten ionizers, infiltrated with Cu-2A/oFe alloy. Structures at the left (upper and lower) were produced with polishing and chemical etching performed in two different steps. Structures at the center and right of Figure 2-3 were produced by two separate polishing operations, described in Table 2-IV as "preliminary" and "final". According to actual pore counts, given under each micrograph, the double polishing procedure is effective in revealing higher pore densities. A detailed outline of the double polishing procedure is given in Table 2-IV. This procedure provides the best surface yet obtained at EOS. Final polishing on the etch cloth is apparently very critical and, if continued for too long, can lead to undesirable surface relief and to pore counts larger than would actually occur on a flat plane. However, if Linde B alumina, with modified Murakami's slurry, is used as described in Table 2-IV, a final polishing time of from 5 to 10 seconds can be specified.

2.2.10 Determination of Pore Density and Average Pore Diameter

Considerable effort was exerted in determining porosity by the pore count method. After careful polishing and etching of the tungsten ionizers, photomicrographs were taken at magnifications of 2000X or 1200X. (coarser structures were taken at 1200X to include sufficient pores.) Rectangles of 8cm x 10cm were drawn on the photos. All pores included within the 80-cm^2 area were counted; pores intersected by the rectangle boundries were tallied as 1/2 pores. Calculations were made as follows:

$$\text{Pores/cm}^2 = (\text{Pores Counted})(\text{Mag.})^2/80$$

$$\frac{\pi \bar{d}^2}{4} = \frac{\text{Vol. \% Open Pores}}{(100)(\text{Pores/cm}^2)} \qquad \bar{d}\ (\text{in } \mu) = 1128 \sqrt{\frac{\text{Vol. \% Open Pores}}{\text{Pores/cm}^2}}$$

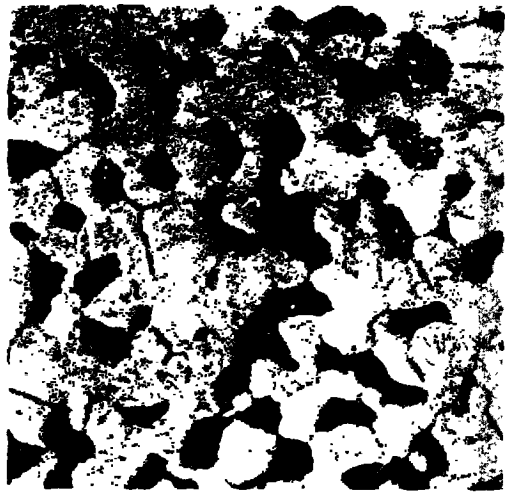

NEG. 1525 BUTTON E3-P-1
LINDE ALUMINA $(4.01)(10)^6$PORES/cm^2
5-10 sec. SWAB ETCH AVG. PORE DIA. = 2.50μ

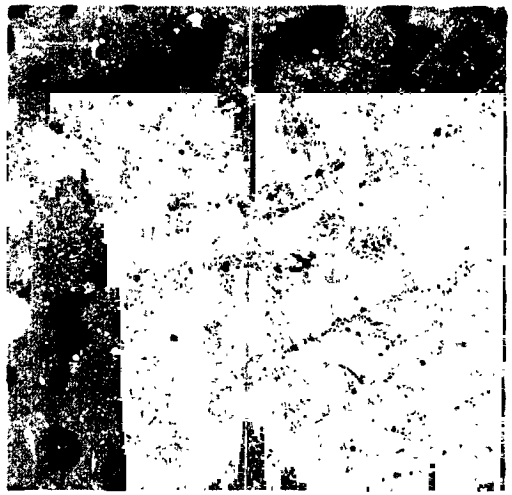

NEG. 1735 BUTTON E3-P-1
LINDE ALUMINA $(4.20)(10)^6$PORES/cm^2
5 sec. ON ETCH CLOTH AVG. PORE DIA. = 2.44μ

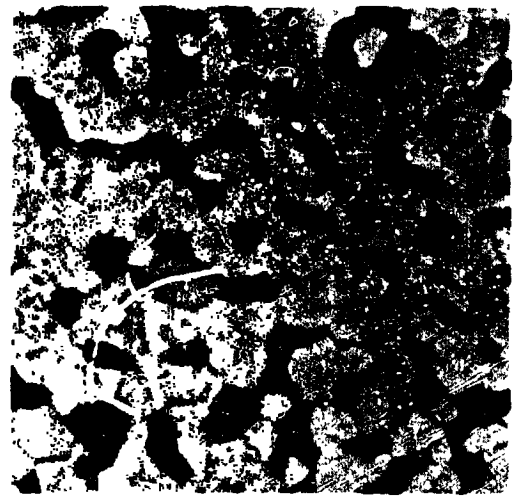

NEG. 1845 BUTTON E3-P-1
LINDE ALUMINA $(4.19)(10)^6$PORES/cm^2
10 sec. ON ETCH CLOTH AVG. PORE DIA. = 2.45μ

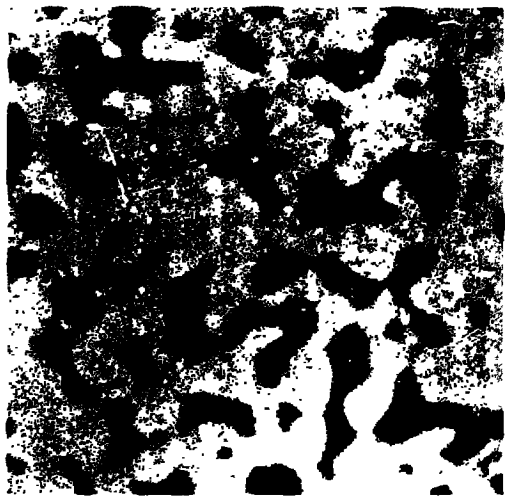

NEG. 1518 BUTTON E4-G-8
LINDE ALUMINA $(4.03)(10)^6$PORES/cm^2
5-10 sec. SWAB ETCH AVG. PORE DIA. = 2.37μ

NEG. 1737 BUTTON E4-G-8
LINDE ALUMINA $(4.20)(10)^6$PORES/cm^2
5 sec. ON ETCH CLOTH AVG. PORE DIA. = 2.32μ

NEG. 1743 BUTTON E4-G-8
LINDE ALUMINA $(5.15)(10)^6$PORES/cm^2
10 sec. ON ETCH CLOTH AVG. PORE DIA. = 2.10μ

FIG. 2-3 EFFECT OF POLISHING TECHNIQUES ON APPEARANCE OF SPHERICAL TUNGSTEN POWDER IONIZERS (2000X)

TABLE 2-IV

METALLOGRAPH PREPARATION OF POROUS TUNGSTEN, INFILTRATED WITH COPPER

I. Initial Surface Condition - Machined or Machine Ground

II. Mounting
- A. Bakelite[a]
- B. Pressure, 4200 psi; maximum temperature $\approx 150^{\circ}C$
- C. Hold at above pressure and temperature for about 6 minutes.

III. Hand Grinding
- A. Wet Papers
  1. 240-grit silicon carbide
  2. 320-grit silicon carbide
  3. 400-grit silicon carbide
  4. 600-grit silicon carbide
- B. Grind in sequence A, keeping specimen as flat as possible.

IV. Polishing
- A. Preliminary (to remove most of surface deformation)
  1. Linde A alumina (0.3μ) slurry with H_2O on nylon cloth[b]
  2. Wheel speed, 1150 rpm; pressure applied, heavy
  3. Polish with hand rotation for the minimum time necessary to remove microscopic scratches.
- B. Final (to remove residual surface deformation)
  1. Linde B alumina (0.05μ) slurry with modified Murakami's etchant[d] on microcloth[c]
  2. Wheel speed, 163 rpm; pressure applied, light
  3. Polish with hand rotation for 5-10 sec. or until grain boundries become faintly visible.

V. Differential Oxidation Etch (to provide contrast between tungsten matrix and infiltrant)
- A. Heat in air oven at 140-155°C for a minimum of 10 minutes.
- B. Repeat A until desired contrast is obtained.

(a) Buehler Catalog number 20-3300
(b) Buehler Catalog number 40-7058
(c) Buehler Catalog number 40-7208
(d) 15 gm KOH, 1 gm $K_3Fe(CN)_6$, 250 ml H_2O

3. IONIZERS FROM TUNGSTEN MICROSPHERES AND TANTALUM PARTICLES

It was demonstrated in the previous program (Ref. 2, Section 6) that densification of tungsten microspheres was greatly retarded by additions of tantalum particles. This effect is illustrated clearly in Figure 3-1. Additional study of W-Ta mixtures was considered necessary to optimize tantalum content and particle size in relation to the various criteria by which ionizers are rated. The range 0-10 A/o Ta was selected for detailed investigation. In this range, two particle-size distributions of tantalum (both predominantly below 6μ) were chosen.

3.1 Preliminary W-10 Ta Ionizers

Before starting extensive fabrication on Phase I of the program, it was desired to learn how the W-10A/o Ta alloy would perform as an ionizer. Two series of ionizer buttons were prepared by standard techniques, a control series from 2-5μ (Lot E4) tungsten microspheres only, the other from 2-5μ tungsten plus 10 atom percent 1-3μ tantalum.

Density and permeability parameters are listed in Table 3-I for the control series, and in Table 3-II for the W-10 Ta series. Average densities of both ionizer series were very near 80 percent of maximum theoretical. Average nitrogen permeability of the unalloyed control series was 0.25μP*, while that of the W-10A/o Ta series was 0.16μP. The latter low value thus indicated that the pore structure was restricted by the tantalum particle addition.

Microstructures of typical tungsten (control series) and W-10 Ta buttons are compared in Figure 3-2. Data given under the unalloyed and W-10 Ta micrographs indicate closely comparable mean pore diameters, however, the W-10 Ta structure evidenced about 14 percent fewer pores/cm^2.

---

* The quantity μP is defined as 10^{-6} gm·cm·sec^{-1}·$torr^{-1}$

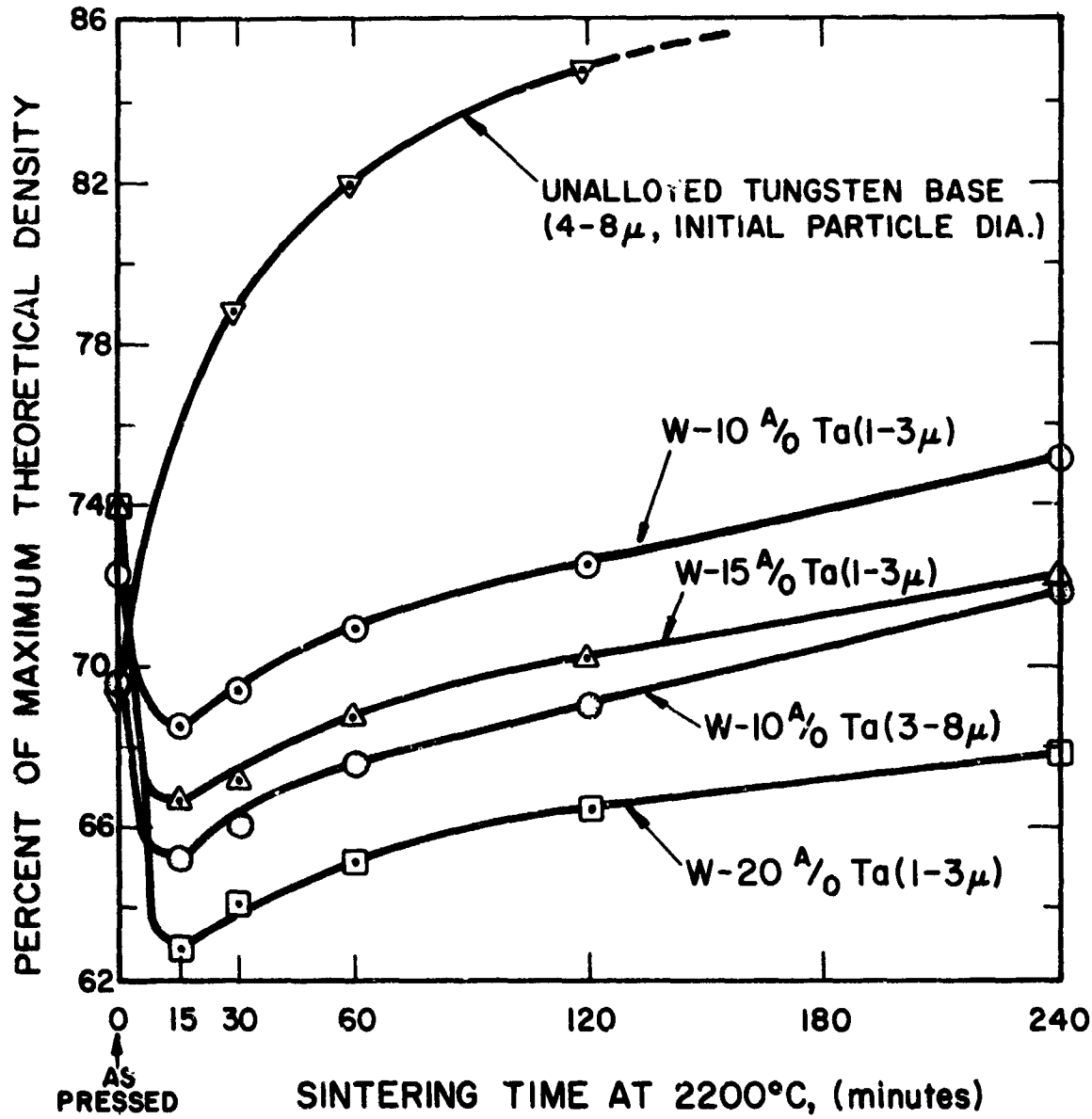

FIG. 3-1 EFFECT OF TANTALUM ON 2200°C SINTERING RATE OF LOT E7A TUNGSTEN MICROSPHERES OF 4-8μ DIAMETER (Atom percentages and size ranges of the tantalum additives are rated on respective curves above. All sintering performed at 5×10^{-5} torr)

TABLE 3-I

PARAMETERS OF IONIZER BUTTONS PREPARED FROM
LOT E4 (2-5μ) SPHERICAL TUNGSTEN POWDER
(Surface ground to 6 rms finish)

Button No.	Face Area, cm^2	Thick., cm	Vol., cm^3	Wt., gm	Density, gm/cm^3	% of Max. Theor. Density	δt, sec.	Mass Perm.* Coef., μP
E4-G-1	.17532	.10135	.01777	.2722	15.32	79.38	8.98	.286
E4-G-2	.17547	.10185	.01787	.2764	15.47	80.16	11.43	.226
E4-G-3	.17512	.09830	.01721	.2648	15.39	79.74	9.39	.266
E4-G-4	.17547	.10236	.01796	.2750	15.31	79.33	9.67	.268
E4-G-5	.17512	.10211	.01788	.2735	15.30	79.27	9.30	.279
E4-G-6	.17547	.10211	.01792	.2762	15.41	79.84	11.02	.235
E4-G-7	.17512	.10160	.01779	.2778	15.62	80.93	13.73	.188
Avgs.	----	.10138	----	----	15.40 →	79.79	----	.250

* Permeability Coefficient expressed in microperms, where
$1\ \mu P = 10^{-6} \cdot gm \cdot cm^{-1} \cdot sec^{-1} \cdot torr^{-1}$

TABLE 3-II

PARAMETERS OF IONIZER BUTTONS PREPARED FROM
LOT E4 (2-5μ) SPHERICAL TUNGSTEN PLUS 10 A/o OF
LOT BF (1-3μ) TANTALUM (Surface ground to 6 rms finish)

Button No.	Face Area, cm^2	Thick., cm	Vol., cm^3	Wt., gm	Density, gm/cm^3	% of Max. Theor. Density	δt, sec.	Mass Perm. Coef., μP
34-10Ta-1	.17831	.10490	.01870	.2873	15.36	80.71	16.62	.157
4-10Ta-2	.17831	.10414	.01857	.2855	15.37	80.77	15.74	.165
4-10Ta-3*	.17831	.10465	.01866	.2868	15.37	80.77	16.28	.160
4-10Ta-4	.17816	.10439	.01860	.2857	15.36	80.71	14.59	.178
4-10Ta-5	.17831	.10465	.01866	.2872	15.39	80.87	17.40	.150
4-10Ta-6	.17816	.10465	.01864	.2876	15.42	81.08	17 78	.147
4-10Ta-7	.17831	.10414	.01857	.2853	15.36	80.71	16.37	.158
4-10Ta-8	.17851	.10414	.01859	.2848	15.32	80.50	14.88	.174
4-10Ta-9	.17831	.10465	.01866	.2871	15.39	80.87	17.02	.153
gs.	---	.10448	---	---	15.37	→ 80.77	---	.160

Used for ionization performance testing.

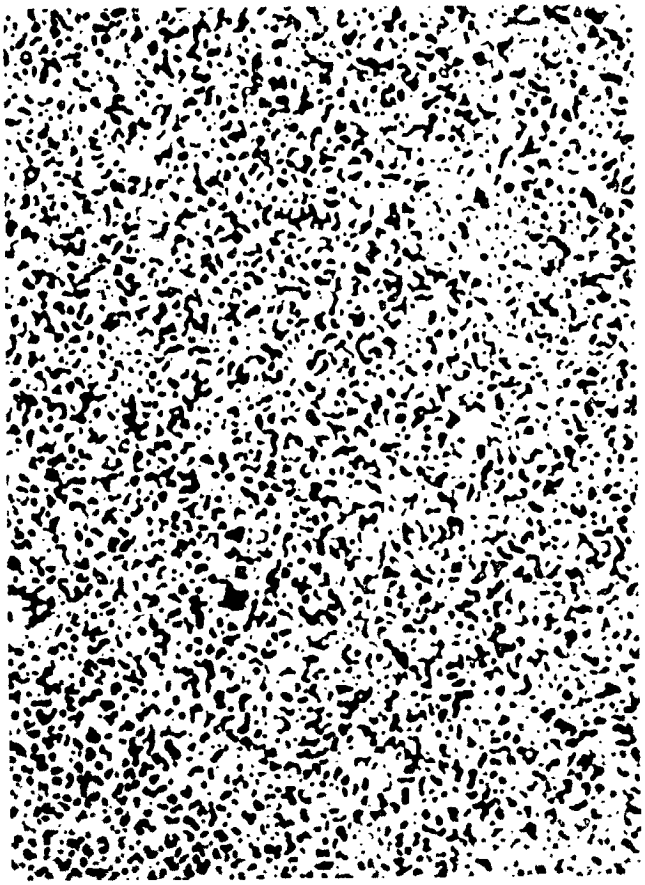

NEG. 1722 AVG. PORE DIA. = 2.37μ
PURE TUNGSTEN 4.03 X 10^6 PORES/cm^2

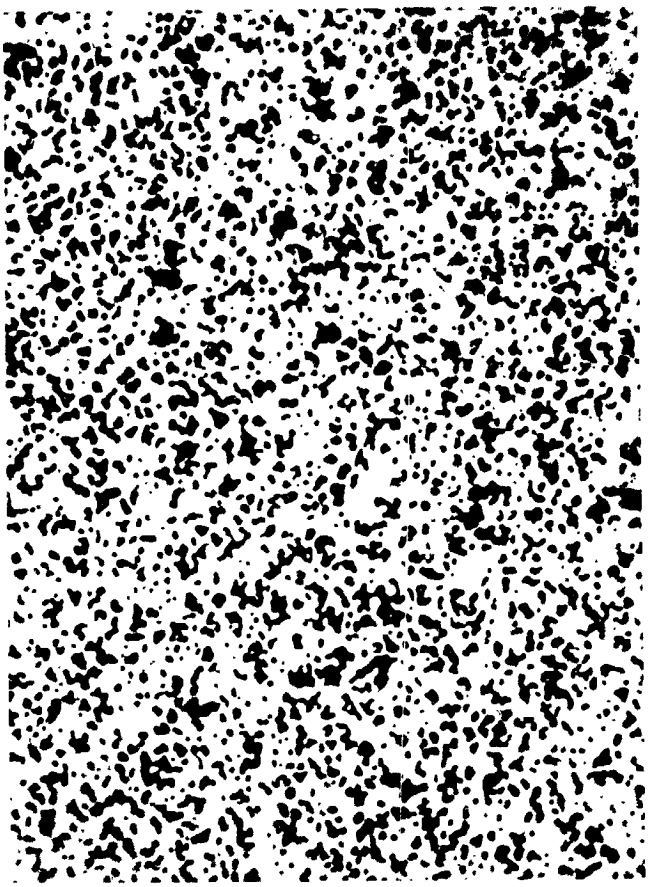

NEG. 1723 AVG. PORE DIA. = 2.34μ
W-10 A/o Ta 3.51 X 10^6 PORES/cm^2

FIG. 3-? EFFECT OF 10 ATOM PERCENT TANTALUM ON PORE STRUCTURE OF SPHERICAL POWDER IONIZER [2-5μ (E4) tungsten base; 1-3μ (BF) tantalum; 400X]

Further, the pore size of the W-10 Ta buttons is notably less uniform than that of the unalloyed tungsten. Whether the decrease in pore uniformity, pores per unit area, and permeability (occasioned by tantalum addition) is outweighed by increased structural stability can be established only by subsequent life testing.

Cesium ionization of one preliminary W-10A/o Ta ionizer was investigated to a maximum ion current density of 85 mA/cm^2. The neutral fraction was similar to E6 (3-6μ) spherical powder ionizers and the neutral fraction-vs-ionizer temperature curves indicated a work function of 4.65 eV. Critical temperatures were similar to those of the ionizers made from 1-4μ and 3-6μ spherical tungsten powder. Details of performance are given in Section 7 of this report

Performance of the preliminary W-10 Ta ionizer, in conjunction with its indicated superiority of thermal stability, was highly encouraging. Therefore, it was decided to use tantalum as the secondary alloying element in Phase I.

3.2 Ionizers Containing 0.0 to 10 A/o of Tantalum

The following mixtures, containing 1.7-5μ tungsten (Lot L), were prepared and pressed hydrostatically at 59,000 psi:

Comp., A/o	No. of Compacts [a] Pressed
Tung. Base (1.7-5μ)	5
Tung. Base - 0.5 Ta	5 with 1-3μ Ta[b] + 5 with 1-5μ Ta[c]
Tung. Base - 2.0 Ta	5 with 1-3μ Ta + 5 with 1-5μ Ta
Tung. Base - 5.0 Ta	5 with 1-3μ Ta + 5 with 1-5μ Ta
Tung. Base - 10.0 Ta	5 with 1-3μ Ta + 5 with 1-5μ Ta

(a) Barrel compacts, about 3/4" long with a maximum diameter of 3/8"
(b) Lot BF tantalum
(c) Lot CF tantalum

3.2.1 Effect of Tantalum on Sintering Rate

One compact of each of the nine categories listed above was vacuum sintered at 2000°C, and densities were determined at intervals of 30, 60, 120, and 240 minutes. Density data for two alloy series are listed in Tables 3-III and 3-IV. Data of Tables 3-III and 3-IV are plotted in Figures 3-3 and 3-4 as density vs sintering time. General trends, shown by these curves, are as follows:

1. Densification is accelerated by 0.5 A/oTa, affected very little by 2 A/oTa, and retarded significantly by 5 and 10 A/o Ta additions:

2. Retardation of densification, or improved dimensional stability, at the higher tantalum levels is consistent with trends reported previously; the retarding effect of 1-5μ Ta is somewhat greater than that of 1-3μ Ta particles.

Validity of the preceding trends is confirmed by agreement of the 1-3μ particle series with the 1-5μ series. The fact that 0.5 A/o Ta additions accelerated initial densification, as compared with the pure tungsten powders, is not well understood. Since this same effect was observed subsequently for 1.53 A/o Ta, added as a vapor coating on the tungsten, one can rule out explanations based on physical form or distribution of the tantalum. A plausible explanation is that only a small amount of tantalum is required to getter interstitial impurities (O, N, H) and that diffusion is thereby accelerated. Small additions could thus account for accelerated densification rates, while larger additions apparently introduce a retarding mechanism which dominates.

The curves of Figure 3-1 show that addition of 10-20 percent tantalum actually caused densities to decrease during the first 15 minutes of sintering at 2200°C. In other words, these large amounts of tantalum caused sample volumes to increase initially, and then to decrease at a lessening rate. The countering effects of two sintering mechanisms - one acting to shrink, the other to expand - together with the resulting curve, are illustrated in Figure 3-5. Initial volume expansion

TABLE 3-III

DENSIFICATION-RATE DATA FOR COMPACTS MADE FROM MIXTURES OF 1.7-5μ TUNGSTEN MICROSPHERES (Lot L) AND 1-3μ TANTALUM POWDER (LotBF) (Pressed Hydrostatically at 59,000 psi and Sintered in 10^{-5} torr Range)

Compact Identity	Weight Data, gms. *					Density	
	S	P+M_1	P+M_1+S	(P+M_2+S)	M_1-M_2	13.546 S/M_1-M_2 gm/cm^3	% of Theor.
			As-pressed				
Pure W	17.2229	203.5798	220.8027	203.4477	17.3550	13.44	69.64
W-.5Ta	17.6873	203.5798	221.2581	203.5230	17.7351	13.50	69.98
W- 2Ta	16.8669	203.5798	220.4467	203.4467	17.1908	13.29	69.07
W- 5Ta	17.8596	203.5798	221.4394	203.2054	18.1340	13.34	69.59
W-10Ta	16.4481	203.5793	220.0279	203.1199	16.9080	13.18	69.26
			After 30 minutes at 2000° C				
Pure W	17.1256	203.5798	220.7054	205.7968	14.9086	15.56	80.62
W-.5Ta	17.6276	203.5798	221.2074	206.6848	14.5226	16.44	85.23
W- 2Ta	16.8339	203.5798	220.4137	205.7215	14.6922	15.52	80.67
W- 5Ta	17.8021	203.5798	221.3819	204.8034	16.5785	14.55	75.90
W-10Ta	16.3935	203.5798	219.9733	203.2437	16.7296	13.27	69.73
			After 60 minutes at 2000° C				
Pure W	17.1231	203.5798	220.7029	206.5501	14.1528	16.39	84.92
W-.5Ta	17.6244	203.5798	221.2042	207.2724	13.9318	17.14	88.85
W- 2Ta	16.8335	203.5798	220.4133	206.4587	13.9546	16.34	84.93
W- 5Ta	17.7959	203.5798	221.3757	205.5055	15.8702	15.19	79.24
W-10Ta	16.3827	203.5798	219.9625	203.9306	16.0319	13.84	72.73
			After 120 minutes at 2000° C				
Pure W	17.1204	203.5798	220.7002	207.0384	13.6618	16.98	87.98
W-.5Ta	17.6261	203.5798	221.2059	207.5176	13.6883	17.44	90.41
W- 2Ta	16.8332	203.5798	220.4130	207.0168	13.3962	17.02	88.46
W- 5Ta	17.7916	203.5798	221.3714	206.0317	15.3397	15.71	81.95
W-10Ta	16.3736	203.5798	219.9534	204.5513	15.4021	14.40	75.67
			After 240 minutes at 2000° C				
Pure W	17.1235	203.5798	220.7033	207.5355	13.1678	17.62	91.30
W-.5Ta	17.6292	203.5798	221.2090	207.8982	13.3108	17.94	93.00
W- 2Ta	16.8360	203.5798	220.4158	207.5355	12.8803	17.71	92.05
W- 5Ta	17.7930	203.5798	221.3728	206.8877	14.4851	16.64	86.80
W-10Ta	16.3665	203.5798	219.9463	205.1369	14.8094	14.97	78.67

*

S = wt of sample in air

P = wt of empty pycnometer

M_1 = max wt. of Hg pycnometer can hold

M_2 = wt of Hg in pycnometer with sample immersed

(P+M_2+S) = total wt. of pycnometer, residual Hg and immersed sample

M_1-M_2 = P+M_1+S -(P+M_2+S) = Wt. of displaced Hg

TABLE 3-IV

DENSIFICATION-RATE DATA FOR COMPACTS MADE FROM MIXTURES OF 1.7-5μ TUNGSTEN MICROSPHERES (Lot L) AND 1-5μ TANTALUM POWDER (Lot CF) (Pressed hydrostatically at 59,000 psi and Sintered in 10^{-5} torr Range)

Compact Identity	Weight Data, gms.* S	P+M_1	P+M_1+S	(P+M_2+S)	M_1-M_2	Density 13.546 S/M_1-M_2 gm/cm^3	% of Theor.
			As-pressed				
Pure W	17.2229	203.5798	220.8027	203.4477	17.3550	13.44	69.64
W-.5Ta	16.5012	203.5798	220.0810	203.1487	16.9323	13.20	68.43
W- 2Ta	17.3740	203.5798	220.9538	203.3171	17.6367	13.34	69.33
W- 5Ta	17.9122	203.5798	221.4920	203.334.	18.1578	13.36	69.69
W-10Ta	16.2285	203.5798	219.8083	203.0961	16.7122	13.15	69.10
			After 30 minutes at 2000° C				
Pure W	17.1256	203.5798	220.7054	205.7968	14.9086	15.56	80.62
W-.5Ta	16.4666	203.5798	220.0464	206.3872	13.6592	16.33	84.66
W- 2Ta	17.3108	203.5798	220.8906	205.6493	15.2413	15.39	79.99
W- 5Ta	17.8583	203.5798	221.4381	204.6829	16.7552	14.44	75.33
W-10Ta	16.1557	203.5798	219.7355	202.9848	16.7507	13.06	68.63
			After 60 minutes at 20 0° C				
Pure W	17.123.	203.5798	220.7029	206.5501	14.1528	16.39	8′ .92
W-.5Ta	16.4658	203.5798	220.0456	206.8421	13.2035	16.89	87.56
W- 2Ta	17.3086	203.5798	220.8884	206.4036	14.4848	16.19	84.15
W- 5Ta	17.8549	203.5798	221.4347	205.3152	16.1195	15.00	78.25
W-10Ta	16 1465	203.5798	219.7263	203.3428	16.3835	13.35	70.15
			After 120 minutes at 2000° C				
Pure W	17.1204	203.5798	220.7002	207.0384	13.6618	16.98	87.98
W-.5Ta	16.4679	203.5798	220.0477	207.3178	12.7299	17.52	90.82
W- 2Ta	17.3089	203.5798	220.8887	207.0027	13.8860	16.89	87.79
W- 5Ta	17.8521	203.5798	221.4319	205.8428	15.5891	15.51	80.91
W-10Ta	16.1387	203.5798	219.7185	204.2819	15.4366	14.16	74.41
			After 240 minutes at 2000° C				
Pure W	17.1235	203.5798	220.7033	207.5355	13.1678	17.62	91.30
W-.5Ta	16.4722	203.5798	220.0520	207.8182	12.2338	18.24	94.56
W- 2Ta	17.3125	203.5798	220.8923	207.4531	13.4392	17.45	90.70
W- 5Ta	17.8539	203.5798	221.4337	206.6195	14.8142	16.33	85.19
W-10Ta	16.1335	203.5798	219.7133	204.7381	14.9752	14.59	76.67

* S = wt of sample in air
P = wt of empty pycnometer
M_1 = max wt.of Hg pycnometer can hold
M_1-M_2 = P+M_1+S -(P+M_2+S)= wt of displaced Hg
M_2 = wt of Hg in pycnometer with sample immersed
(P+M_2+S)= total wt of pycnometer, residual Hg, and immersed sample

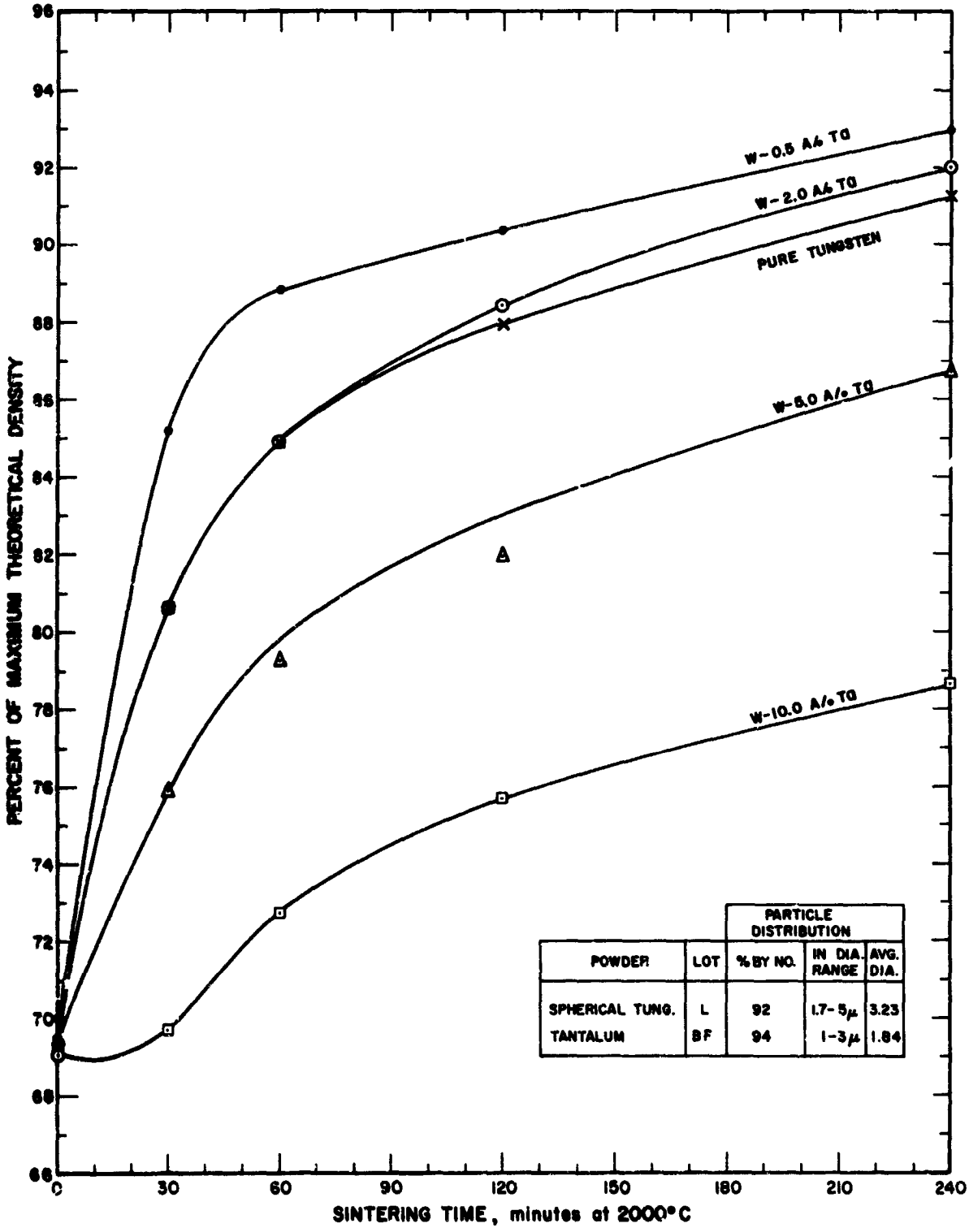

FIG. 3-5 DENSIFICATION RATE CURVES FOR TUNGSTEN POWDER AND W-Ta POWDER MIXTURES (Pressed hydrostatically at 59000 psi and sintered at 2000°C in 10^{-5} torr range; average diameter of Ta particles = 1.84μ)

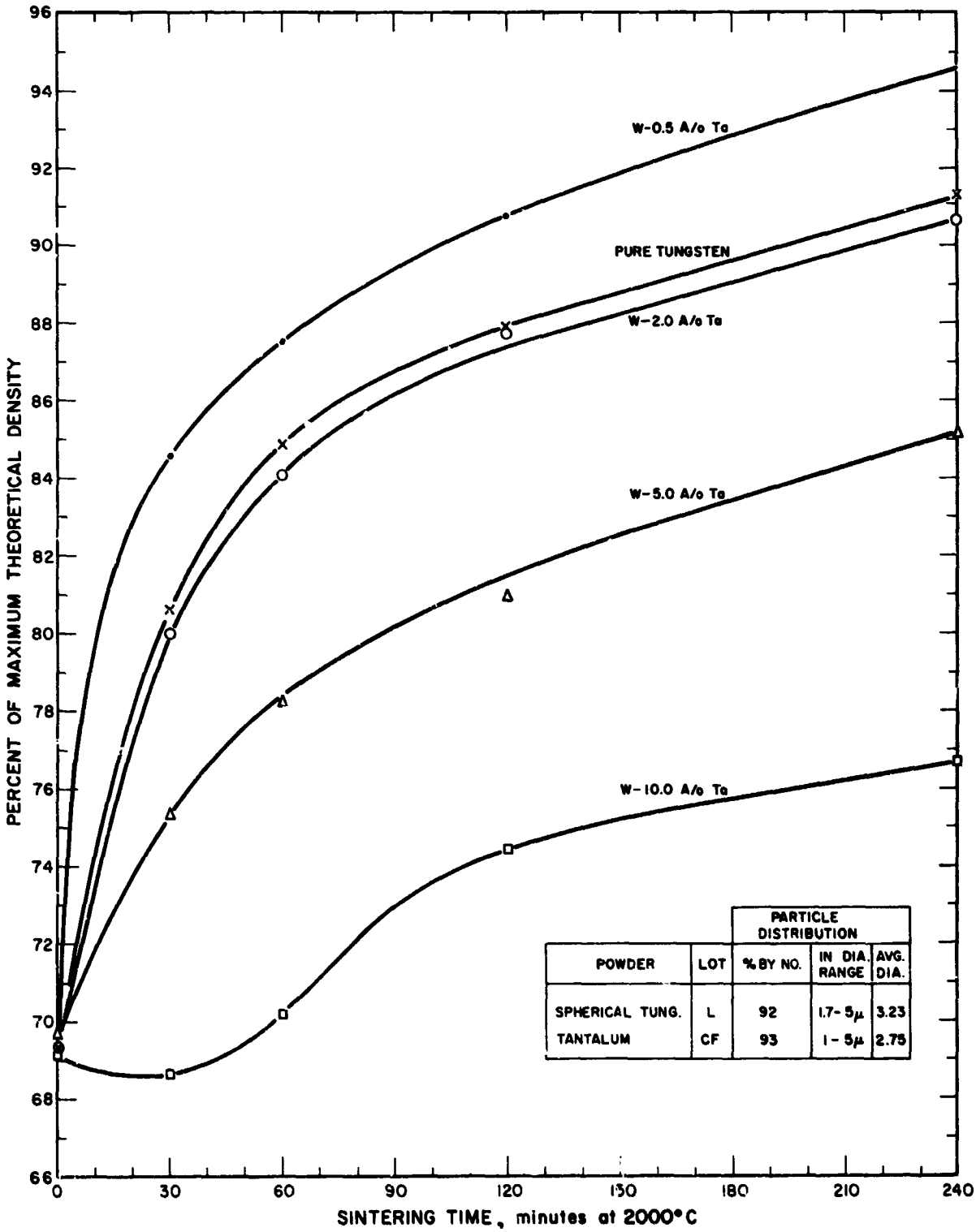

FIG. 3-4 DENSIFICATION RATE CURVES FOR TUNGSTEN POWDER AND W-Ta POWDER MIXTURES (Pressed hydrostatically at 59000 psi and sintered at 2000°C in 10^{-5} torr range; average diameter of Ta particles = 2.75μ)

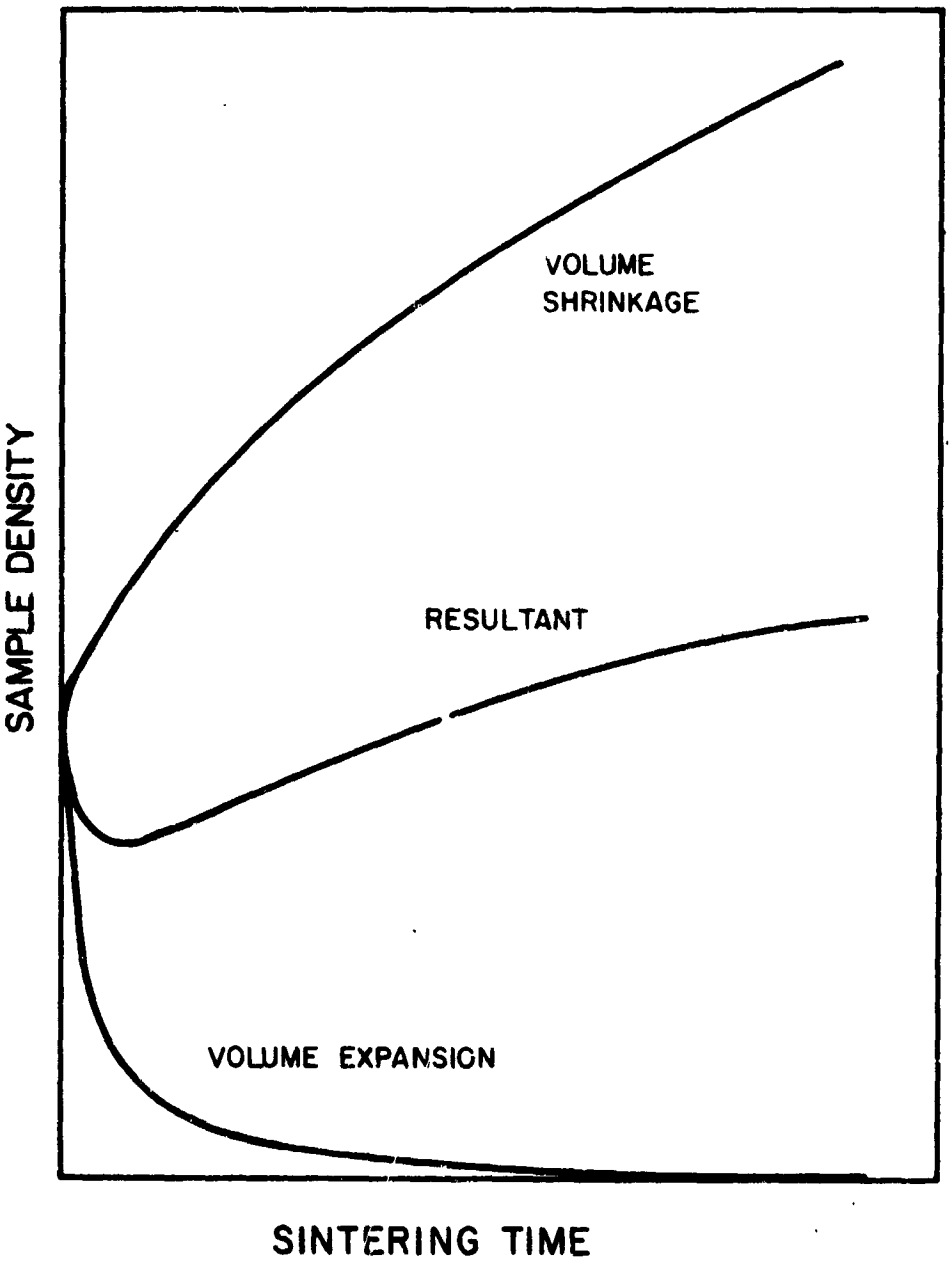

FIG. 3-5 EFFECT OF OPPOSED SINTERING MECHANISMS

of the W-Ta mixtures is believed to be caused by rapid diffusion of the tantalum into the tungsten particles. The tungsten particles are thus enlarged, and additional void spaces are created. Dominance of this expanding mechanism would be expected to increase with tantalum addition, as confirmed by Figure 3-1.

Since all curves of Figures 3-3 and 3-4 cross the level which corresponds to 76 percent density, their slopes at this common level were measured to provide a comparison of instantaneous sintering rates. These data are listed in Table 3-V. The pure tungsten powder used as a control reached 76 percent density in 14 minutes, at which level its densification rate was 0.39%/min. In contrast, W-10A/o (1-5μ)Ta required 198 minutes (or 14 times longer) to reach 76 percent density, at which level its densification rate was only 0.02%/min (or 1/20 that of the pure tungsten powder).

3.2.2 Effect of Tantalum on Nitrogen Permeability

The sintering rate information discussed in the preceding section, was utilized in vacuum sintering additional compacts of all W-Ta mixtures, at temperatures and times necessary to reach approximately 80 percent density. These compacts were infiltrated, machined to button form, and vacuum distilled by standard procedures.

Final densities and nitrogen permeabilities of the mixed powder W-Ta buttons are listed in Appendix Tables A-G, and plotted in Figure 3-6. The data scatter band in Figure 3-6 for each of the button categories indicates a normal trend of decreasing nitrogen permeability with increasing density. The pure tungsten control buttons exhibit unusually large variances in permeability, compared with that of previous spherical tungsten controls and with the small variances in permeability of the four W-Ta alloys. The lower permeability of the W-Ta alloys is again illustrated, confirming the tendency of Ta to restrict the pore channels.

An indication of dimensional stability of the four W-Ta alloys (relative to one another and to pure tungsten) is given by the sintering conditions required to reach target density, as noted in Figure 3-6.

TABLE 3-V

EFFECT OF TANTALUM ADDITIONS TO SPHERICAL TUNGSTEN POWDER[(a)] ON INSTANTANEOUS SINTERING RATE (AT 76% DENSITY LEVEL) AND ON TIME REQUIRED TO REACH 76% DENSITY

Tantalum Particle Size Range	Av	A/o Tantalum Added	Instantaneous Sint. Rate at 76% Density Level, Δ% density/minute	Time at 2000°C to Reach 76% Den., Minutes
1-3μ (Lot BF)	1.84μ	0.0	0.39	14
		0.5	0.57	11
		2.0	0.39	14
		5.0	0.18	31
		10.0	0.03	131
1-5μ (Lot CF)	2.75μ	0.0	0.39	14
		0.5	1.00	4
		2.0	0.36	16.5
		5.0	0.13	35
		10.0	0.02	198

(a) Av particle diam = 3.23μ (Lot L)

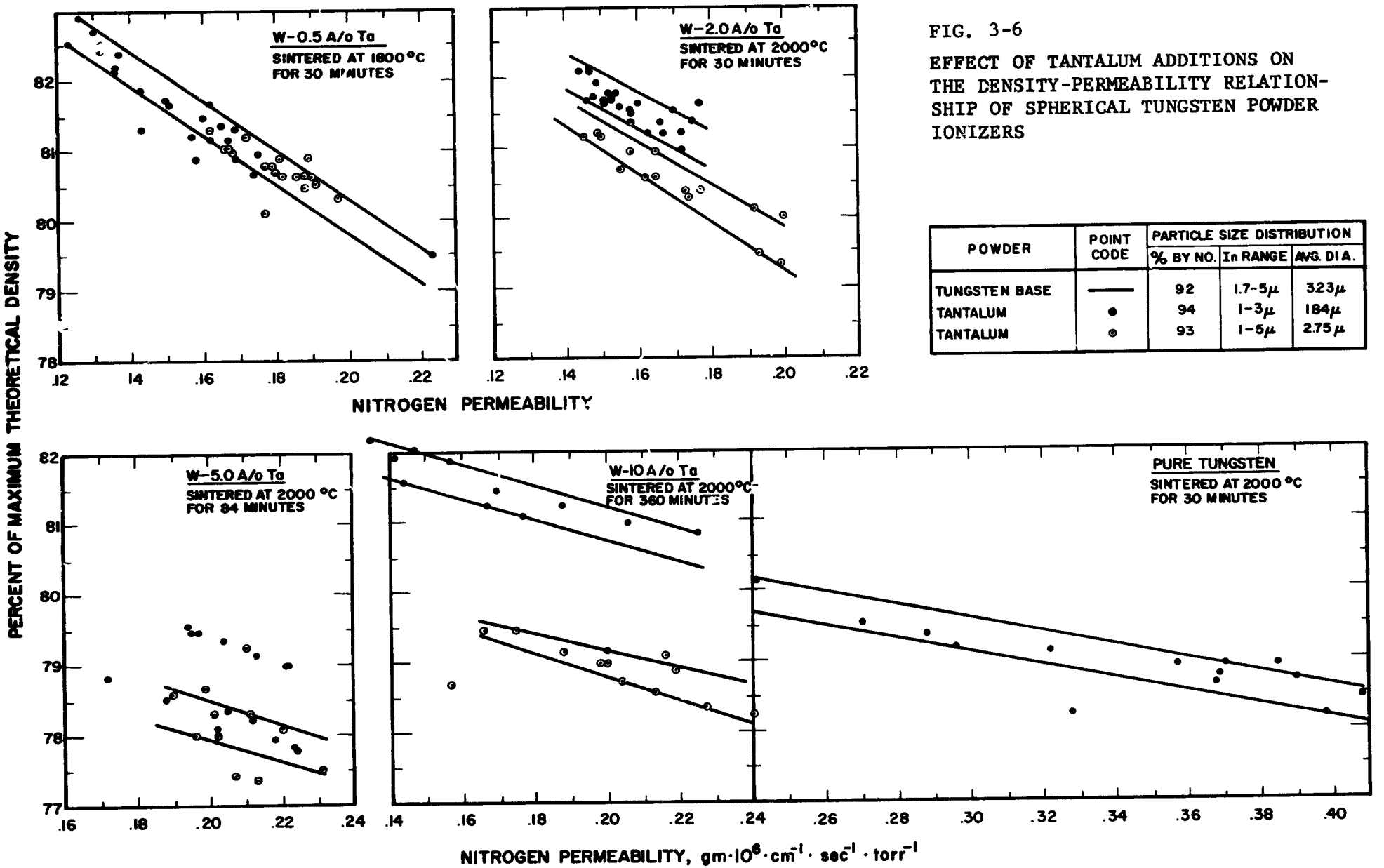

FIG. 3-6

EFFECT OF TANTALUM ADDITIONS ON THE DENSITY-PERMEABILITY RELATIONSHIP OF SPHERICAL TUNGSTEN POWDER IONIZERS

POWDER	POINT CODE	PARTICLE SIZE DISTRIBUTION		
		% BY NO.	In RANGE	AVG. DIA.
TUNGSTEN BASE	——	92	1.7-5μ	323μ
TANTALUM	●	94	1-3μ	184μ
TANTALUM	⊙	93	1-5μ	2.75μ

The 10 A/o (1-5μ) Ta addition is unquestionably the most effective in retarding densification and imparting dimensional stability.

3.2.3 Effect of Tantalum on Pore Volumes

Pore volume, density, and mercury intrusion data for relatively large W-Ta samples* are summarized in Table 3-VI. In general, the volume percent of occluded pores is shown to increase with increasing Ta content. Similarly, at any Ta level, addition of the 1-5μ particles yields a somewhat larger volume of occluded pores than addition of the 1-3μ particles. Based on volumes of Hg intruded vs pressure applied, the pore networks of the W-Ta samples appear to be only slightly more restricted than that of the pure tungsten powder. This indication does not agree with the rather large difference in nitrogen permeabilities shown in Figure 3-6. However, final comparisons of structure are made metallographically, with pore densities and average pore diameters being determined by the counting method.

3.2.4 Effect of Tantalum on Pore Structure

The most important criterion used in selecting ionizers for performance testing is pore structure. Almost without exception, tungsten ionizers having higher pore densities and finer pore sizes have performed more efficiently. Therefore, considerable effort was exerted in defining the W-Ta structures.

Typical pore sturctures of the W-Ta alloys are shown in Figures 3-7 to 3-10 at magnifications of 400X and 2000X. Comparisons of these photomicrographs indicates a general decrease in pore uniformity with tantalum addition. This effect is most pronounced at the 10 Ta level and for the larger (1-5μ) Ta particle additive.

Microscopic pore counts were conducted, with results listed in Tables 3-VII and 3-VIII for the 1-3μ and the 1-5μ Ta series, respectively. The pore density and pore diameter of each composition was obtained by averaging the pore counts from four 2000X micros, and by calculating as explained in the table footnotes. Average pore diameter is

* Samples equivalent in volume to approximately 18 to 20 standard ionizer buttons

TABLE 3-VI

DENSITY, PORE VOLUME, AND MERCURY INTRUSION DATA
FOR SINTERED W-Ta MIXTURES, SHOWING EFFECT OF TANTALUM
CONTENT AND PARTICLE SIZE (Phase I)

Composition, Atom %	Pure Tungsten	W - 0.5Ta		W - 2.0Ta		W - 5.0Ta		W - 10.0Ta	
Sample Identity	Control	L.5B Ta	L.5C Ta	LB2 Ta	LC2 Ta	LB5 Ta	LC5 Ta	LB10 Ta	LC10 Ta
Tung. Particle Size *	1.7-5μ	1.7-5μ	1.7-5μ	1.7-5μ	1.7-5μ	1.7-5μ	1.7-5μ	1.7-5μ	1.7-5μ
Ta Particle Size *	----	1-3μ	1-5μ	1-3μ	1-5μ	1-3μ	1-5μ	1-3μ	1-5μ
Sintering Temp., °C	2000	1800	1800	2000	2000	2000	2000	2000	2000
Sintering Time, minutes	30	30	30	30	30	84		360	360
Vol. of Sample, V_s, cm^3	0.34125	0.33666	0.33346	0.34688	0.35241	0.34128		0.33902	0.34820
Density, % of Max. Theor.	79.22	80.82	79.57	80.93	80.77	80.54	**	82.71	80.56
Total Pore Vol., % of V_s	20.78	19.18	20.43	19.07	19.23	19.46		17.29	19.44
Open Pore Vol., % of V_s	19.69	18.09	18.98	17.44	17.25	17.05		15.07	16.94
Occluded Pore Vol., % of V_s	1.09	1.09	1.45	1.63	1.98	2.41		2.22	2.50
Mercury Pressure Range, psi	Mercury Intruded Over Respective Pressure Ranges								
	$\Delta V, cm^3$ / % of V_s	$\Delta V, cm^3$ / % of V_s	$\Delta V, cm^3$ / % of V_s	$\Delta V, cm^3$ / % of V_s	$\Delta V, cm^3$ / % of V_s	$\Delta V, cm^3$ / % of V_s	$\Delta V, cm^3$ / % of V_s	$\Delta V, cm^3$ / % of V_s	$\Delta V, cm^3$ / % of V_s
73-102	.0002 / 0.06	Nil / Nil	Nil / Nil	Nil / Nil	Nil / Nil	Nil / Nil	Nil / Nil	Nil / Nil	.0001 / 0.03
102-160	.0560 / 16.41	Nil / Nil	Nil / Nil	Nil / Nil	Nil / Nil	Nil / Nil	Nil / Nil	.0001 / 0.03	.0378 / 10.85
160-235	.0100 / 2.39	.0518 / 15.39	.0538 / 16.13	.0529 / 15.25	.0467 / 13.25	.0532 / 15.59	**	.0475 / 14.01	.0163 / 4.68
235-335	.0003 / 0.09	.0081 / 2.41	.0078 / 2.34	.0058 / 1.67	.0117 / 3.32	.0027 / 0.79		.0024 / 0.71	.0030 / 0.86
335-568	.0002 / 0.06	.0001 / 0.03	.0012 / 0.36	.0012 / 0.35	.0016 / 0.45	.0018 / 0.53		Nil / Nil	.0009 / 0.26
568-1735	.0003 / 0.09	.0003 / 0.09	.0003 / 0.09	.0003 / 0.09	.0003 / 0.09	.0001 / 0.03		.0001 / 0.03	.0003 / 0.09
1735-3485	.0002 / 0.06	.0004 / 0.12	.0001 / 0.03	.0001 / 0.03	.0003 / 0.09	.0002 / 0.06		.0009 / 0.26	.0005 / 0.14
3485-4360	Nil / Nil	.0001 / 0.03	.0001 / 0.03	.0001 / 0.03	.0002 / 0.06	.0002 / 0.06		.0001 / 0.03	.0001 / 0.03
4360-4985	Nil / Nil	.0001 / 0.03	Nil / Nil	.0001 / 0.03	.0001 / Nil	Nil / Nil		Nil / Nil	Nil / Nil
Totals	.0672 / 19.70	.0609 / 18.10	.0633 / 18.98	.0605 / 17.45	.0608 / 17.26	.0582 / 17.06		.0511 / 15.07	.0590 / 16.94

*

Powder Used	Lot No.	Particle Distribution: % by No	In Range	Avg. Dia.
Spherical Tung.	L	92	1.7-5μ	3.23μ
Tantalum	BF	94	1-3μ	1.84μ
Tantalum	CF	93	1-5μ	2.75μ

** Sample LC5 Ta was sintered for only 30 min., therefore its density was too low for comparison with other samples in table.

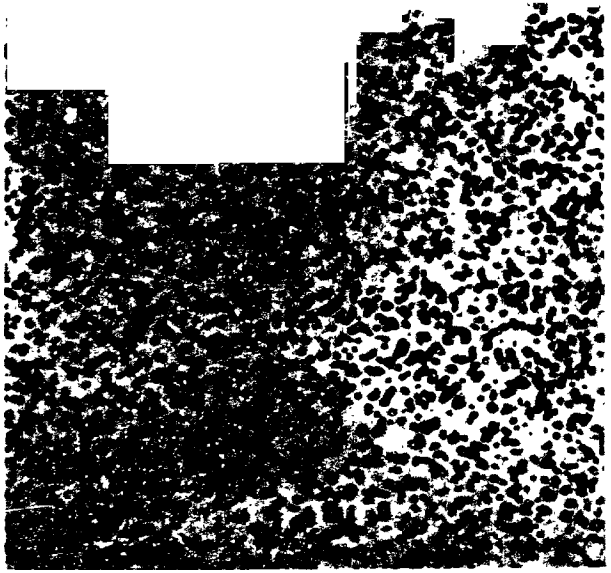

Neg. 1951 400X

Neg. 1943 1-3μ Ta 400X

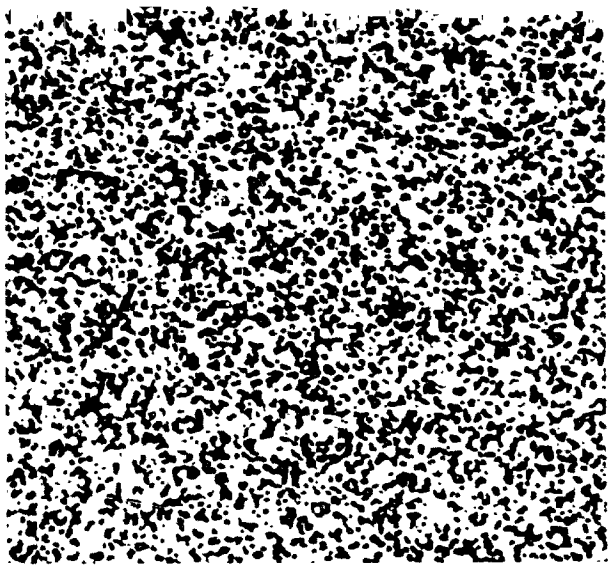

Neg. 1944 1-5μ Ta 400X

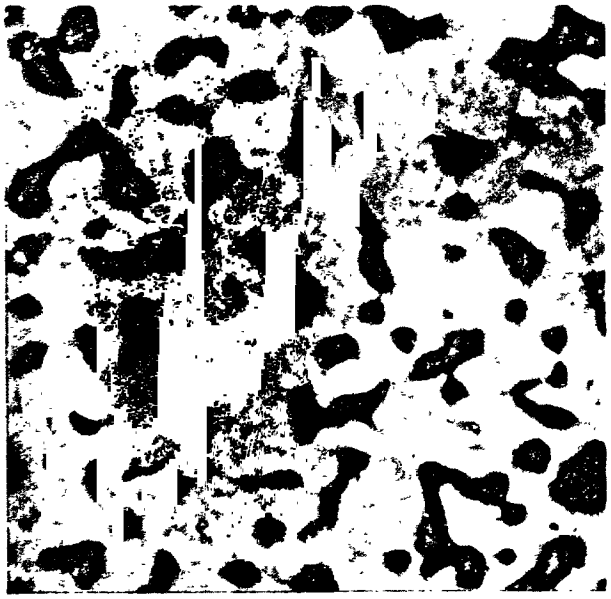

Neg. 1989 2000X

Neg. 1990 1-3μ Ta 2000X

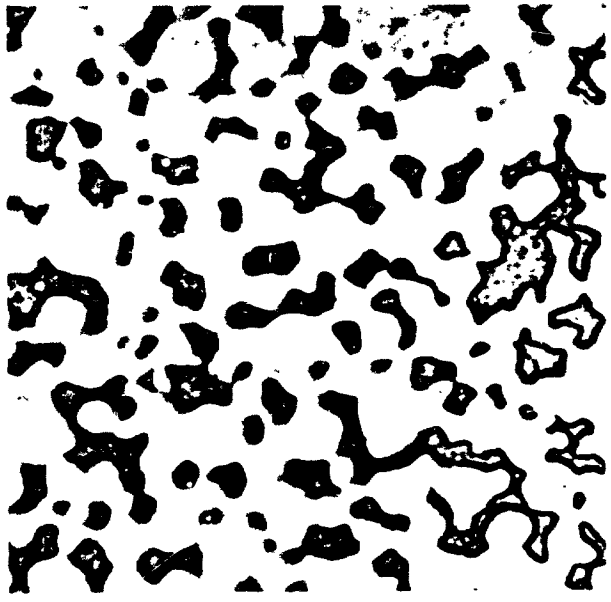

Neg. 1994 1-5μ Ta 2000X

←——Pure Tungsten——→ ←——W-0.5 A/o Ta——→

FIG. 3-7 EFFECT OF 0.5 A/o ADDITIONS OF 1-3μ AND 1-5μ TANTALUM PARTICLES ON PORE STRUCTURE OF ≈80% -DENSE TUNGSTEN (Made from 1.7-5μ Microspheres)

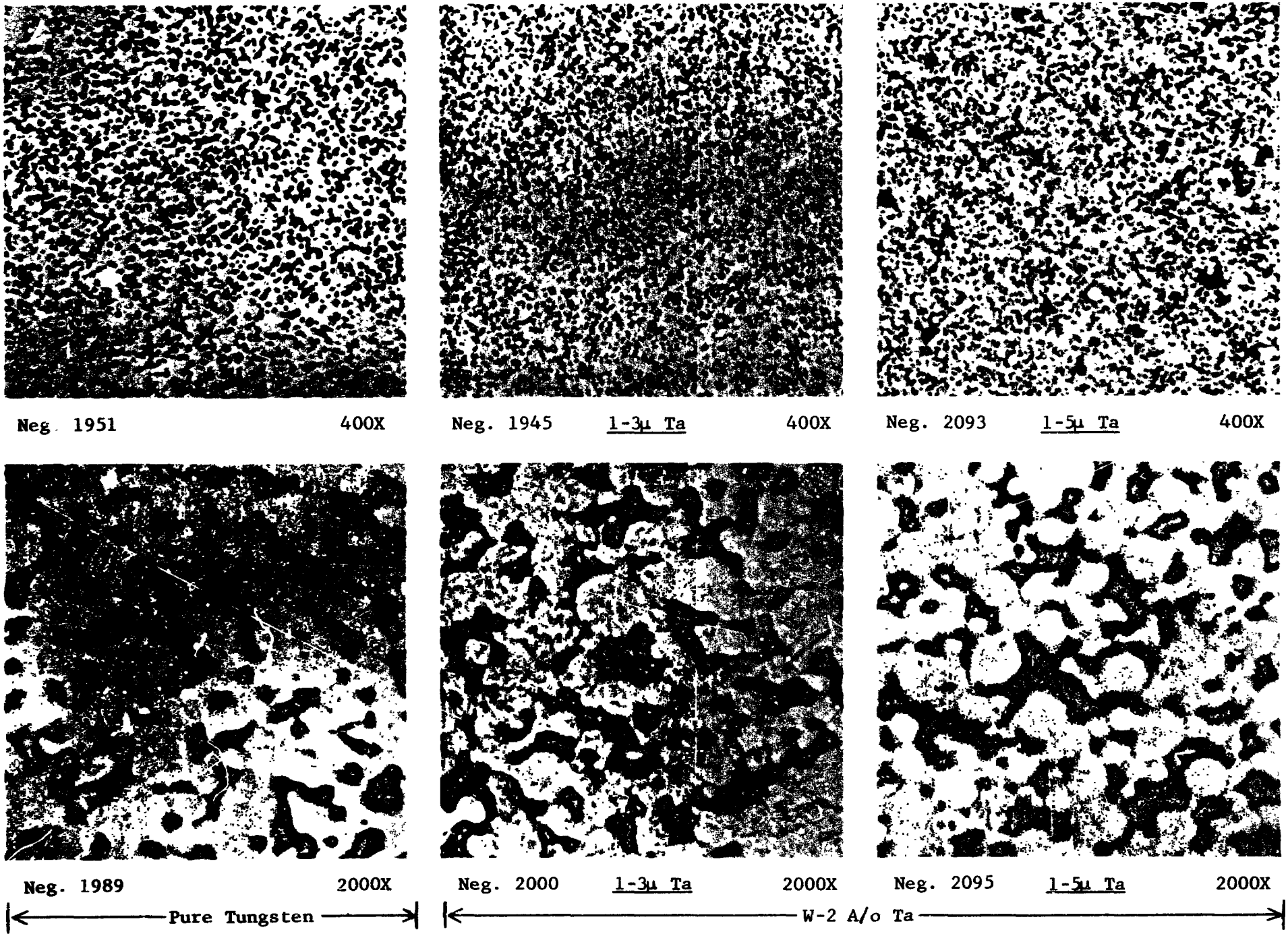

FIG. 3-8 EFFECT OF 2 A/o ADDITIONS OF 1-3μ AND 1-5μ TANTALUM PARTICLES ON PORE STRUCTURE OF ≈80%-DENSE TUNGSTEN

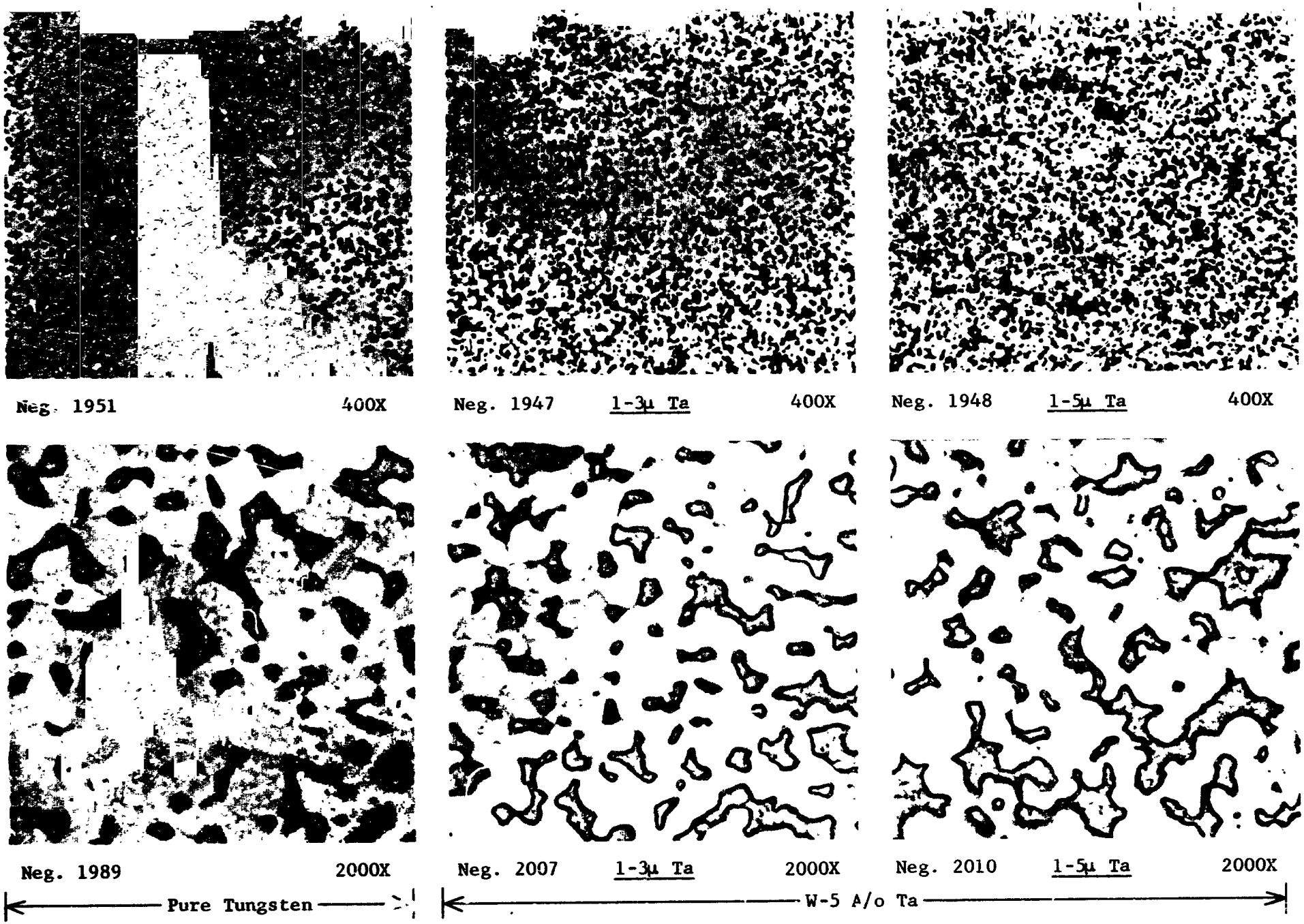

FIG. 3-9 EFFECT OF 5 A/o ADDITIONS OF 1-3μ AND 1-5μ TANTALUM PARTICLES ON PORE STRUCTURE OF ≈80%-DENSE TUNGSTEN (Made from 1.7-5μ Microspheres)

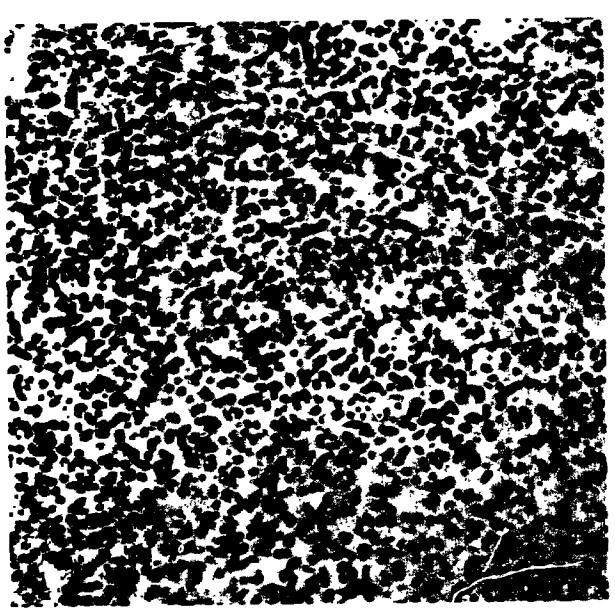

Neg. 1951 400X

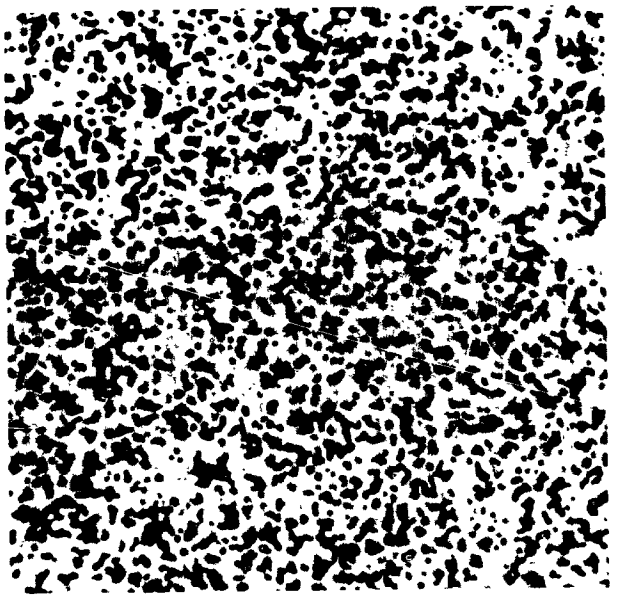

Neg. 1949 1-3μ Ta 400X

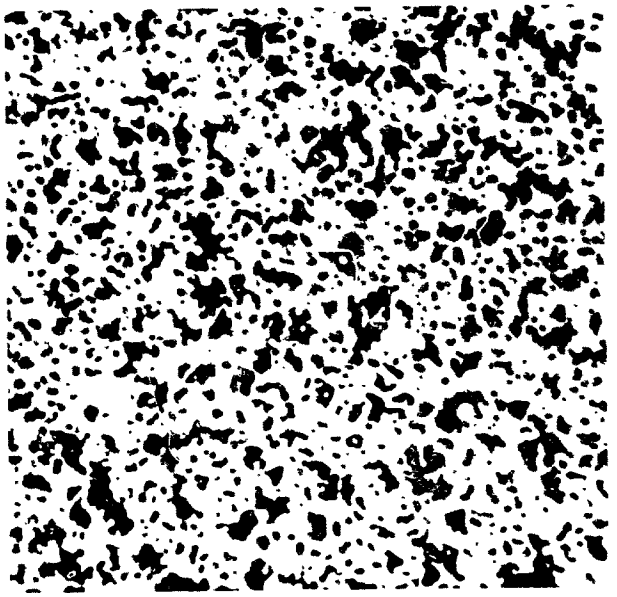

Neg. 1950 1-5μ Ta 400X

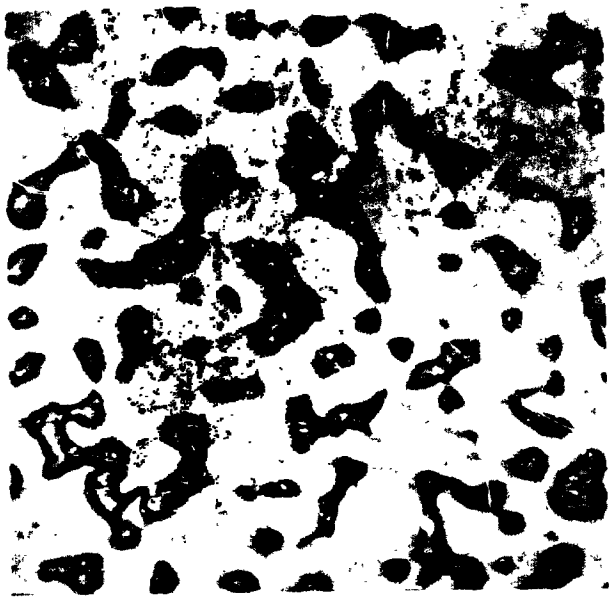

Neg. 1989 2000X

Neg. 2016 1-3μ Ta 2000X

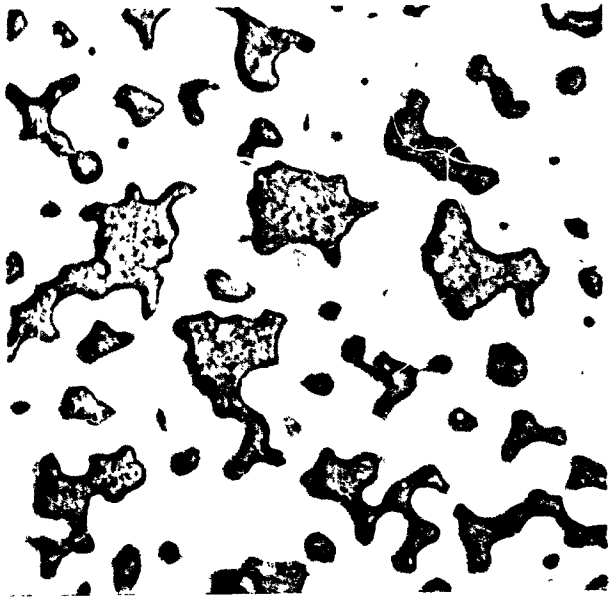

Neg. 2021 1-5μ Ta 2000X

Pure Tungsten

W-10 A/o Ta

FIG. 3-10 EFFECT OF 10 A/o ADDITIONS OF 1-3μ AND 1-5μ TANTALUM PARTICLES ON PORE STRUCTURE OF ≈80%-DENSE TUNGSTEN

TABLE 3-VII

EFFECT OF TANTALUM, ADDED AS 1-3μ PARTICLES, ON PORE DENSITY AND AVERAGE PORE DIAMETER OF TUNGSTEN SPHERICAL-POWDER IONIZERS

Sample Identity	Density, % of Theor.	Negative No.	Pores Counted at 2000X in 80 cm^2 Half Pores	Whole Pores	Total Pores	Pores/cm^2 at 1X (a)	Vol.% of Open Pores (b)	Av Pore Dia., μ (c)
			Pure Tungsten					
Control	79.22	1986	15	63	70.5			
		1987	14	81	88.0			
		1988	19	72	81.5			
		1989	17	76	84.5			
				Average =	81.1	4.06×10^6	19.69	2.48
			W-0.5 A/o Ta					
L.5B Ta	80.82	1990	13	112	118.5			
		1991	16	110	118.0			
		1992	14	103	110.0			
		1993	15	104	111.5			
				Average =	114.5	5.73×10^6	18.09	2.00
			W-2 A/o Ta					
LB2 Ta	80.93	1998	17	95	103.5			
		1999	21	91	101.5			
		2000	18	86	95.0			
		2001	14	100	107.0			
				Average =	101.8	5.09×10^6	17.44	2.09
			W-5 A/o Ta					
LB5 Ta	80.54	2006	16	80	88.0			
		2007	12	91	97.0			
		2008	15	80	87.5			
		2009	18	76	85.0			
				Average =	89.4	4.47×10^6	17.05	2.20
			W-10 A/o Ta					
LB10 Ta	82.71	2014	12	63	69.0			
		2015	14	56	63.0			
		2016	13	62	68.5			
		2017	14	64	71.0			
				Average =	67.9	3.40×10^6	15.07	2.37

a) Pores/cm^2 at 1X mag. = (Total Pores at 2000X)$(2000)^2$/80 cm^2

b) Vol. % of Open Pores = (100)(Vol. of Hg Intruded) /Vol. of Sample

c) Av Pore Diam, $\mu = 1128 \sqrt{\frac{(\text{Vol.\% of Open Pores})}{(\text{Pores/cm}^2 \text{ at 1X})}}$

TABLE 3-VIII

EFFECT OF TANTALUM, ADDED AS 1-5μ PARTICLES, ON PORE DENSITY AND AVERAGE PORE DIAMETER OF TUNGSTEN SPHERICAL-POWDER IONIZERS

Sample Identity	Density % of Theor.	Negative No.	Pores Counted at 2000X in 80 cm²			Pores/cm² at 1X (a)	Vol.,% of Open Pores (b)	Av Pore Dia.,μ (c)
			Half Pores	Whole Pores	Total Pores			
				Pure Tungsten				
Control	79.22	1986	15	63	70.5			
		1987	14	81	88.0			
		1988	19	72	81.5			
		1989	17	76	84.5			
				Average =	81.1	4.06×10^6	19.69	2.48
				W-0.5 A/o Ta				
L.5C Ta	79.57	1994	22	107	118.0			
		1995	18	100	109.0			
		1996	19	101	110.5			
		1997	23	104	115.5			
				Average =	113.3	5.67×10^6	18.98	2.06
				W-2 A/o Ta				
LC2 Ta	80.77	2095	14	87	94.0			
		2096	14	97	104.0			
		2097	19	96	105.5			
		2098	20	104	114.0			
				Average =	104.4	5.22×10^6	17.25	2.05
	est'd			W-5 A/o Ta				
LC5 Ta	80.45	2010	17	73	81.5			
		2011	21	70	80.5			
		2012	20	83	93.0			
		2013	23	80	91.5			
				Average =	86.6	4.33×10^6	est'd 17.00	2.24
				W-10 A/o Ta				
LC10 Ta	80.56	2018	14	51	58.0			
		2019	12	51	57.0			
		2020	13	65	71.5			
		2021	16	57	65.0			
				Average =	62.9	3.15×10^6	16.94	2.62

(a) Pores/cm² at 1X mag. = (Total Pores at 2000X)$(2000)^2$/80cm²

(b) Vol. % of Open Pores = (100)(Vol. of Hg Intruded) /Vol. of Sample

(c) Av Pore Diam, $\mu = 1128 \sqrt{\frac{(\text{Vol.\% of Open Pores})}{(\text{Pores/cm}^2 \text{ at 1X})}}$

plotted against pore density in Figure 3-11. Here it may be observed that W-0.5A/o Ta compositions have the highest pore density and smallest average pore diameter, while W-10A/o Ta compositions have the lowest pore density and largest pore diameter. As indicated on the graph by arrows, increasing the size range of tantalum from 1-3μ to 1-5μ resulted in lower pore densities and larger average pore sizes (at equivalent Ta percentages). The position of the point representing the pure tungsten powder, in relation to the W-Ta curves, indicates that a 6-8 atom percent addition of very fine tantalum particles should provide a structure equivalent in pore density to that of pure tungsten, but having greatly improved thermal stability.

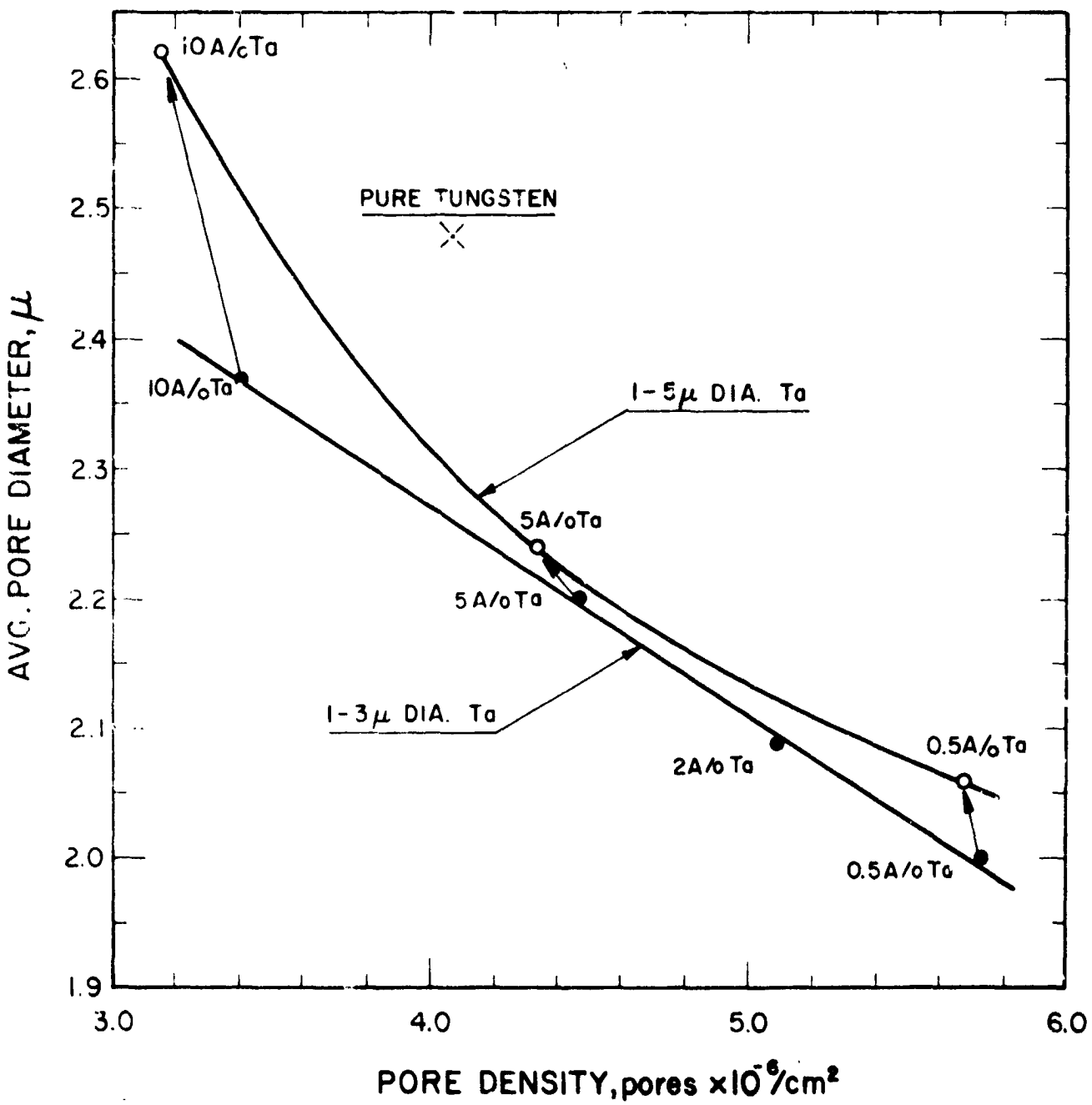

FIG. 3-11 EFFECT OF TANTALUM PARTICLE SIZE ON PORE DIAMETER-TO-DENSITY RELATIONSHIP AT VARIOUS LEVELS OF TANTALUM ADDITION (All compositions sintered to ≈80% of theoretical density)

3.3 Effect of Particle Surface Free Energy on Sintering

The effect of tantalum particles on the sintering rate of tungsten microspheres having been noted, it was desired to learn whether a similar retardation mechanism would obtain if low-energy tungsten microspheres were mixed with higher-energy nonspherical tungsten particles.

To determine this, two samples were prepared from Lot L spherical tungsten powder. (This powder contains 94% by number of particles within the diameter range of 1.7 to 5μ. Average particle diameter is 3.2μ.) To one sample of spherical powder, hydrogen-reduced tungsten powder having an average particle diameter of 1μ was admixed. This gave a heterogeneous duplex powder, consisting of 60 % by weight of spherical and 40% by weight of hydrogen-reduced.

The spherical powder sample and the spherical plus hydrogen-reduced powder mixture were loaded into rubber tubes and pressed hydrostatically at 60,000 psi. Then specimens were cut from each cylinder, measured to determine density, infiltrated with Cu-2%Fe, and examined metallographically. The remaining samples in the two cylinders were measured to determine density, sintered simultaneously at 2000°C for one hour in vacuum, and infiltrated. Finally, sintered densities were measured and the sintered structures were photomicrographed.

Photomicrographs of the two materials, in both the as-pressed and as-sintered conditions, are shown in Figures 3-12 and 3-13. The difference in the sintered structures may be explained as follows:

1. The finer hydrogen-reduced particles reduce the intimacy of sphere contact in compaction; however, exterior dimensions of the pressed compact are determined largely by the skeletal structure or packing of the larger microspheres.
2. Early in sintering, the fine hydrogen-reduced particles (like Ta) diffuse rapidly into the spherical particles. Thus, the spherical particles are expanded, total surface area is reduced, additional void spaces are created, and the

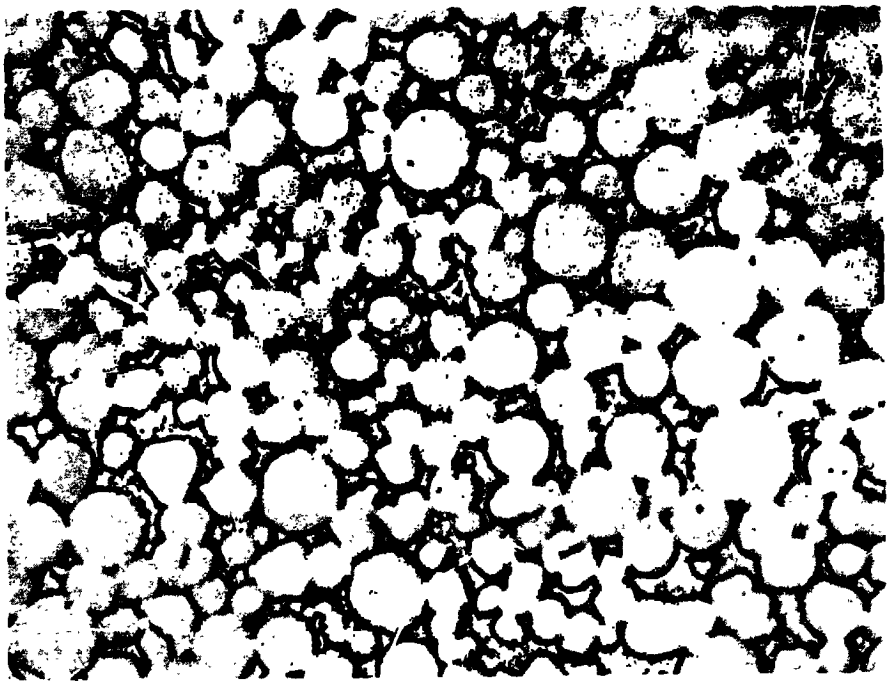

Neg. 1916 Density = 70.83%

As-Pressed

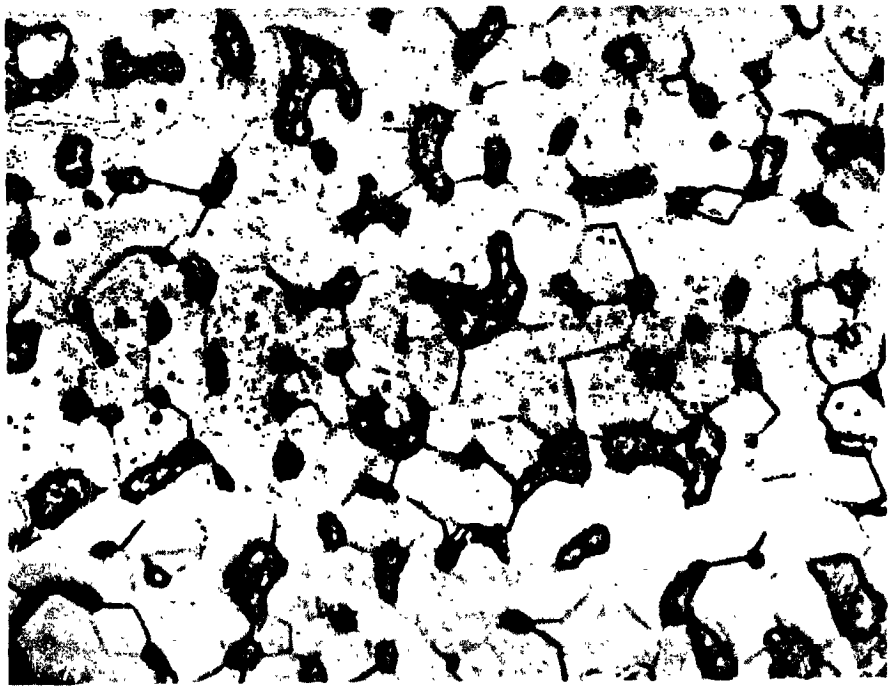

Neg. 1914 Density = 83.21%

As-Sintered
at 2000°C for 1 Hour

FIG. 3-12 APPEARANCE OF 3.2μ SPHERICAL TUNGSTEN POWDER IN THE AS-PRESSED AND AS-SINTERED CONDITIONS (2000X)

Neg. 1915 Density = 71.14%

As-Pressed

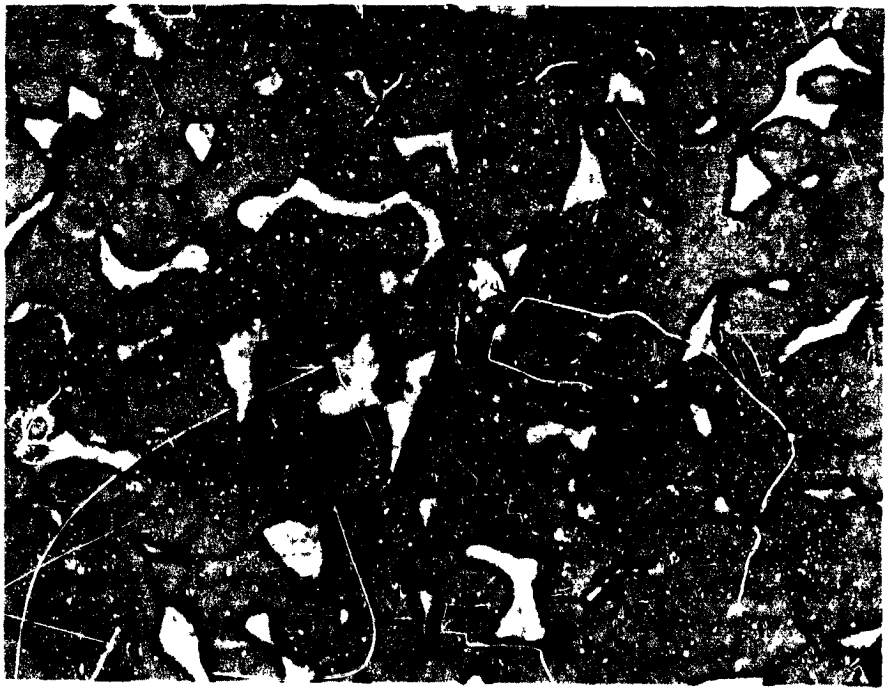

Neg. 1913 Density = 80.05%

As-Sintered
at 2000°C for 1 Hour

FIG. 3-13 APPEARANCE OF "3.2μ SPHERICAL TUNGSTEN + 40 W/o 1μ H_2-REDUCED" POWDER MIXTURE IN THE AS-PRESSED AND AS-SINTERED CONDITIONS (2000X)

number of possible diffusion paths between spherical particles is reduced.

3. As the high-energy particles are absorbed, the reduced surface area and the fewer diffusion bridges act to decrease total diffusion within the porous material.

Thus, whether the early rapid diffusion (which induces volume expansion and retards sintering rate) is due to differences in particle surface free energy or particle composition, such diffusion can produce structural changes which, in turn, increase dimensional stability. However, photomicrographs of the sintered structures, comparing the microspheres of tungsten with the heterogeneous tungsten mixture (lower photomicrographs, Figures 3-12 and 3-13) illustrate that the gain in dimensional stability is accompanied by a sacrifice in pore density and size.

In summary, the addition of secondary particles to sized tungsten microspheres (whether such particles are heterogeneous in surface energy or in composition) can increase dimensional stability but can simultaneously coarsen pore structure. It is believed that the mechanism demonstrated by this experiment will be very helpful in guiding future research on the stabilization of porous tungsten.

4. IONIZERS FROM TUNGSTEN MICROSPHERES, PRECOATED BY VACUUM DEPOSITION WITH TANTALUM, OSMIUM AND RHENIUM

This phase of the program was undertaken to determine whether precoatings of Ta, Re, and Os on tungsten would

(1) improve uniformity of secondary element distribution and thereby promote uniform ionizer pore structures,

(2) promote ready and uniform alloying by diffusion by placing the secondary element in closest possible contact with the tungsten microspheres,

(3) eliminate the voids formed when secondary particles diffuse into parent tungsten particles, and

(4) yield ionizers having improved performance and structural stability at operating temperatures.

Procedures used in vapor depositing these elements on tungsten were described in Section 2. It was noted that the coatings applied were considerably thinner than the desired thicknesses, tabulated as follows:

Coating Element	Coating Applied W/o	Coating Applied A/o	Coating Applied Thick., Å	Goal, Å
Ta	1.51	1.53	102	500
Ta	11.65	11.82	837	1000
Re	0.86	0.85	45	500
Re	2.80	2.77	150	1000
Os	0.35	0.34	17	500
Os	2.66	2.57	133	1000

As indicated by results to be discussed in this section, the thinner coatings proved to be of greater technical value than the thicker ones - so much so that less information would have been obtained had the 500Å and 1000Å thickness goals been achieved.

The six precoated powder batches were dried and blended by standard procedures to insure homogeniety and uniform packing characteristics. Five standard (barrel) compacts of each powder batch were pressed hydrostatically at 59,000 psi.

4.1 Effect of Vapor Precoatings on Sintering Rate

One compact form each of the six precoated batches was chosen at random for the sintering rate study. These six samples were vacuum sintered at 2000°C, and density determinations were made at sintering time intervals of 30, 60, 120, and 240 minutes. Density data obtained for the thinner coatings of Ta, Os, and Re are listed in Table 4-I, and for the thicker coatings in Table 4-II. Density-vs-time curves for the thinner coatings are plotted in Figure 4-1, and for the thicker coatings in Figure 4-2.

It is apparent from Figure 4-1 that the 102Å Ta (1.53 A/o) coating accelerated the rate of sintering in the useful 78% to 85% density range. This is in good agreement with the acceleration noted previously for 0.5 A/o Ta particle additions. Figure 4-1 also shows that densification was retarded by the 17Å Os and 45Å Re coatings, though not to a significant degree. Figure 4-2 shows that all of the thicker coatings were quite effective in retarding densification; the 133Å Os coating was extremely effective, however, the initial decrease in density (or increase in volume) indicates rapid interparticle or transgranular diffusion accompanied by coarsening of the pore structure. This was subsequently verified by metallographic examination of sintered ionizer buttons, being most pronounced for the 133Å Os and 150Å Re coated tungsten.

4.2 Effect of Vapor Precoatings on Nitrogen Permeability

Additional compacts of six coated powder batches were sintered to densities of approximately 80%, infiltrated, machined to buttons, and vacuum distilled. Final densities and nitrogen permeabilities of all buttons were determined and are listed in Appendix tables, as follows:

TABLE 4-I

DENSIFICATION RATE DATA FOR TUNGSTEN MICROSPHERES (Lot L), THINLY COATED BY VACUUM DEPOSITION WITH TANTALUM, OSMIUM AND RHENIUM; (Pressed Hydrostatically at 59,000 psi and Sintered in 10^{-5} torr Range)

Sample Identity	Weight Data, grams*					Sample Density gm/cm^3 $(13.546S/M_1-M_2)$	% theor. $(100\rho/19.3)$
	S	P+M_1	P+M_1+S	(P+M_2+S)	M_1-M_2		
As-Pressed							
Pure W	17.3453	203.5798	220.9251	203.3167	17.6084	13.34	69.12
W-102ÅTa	16.0851	203.5798	219.6649	203.2392	16.4257	13.27	68.76
W-17ÅOs	17.2832	203.5798	220.8630	203.2091	17.6539	13.26	68.70
W-45ÅRe	17.2706	203.5798	220.8504	203.1731	17.6773	13.23	68.55
After 30 Minutes at 2000°C							
Pure W	17.2771	203.5798	220.8569	206.1221	14.7348	15.88	82.28
W-Ta	16.0505	203.5798	219.6303	205.6808	13.9495	15.59	80.78
W-Os	17.2001	203.5798	220.7799	205.7569	15.0230	15.51	80.36
W-Re	17.1898	203.5798	220.7696	205.7305	15.0391	15.48	80.21
After 60 Minutes at 2000°C							
Pure W	17.2787	203.5798	220.8585	206.4700	14.3885	16.27	84.30
W-Ta	16.0510	203.5798	219.6308	206.5566	13.0742	16.63	86.17
W-Os	17.2017	203.5798	220.7815	206.3229	14.4586	16.12	83.52
W-Re	17.1911	203.5798	220.7709	206.1346	14.6363	15.91	82.44
After 120 Minutes at 2000°C							
Pure W	17.2807	203.5798	220.8605	206.8795	13.9810	16.74	86.74
W-Ta	16.0529	203.5798	219.6327	206.9204	12.7123	17.11	88.65
W-Os	17.2036	203.5798	220.7834	206.7539	14.0295	16.61	86.06
W-Re	17.1927	203.5798	220.7725	206.7635	14.0090	16.62	86.11
After 240 Minutes at 2000°C							
Pure W	17.2856	203.5798	220.8654	207.2787	13.5867	17.23	89.27
W-Ta	16.0574	203.5798	219.6372	207.2438	12.3934	17.55	90.93
W-Os	17.2081	203.5798	220.7879	207.0894	13.6985	17.02	88.19
W-Re	17.1961	203.5798	220.7759	206.9436	13.8323	16.84	87.25

*S = wt of sample in air
P = wt of empty pycnometer bottle
M_1 = max. wt of Hg pycnometer can hold
M_2 = wt of Hg in pycnometer after immersion of sample
(P+M_2+S) = total wt of pycnometer, residual Hg and immersed sample
M_1-M_2 = P+M_1+S - (P+M_2+S) = wt of Hg displaced by sample
13.546 S/M_1-M_2 = density of sample

TABLE 4-II

DENSIFICATION RATE DATA FOR TUNGSTEN MICROPHERES (LOT L), THICKLY COATED BY VACUUM DEPOSITION WITH TANTALUM, OSMIUM, AND RHENIUM, (Pressed Hydrostatically at 59,000 psi and Sintered in 10^{-5} torr Range)

Sample Identity	Weight Data, grams*					Sample Density, gm/cm^3		% of Theor.
	S	$(P+M_1)$	$(P+M_1+S)$	$(P+M_2+S)$	M_1-M_2	Max. Theor.	Actual	Density
			As-Pressed					
ure W	17.4857	203.5798	221.0655	203.3000	17.7655	19.30	13.33	69.07
+837ÅTa	16.6754	203.5798	220.2552	201.7113	18.5439	18.97	12.18	64.21
+133ÅOs	17.2394	203.5798	220.8192	203.0206	17.7986	19.87	13.12	66.83
+150ÅRe	17.2739	203.5798	220.8537	202.7361	18.1176	19.59	12.92	65.95
			After 30 Minutes at 2000°C					
ure W	17.4169	203.5798	220.9967	205.2901	15.7066	19.30	15.02	77.82
+Ta	16.4878	203.5798	220.0676	202.6126	17.4550	18.97	12.80	67.47
+Os	17.1330	203.5798	220.7128	202.2441	18.4687	19.87	12.57	63.26
+Re	17.1837	203.5798	220.7635	204.8652	15.8983	19.59	14.64	74.73
			After 60 Minutes at 2000°C					
ure W	17.4188	203.5798	220.9986	205.9185	15.0801	19.30	15.66	81.14
+Ta	16.4439	203.5798	220.0237	203.4172	16.6065	18.97	13.41	70.69
+Os	17.1254	203.5798	220.7052	204.3408	16.3644	19.87	14.18	71.36
+Re	17.1702	203.5798	220.7500	205.5140	15.2360	19.59	15.27	77.95
			After 120 Minutes at 2000°C					
ure W	17.4209	203.5798	221.0007	206.6517	14.3490	19.30	16.45	85.23
+Ta	16.4025	203.5798	219.9823	204.0339	15.9484	18.97	13.93	73.43
+Os	17.1247	203.5798	220.7045	204.4825	16.2220	19.87	14.30	71.97
+Re	17.1615	203.5798	220.7413	205.7454	14.9959	19.59	15.50	79.12
			After 240 Minutes at 2000°C					
ure W	17.4262	203.5798	221.0060	207.0571	13.9489	19.30	16.92	87.67
+Ta	16.3614	203.5798	219.9412	204.8050	15.1362	18.97	14.64	77.17
+Os	17.1300	203.5798	220.7098	204.7697	15.9401	19.87	14.56	73.28
W+Re	17.1558	203.5798	220.7356	206.0398	14.6958	19.59	15.81	80.70

S = wt of sample in air
P = wt of empty pycnometer bottle
M_1 = max. wt of Hg pycnometer can hold
M_2 = wt of Hg in pycnometer after immersion of sample
$(P+M_2+S)$ = total wt of pycnometer, residual Hg and immersed sample
$M_1-M_2 = (P+M_1+S) - (P+M_2+S)$ = wt of Hg displaced by sample
$13.546\ S/M_1-M_2$ = density of sample

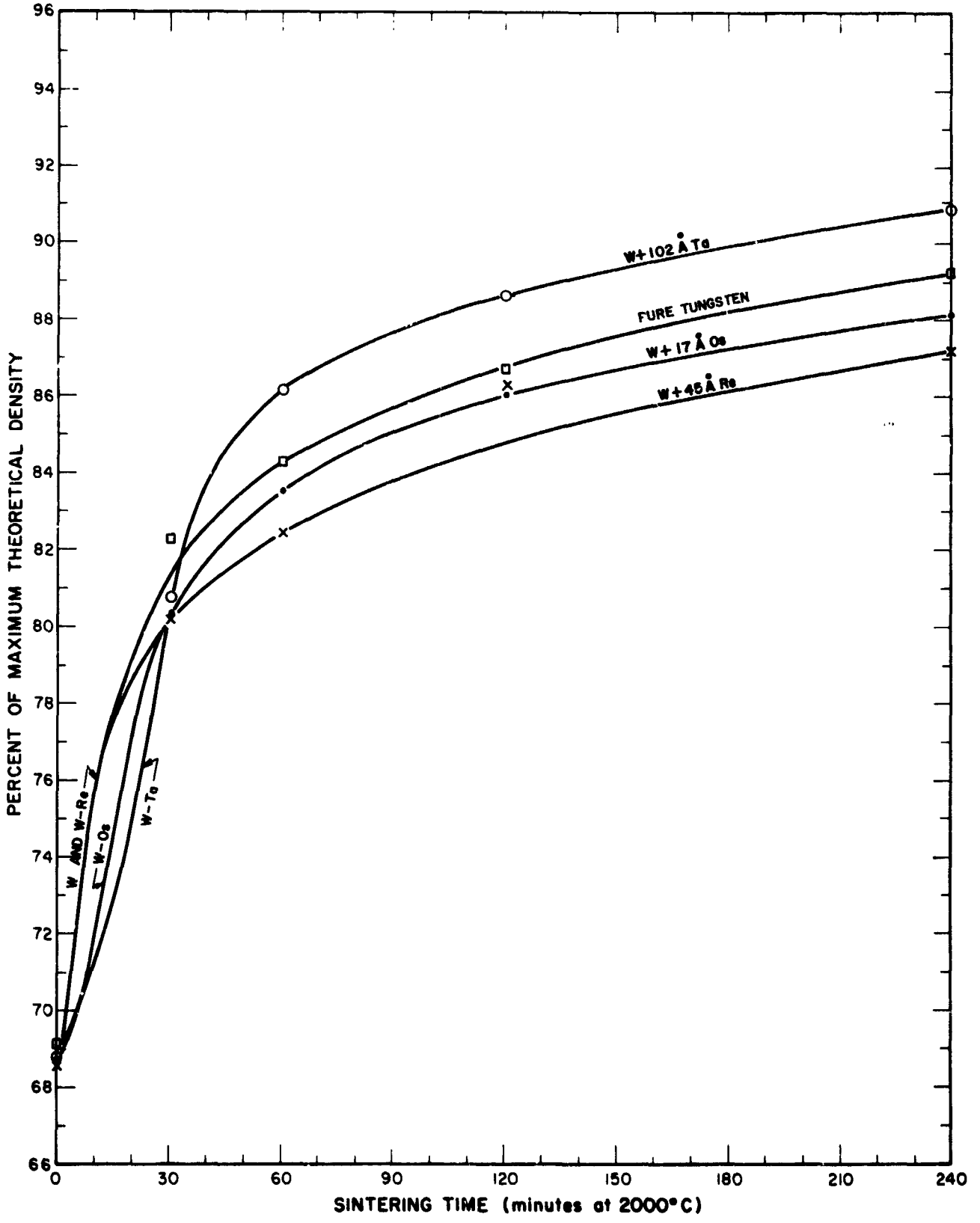

FIG. 4-1 DENSIFICATION RATE CURVES FOR SPHERICAL TUNGSTEN POWDER, VACUUM-DEPOSITION COATED WITH THIN METAL LAYERS (Pressed hydrostatically at 59000 psi, and sintered at 2000°C in 10^{-5} torr range)

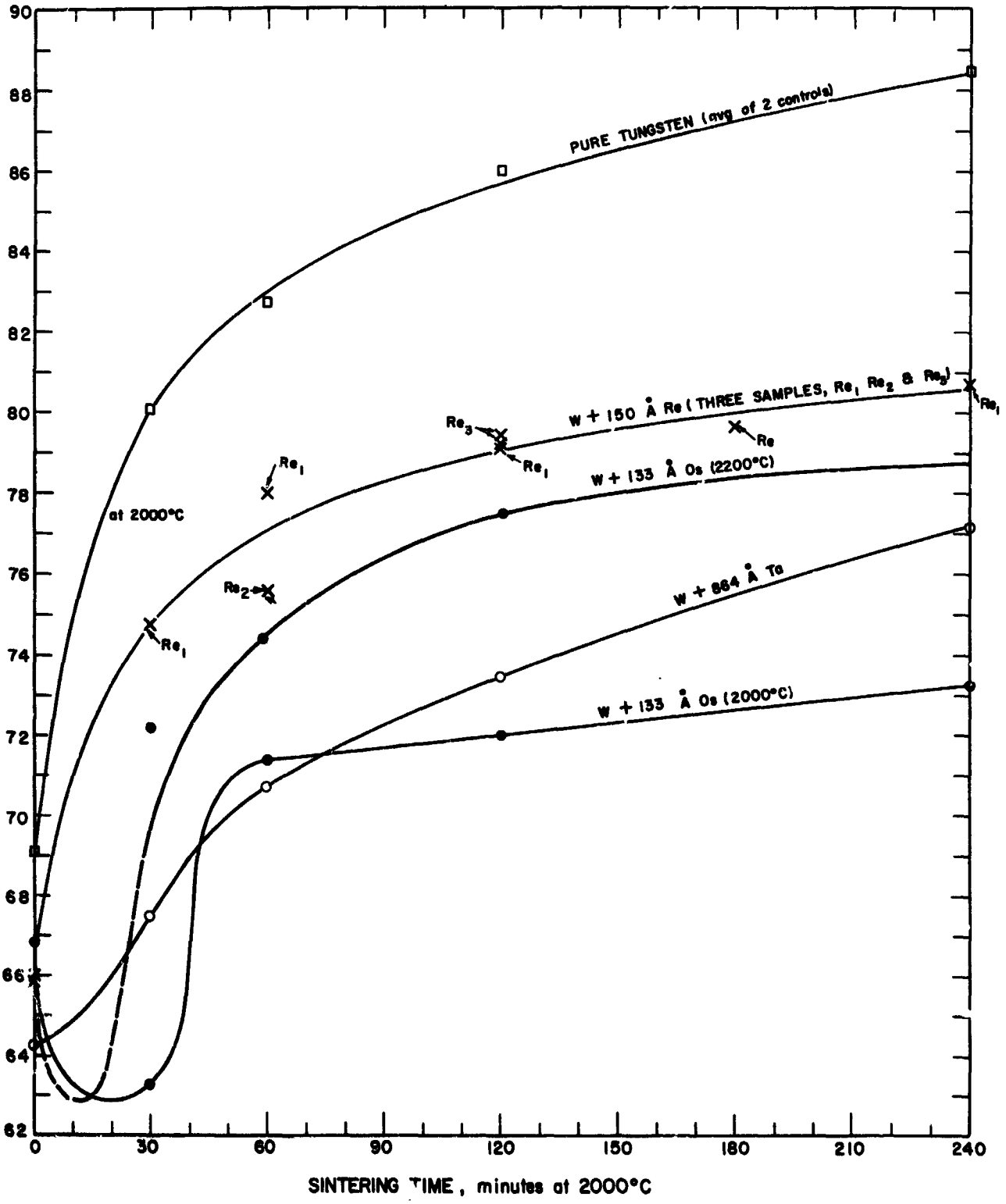

FIG. 4-2 DENSIFICATION RATE CURVES FOR SPHERICAL TUNGSTEN POWDER, VACUUM-DEPOSITION COATED WITH RELATIVELY THICK METAL LAYERS (Pressed hydrostatically at 59000 psi, and sintered at 2000°C in 10^{-5} torr range)

Precoating		Table
102Å	Ta	H
837Å	Ta	I
17Å	Os	J
133Å	Os	K
45Å	Re	J
150Å	Re	L

Density and permeability data of Tables H - L are plotted in Figure 4-3. The following observations are applicable:

1. data points for each button category lie within clearly defined bands;
2. coating with osmium and rhenium effected a shift toward higher permeability, indicating an opening of the pore network (as compared with that of uncoated tungsten);
3. coating with tantalum effected a shift toward lower permeability, indicating restriction of the pore network (again as compared with uncoated tungsten);
4. these effects on permeability indicate that the mechanism of diffusion in sintering may be altered by the coating element.

4.3 Effect of Vapor Precoatings on Pore Volumes

Samples of all precoated ionizer materials were intruded with mercury, principally to determine the volumes of open and occluded pores. The pore volume and mercury intrusion data are listed for both thinly and thickly coated samples in Appendix Tables M and N, respectively. Contrary to expectation, no correlation was found between open pore volume and permeability, as is apparent in the tabulation on the following page.

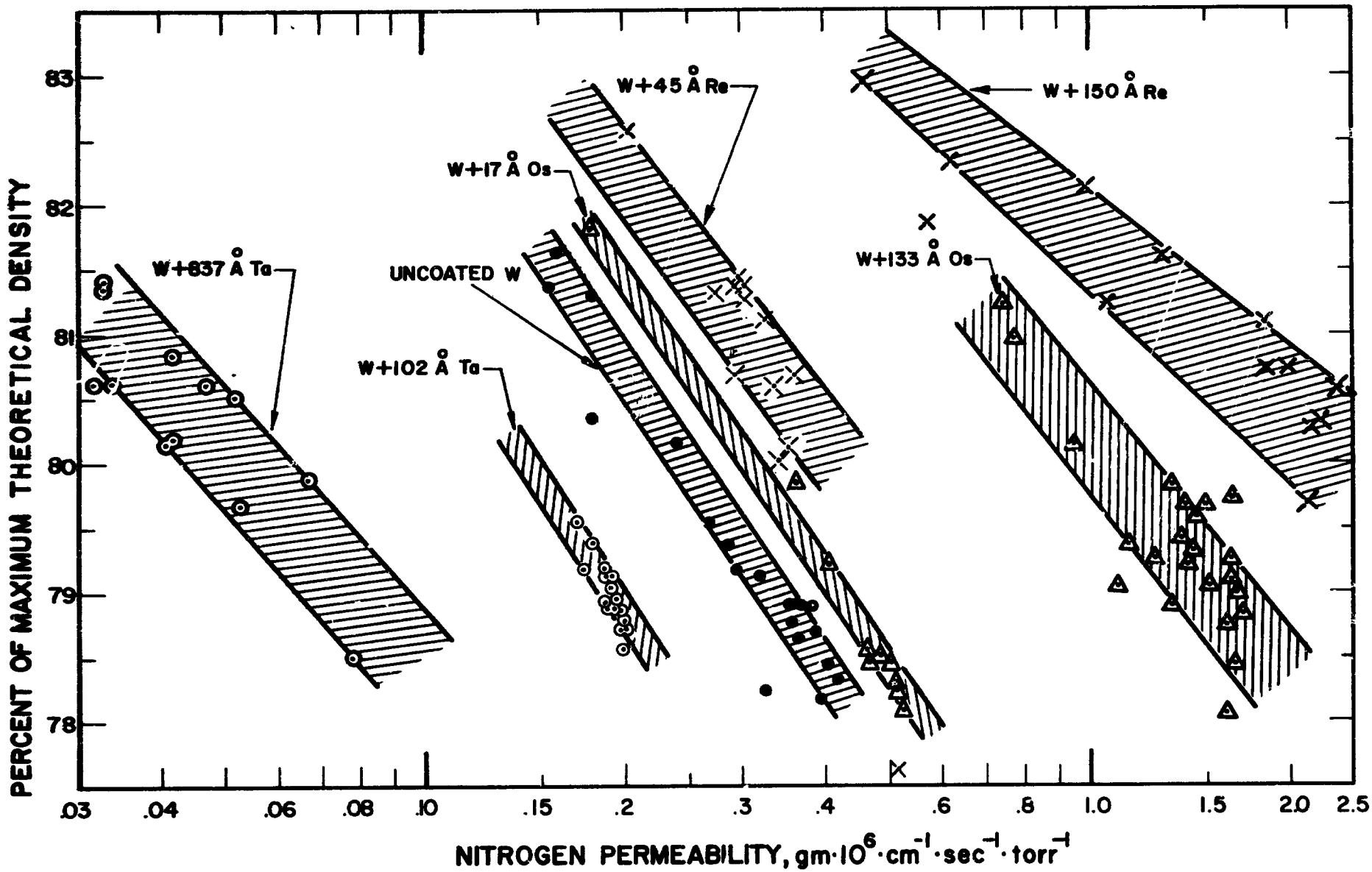

FIG. 4-3 EFFECT OF TANTALUM, OSMIUM, AND RHENIUM COATINGS, VAPOR DEPOSITED ON 1.7-5μ SPHERICAL TUNGSTEN POWDER, ON THE DENSITY-PERMEABILITY RELATIONSHIPS OF SINTERED IONIZER BUTTONS

Vapor Coating	Open Pore Volume, %	N_2 Permeability, μP
150Å Re	14.46	1.51
837Å Ta	15.70	0.05
133Å Os	18.27	1.39
45Å Re	18.94	0.29
102Å Ta	19.20	0.19
None	19.69	0.31
17Å Os	20.73	0.46

4.4 Effect of Vapor Precoatings on Pore Structure

Typical microstructures of all precoated ionizers are compared at a magnification of 400X in Figure 4-4. The more thinly coated compositions are compared at 2000X in Figure 4-5, and the more thickly coated compositions at 1200X in Figure 4-6. Inspection of the photomicrographs verifies that the 150 Å Re and 133 Å Os coatings effected a marked coarsening of grain and pore structures, while the 837 Å Ta coating did not.

Pore count data of Tables 4-III and 4-IV, together with other pertinent data, are summarized in Table 4-V. It may be observed that all three of the more thickly coated powders require greater sintering temperature and/or time to bring them to the desired density range. While this indicates that these coatings increase dimensional stability, their effect on pore stability is not evident. Pore stability must be determined from study of the sintered microstructures, pore densities, and average pore sizes. The pore-density and pore-diameter data, summarized in Table 4-V, indicate that thick coatings of rhenium and osmium yield much coarser pore structures than the thick coating of tantalum. On the other hand, the pore restriction effect of the tantalum coatings (as implied by their low permeabilities) could be unfavorable if subsequent service conditions induce continued sintering. This possibility was investigated in simulated life tests, as discussed in Section 6.

4.5 Correlation of Sintering Mechanisms with Pore Structures

One approach to analyzing the effects of vapor coatings and particle additions on sintering mechanisms is correlation of a diffusion-dependent parameter with a parameter which reflects pore structure. Such corre-

Neg. 1951 Uncoated Tungsten

Compared at 400X Magnification

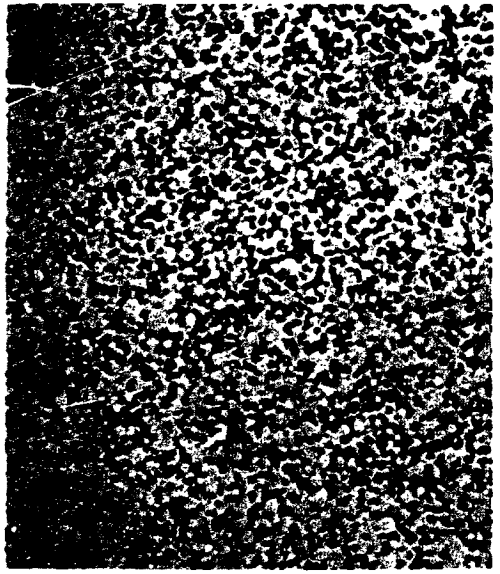

Neg. 2067 W+102Å Ta

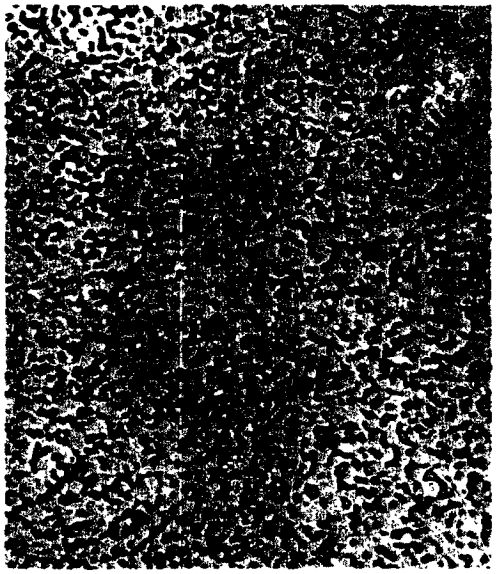

Neg. 2065 W+45Å Re

Neg. 2068 W+17Å Os

Neg. 2104 W+837Å Ta

Neg. 2103 W+150Å Re

Neg. 2101 W+133Å Os

FIG. 4-4 PORE STRUCTURE OF IONIZERS, MADE FROM VAPOR-COATED (1.7-5μ) TUNGSTEN MICROSPHERES, AND SINTERED TO ≈ 80% OF THEORETICAL DENSITY (400X)

Neg. 1989 Uncoated Tungsten

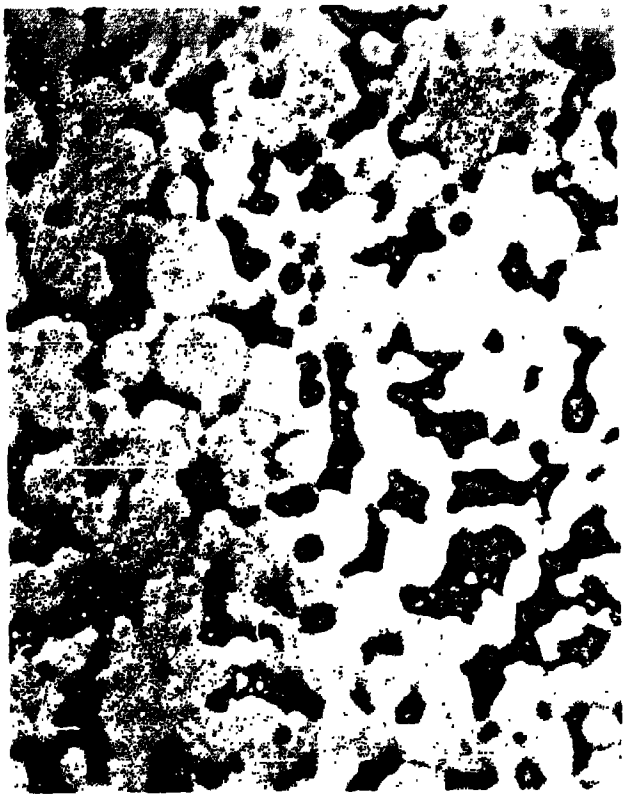

Neg. 2072 W+102Å Ta

Neg. 2076 W+45Å Re

Neg. 2080 W+17Å Os

FIG. 4-5 PORE STRUCTURE OF IONIZERS, MADE FROM VAPOR-COATED (1.7-5μ) TUNGSTEN MICROSPHERES, AND SINTERED TO ≈80% OF THEORETICAL DENSITY (2000X)

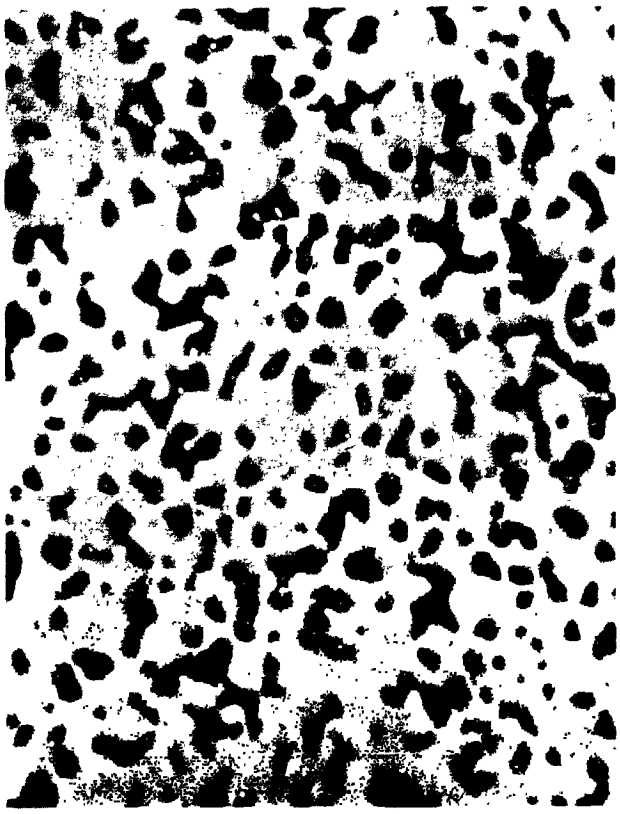

Neg. 2128 Uncoated Tungsten

Neg. 2122 W+837Å Ta

Neg. 2109 W+150Å Re

Neg. 2108 W+133Å Os

FIG. 4-6 PORE STRUCTURE OF IONIZERS, MADE FROM VAPOR-COATED (1.7-5μ) TUNGSTEN MICROSPHERES, AND SINTERED TO ≈80% OF THEORETICAL DENSITY (1200X)

TABLE 4-III

EFFECT OF THIN Ta, Re, AND Os (VAPOR-DEPOSITED) COATINGS ON PORE DENSITY AND AVERAGE PORE DIAMETER OF TUNGSTEN SPHERICAL POWDER IONIZERS

Sample Identity	Sample Density, % of Theor.	Negative No.	Pores Counted at 2000X in 80 cm^2 Half Pores	Whole Pores	Total Pores	Pores/cm^2 at 1X (a)	Vol.% of Open Pores (b)	Av Pore Diam, μ (c)
			Pure Tungsten					
Control	79.22	1986	15	63	70.5			
		1987	14	81	88.0			
		1988	19	72	81.5			
		1989	17	76	84.5			
			Average =		81.1	4.06×10^6	19.69	2.48
			W+ 102Å Ta					
aLTa	78.96	2072	16	107	115.0			
		2073	18	114	123.0			
		2074	13	108	114.5			
		2075	19	123	132.5			
			Average =		121.3	6.07×10^6	19.20	2.01
			W+ 45Å Re					
aLRe	80.47	2076	17	76	84.5			
		2077	17	65	73.5			
		2078	18	73	82.0			
		2079	17	72	80.5			
			Average =		80.1	4.01×10^6	18.94	2.45
			W+ 17 Å Os					
aLOs	78.45	2080	15	49	56.5			
		2081	19	44	53.5			
		2082	13	47	53.5			
		2083	13	50	56.5			
			Average =		55.0	2.75×10^6	20.73	3.10

(a) Pores/cm^2 at 1X mag. = (Total Pores at 2000X)$(2000)^2$/80 cm^2

(b) Vol. % of Open Pores = (100)(Vol. of Hg Intruded) /Vol. of Sample

(c) Av Pore Diam, $\mu = 1128 \sqrt{\frac{(\text{Vol. \% of Open Pores})}{(\text{Pores/cm}^2 \text{ at 1X})}}$

TABLE 4-IV

EFFECT OF THICK Ta, Re, AND Os (VAPOR-DEPOSITED) COATINGS ON PORE DENSITY AND AVERAGE PORE DIAMETER OF TUNGSTEN SPHERICAL POWDER IONIZERS

Sample Identity	Density, % of Theor.	Negative No.	Pores Counted at Mag. in 80 cm^2 Half Pores	Whole Pores	Total Pores	Pores/cm^2 at 1 X (a)	Vol.% of Open Pores (b)	Av Pore Diam, μ (c)
		*		Pure Tungsten				
Control	79.22	1986	15	63	70.5			
		1987	14	81	88.0			
		1988	19	72	81.5			
		1989	17	76	84.5			
			Average =		81.1	4.06×10^6	19.69	2.48
		*		W+837 Å Ta				
bLTa	81.24	2117	8	62	66.0			
		2118	13	58	64.5			
		2119	13	53	59.5			
		2120	10	62	67.0			
			Average =		64.3	3.22×10^6	15.70	2.49
		**		W+150 Å Re				
bLRe	82.33	2109	15	29	36.5			
		2110	13	34	40.5			
		2111	13	25	31.5			
		2112	10	33	38.0			
			Average =		36.6	0.66×10^6	14.46	5.28
		**		W+133 Å Os				
bLOs	80.65	2105	10	26	31.0			
		2106	15	28	35.5			
		2107	13	23	29.5			
		2108	14	28	35.0			
			Average =		32.8	0.59×10^6	18.27	6.28

* (2000X) ** (1200X)

(a) Pores/cm^2 at 1X = (Total pores at Mag.)(Mag.)^2/80 cm^2

(b) Vol. % of Open Pores = (100)(Vol. of Hg Intruded)/Vol. of Sample

(c) Av Pore Diam, $\mu = 1128 \sqrt{\frac{(\text{Vol. \% of Open Pores})}{(\text{Pores/cm}^2 \text{ at 1X})}}$

TABLE 4-V

FABRICATION PARAMETERS AND PROPERTIES OF IONIZERS, MADE FROM VAPOR-PRECOATED (1.7-5μ) TUNGSTEN MICROSPHERES (a)

Composition, Atom %	Pure Tungsten	W + 1.53 Ta	W + 11.82 Ta	W + 0.85 Re	W + 2.77 Re	W + 0.34 Os	W + 2.57 Os
Equiv. Coating Thickness (b), Å	None	102	837	45	150	17	133
Sintering Conditions (10^{-5} torr range)	2000°C,30 min	1800°C,45 min	2100°C,145 min	1800°C,45 min 1900°C,70 min	2000°C,120 min	1800°C,45 min 1900°C,85 min	2200°C,210 min
(c) Density, % of max. theoretical	79.22	78.96	81.24	80.47	82.33	78.45	80.65
(c) Total Pore Vol.,% of sample vol.	20.78	21.04	18.76	19.53	17.67	21.55	19.35
(c) Open Pore Vol.,% of sample vol.	19.69	19.20	15.70	18.94	14.46	20.73	18.27
(c) Occluded Pore Vol.,% of sample vol.	1.09	1.84	3.06	0.59	3.21	0.82	1.08
(d) Avg. N_2 Permeability, μP (e)	0.31	0.19	0.05	0.29	1.50	0.46	1.39
(d) for Avg. Den.,% of max. theor.	79.38	78.97	80.35	81.31	81.19	78.77	79.36
Avg. Pore Density, pores/cm^2	4.06×10^6	6.07×10^6	3.22×10^6	4.01×10^6	0.66×10^6	2.75×10^6	0.59×10^6
Avg. Pore Diameter, μ	2.48	2.01	2.49	2.45	5.28	3.10	6.28

(a) Spherical tungsten powder from Lot L, with 92% by number of particles in the 1.7-5μ range and average particle diameter of 3.23μ

(b) Equiv. Coating Thickness = $(d_b/2)\left[\frac{(W/c \cdot \rho_b - W/c \cdot \rho_c + 100\rho_c)}{\rho_c\,(100-W/c)} - 1\right]^{1/3}$, where d_b = dia. of base microsphere having average surface area,
W/c = Wt. % of coating element applied,
ρ_b and ρ_c = densities of tung. and coating element, respectively

(c) Determined on porosimeter samples ≈ 3/4" long x 3/16" dia.

(d) Avg. values determined for 12-23 ionizer buttons, 3/16" dia. x 0.04" thick

(e) μP unit = $gm \cdot 10^{-6} \cdot cm^{-1} \cdot sec^{-1} \cdot torr^{-1}$

lation can be obtained from a plot of instantaneous densification rate vs permeability, both data obtained at the same density level. The curves in Figure 4-7 show rate of densification ($\Delta\%$/min) as a function of nitrogen permeability, both parameters having been determined at 78% of maximum theoretical density.

Data points for vapor-coated samples to the right of the tungsten control point in Figure 4-7 indicate pore networks which are more permeable than that of pure tungsten. Metallographic examination showed that these structures had larger grains and larger pore sizes than that of pure tungsten. This indicates that sintering occurred predominantly by transgranular diffusion. Conversely, data points for vapor-coated samples to the left of the tungsten-control point in Figure 4-7 indicate pore networks which are less permeable (or more restricted) than that of pure tungsten. Since restriction of pore networks is probably the result of interparticle bridging and closure of the narrow-necks between pore spaces, it is reasoned that, here, sintering occurred predominantly by grain boundary diffusion. Therefore, the data indicates that rhenium and osmium coatings promote transgranular diffusion and grain growth, while tantalum coatings increase the threshold temperature of transgranular diffusion, such that sintering at 2000°C is predominantly by grain boundary diffusion. In this way, tantalum behaves as a true grain-growth inhibitor.

Based on the preceding analysis, and on the intermediate position of the tantalum-particle points in Figure 4-7, it appears that, when mixtures of tungsten and tantalum particles are sintered at 2000°C, two diffusion mechanisms obtain:

1. early absorption of tantalum particles into adjacent tungsten particles, forming localized regions rich in tantalum;
2. subsequent diffusion within tantalum-rich areas by the grain boundary mechanism, and within tantalum-deficient areas by the transgranular mechanism;
3. restriction of pore necks by bridging within tantalum-rich areas and opening of pore necks within tantalum-

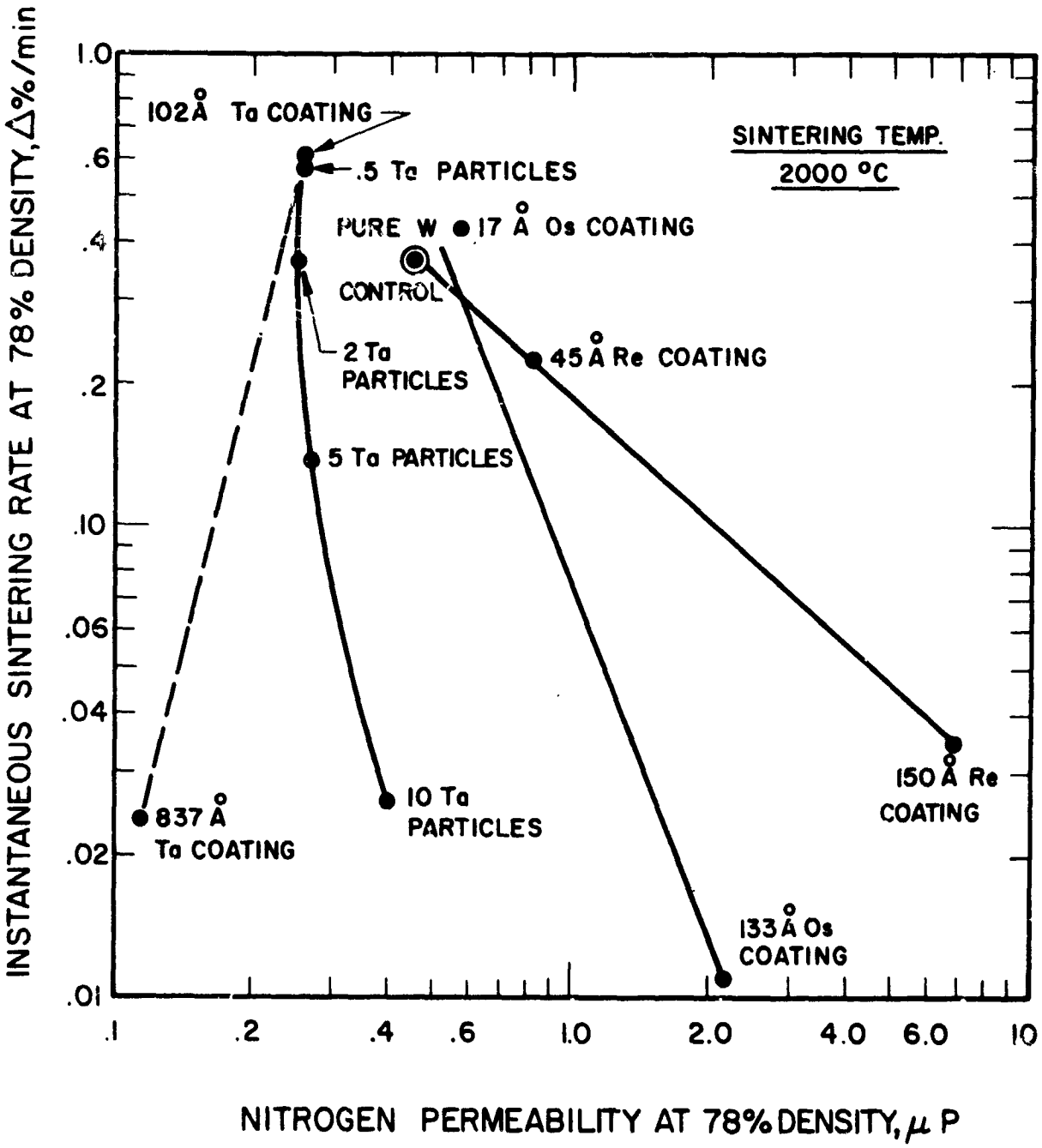

FIG. 4-7 RATE OF DENSITY CHANGE VS NITROGEN PERMEABILITY FOR VARIOUS IONIZER COMPOSITIONS

deficient areas, with the result that bulk permeability is not seriously altered.

In contrast to such heterogeneous diffusion, when tungsten is uniformly coated with sufficient tantalum, sintering at 2000°C occurs homogeneously throughout by grain boundary diffusion, with attendant bridging, closure of pore neck, and reduced permeability.

5. IONIZERS FROM TUNGSTEN MICROSPHERES, WITH ADDITIONS MADE BY HYDROGEN REDUCTION

Addition of secondary elements to tungsten powder by reduction methods offered potential advantages over addition of discrete metallic particles and over precoating by vacuum deposition. While the addition of discrete metal particles is a simple and reproducible method, it can lead to a decrease in uniformity of ionizer pore size, as shown in Section 3. On the other hand, production of composite particles by vacuum deposition of secondary elements on tungsten is a very inefficient and expensive process, since only a small percentage of the metal vapor impinges on the tungsten base particles In addition, vapor coatings of predictable thickness are difficult to achieve, as indicated in Section 4. Therefore, with the objectives of improving uniformity of additive dispersion and ionizer quality, without resort to vapor plating, the reduction method was tried.

5.1 Additions of 0.1A/oRe and 5A/oTa

Tungsten microspheres with diameters predominantly in the 4-8μ range (Lot E7A, described in Ref. 2) were used as the powder base and treated as follows:

1. Superficial oxidation at 400°C for 60 minutes in air, to roughen surfaces;*
2. Division into four equal portions, two of which were set aside for control samples;
3. Inoculation of one portion with 0.1A/oRe by addition of aqueous NH_4ReO_4 solution, and a second portion with 5A/oTa by mixing intimately (in agate mortar as a slurry) with equivalent Ta_2O_5 plus distilled H_2O;

*Oxidation conditions vary with the specific surface area of the powder sample. Powders of increasing particle diameter require progressively increasing temperatures or times for oxidation. Oxidation of the powder sample was halted at the point that a straw colored oxide film first became visible.

4. Simultaneous reduction* of both the control and inoculated powders at 1000°C for 60 minutes in H_2 atmosphere, and hydrostatic compaction at 59,000 psi;
5. Sintering at 2200°C for 60 minutes in two runs, with an untreated control sample included in each run.

Sintered density of the W-5A/oTa sample was only 70.6% (as compared with 82.4% for its tungsten control), indicating appreciable retardation of densification. Sintered structures of both samples are shown in Fig. 5-1. It is apparent that the addition of 5A/oTa as Ta_2O_5 induced serious nonuniformity of pore size. Structure of the W-5A/oTa, after an additional hour at 2200°C, is shown in Fig. 5-2. Additional agglomeration of solid phase and increased pore occlusion are evidenced.

The sintered density of the W-0.1A/oRe sample was 86.4%. The validity of this high value is questionable, since the density of the companion tungsten sample was also extremely high. Further, a significant comparison of the W-5A/oTa and the W-0.1A/oRe structures cannot be made since the latter could not be infiltrated.

5.2 Addition of 4.94A/oRe

Tungsten microspheres with diameters predominately in the 1.7-5μ range (Lot L, described in Section 2) were used as the powder base and treated as follows:

1. Superficial oxidation at 232°C for 30 minutes in air, to roughen surfaces;
2. Division into two equal portions, one of which was set aside for a control sample;
3. Inoculation of the other with 4.94A/oRe by mixing intimately (in agate mortar as a slurry) with equivalent NH_4ReO_4 plus distilled H_2O;
4. Simultaneous reduction of both the control and inoculated powders at 980°C for 10 minutes in H_2 atmosphere, hydrostatic compaction at 60,000 psi, and vacuum sintering at 2200°C for 60 minutes.

*Subsequent experiment indicated that Ta_2O_5 per se is hot reduced by H_2. All reference to such reduction is therefore to be considered in light of this experiment.

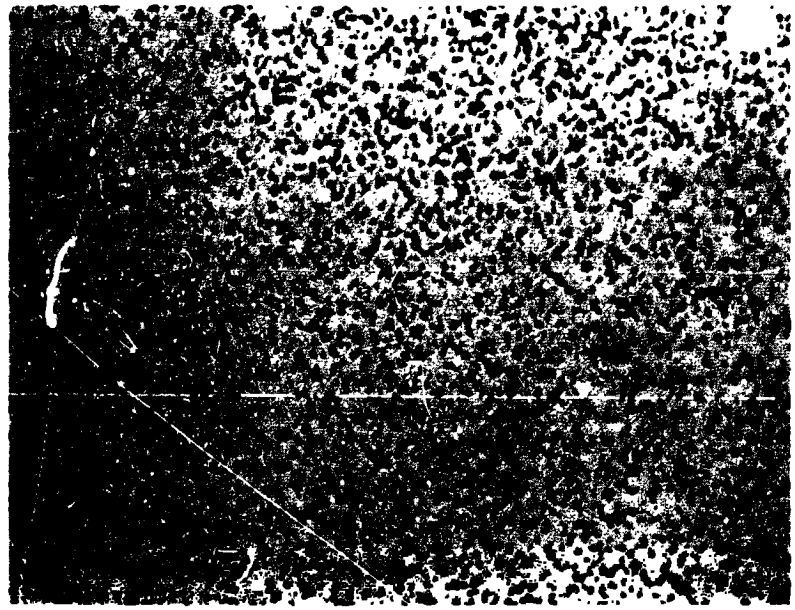

Neg. 1721 Tungsten Control

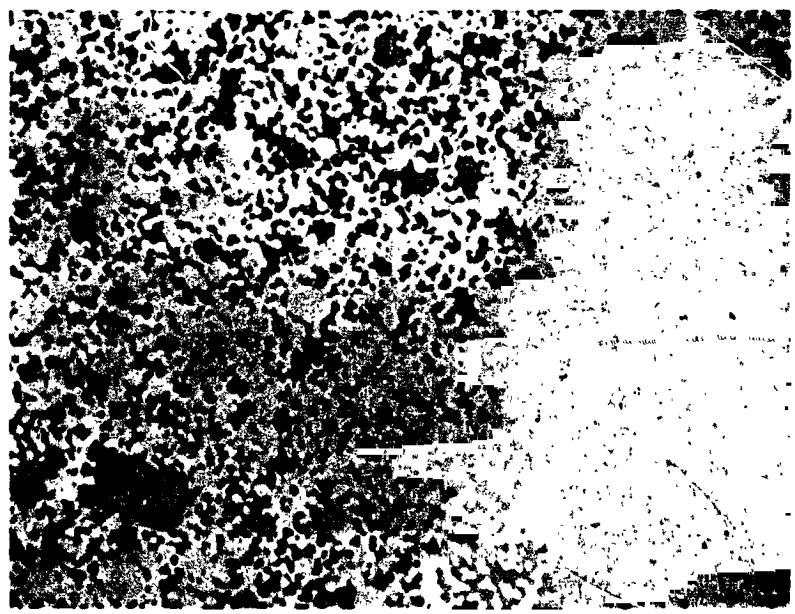

Neg. 1688 W-5A/oTa

FIG. 5-1 COMPARISON OF TUNGSTEN AND W-5A/oTa STRUCTURES AFTER VACUUM SINTERING AT 2200°C FOR 1 HOUR (200X)

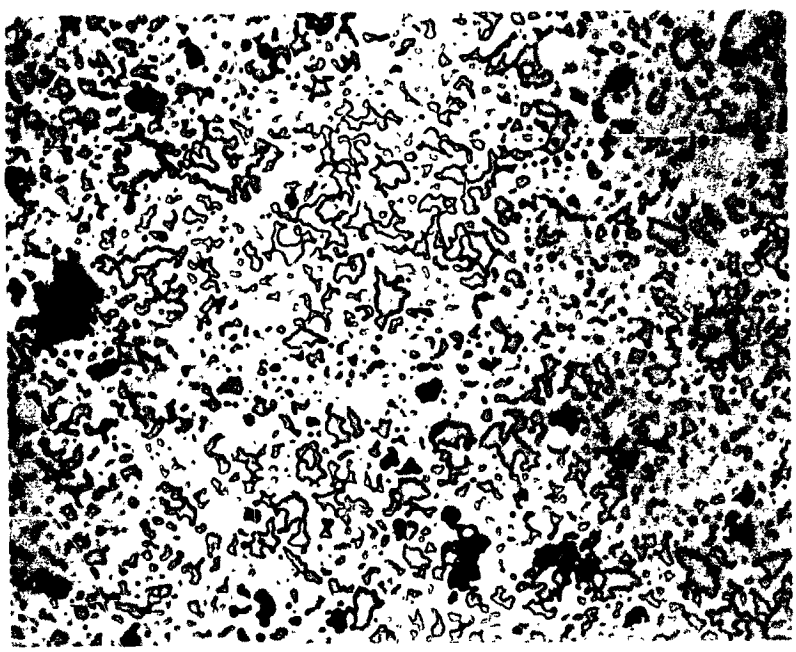

Neg. 1720 W-5A/oTa

FIG. 5-2 STRUCTURE OF W-5A/oTa SAMPLE OF FIG. 5-1 AFTER 1 ADDITIONAL HOUR OF SINTERING AT 2200°C (200X)

Sintered density of the W-4.94A/oRe sample was 87.5% (as compared with 90.2% for its tungsten control). Thus, even at the high sintering temperature of 2200°C, the rhenium addition retarded densification.

Infiltration attempts with Cu-2%Fe were unsuccessful, probably due to the high density of the samples and the occlusion of the pores. Examination of the photomicrographs of Fig. 5-3 shows that the W-4.94A/oRe structure contains fewer pores per unit area than does the tungsten control sample. However, it is difficult to draw very definite conclusions from these noninfiltrated structures.

5.3 Additions of 5A/oRe and 7A/oTa

Tungsten microspheres with diameters predominately in the 1.7-5μ range (Lot L) were used as the base powder and treated as follows:

1. Superficial oxidation at 260°C for 45 minutes in air, to roughen surfaces;
2. Division into two equal portions;
3. Inoculation of one portion with 5A/oRe by mixing intimately (in agate mortar as a slurry) with equivalent NH_4ReO_4 plus distilled H_2O, and the other portion with 7A/oTa by dry mixing (in agate mortar) with equivalent Ta_2O_5;
4. Simultaneous reduction of the inoculated powders at 1200°C for 90 minutes in H_2 atmosphere, hydrostatic compaction at 60,000 psi, and vacuum sintering at 2000°C for 60 minutes;
5. Infiltration of sintered compacts, machining into buttons, and vacuum distillation for subsequent evaluation.

Permeability, pore-volume, and pore-structure parameters are listed in Appendix Tables O, P and Q, respectively, with the most pertinent values summarized in Table 5-I.

Addition of 7A/oTa by chemical reduction greatly reduced both densification rate and final permeability. As previously noted, similar effects were produced by precoating with 837 Å Ta. Also, both

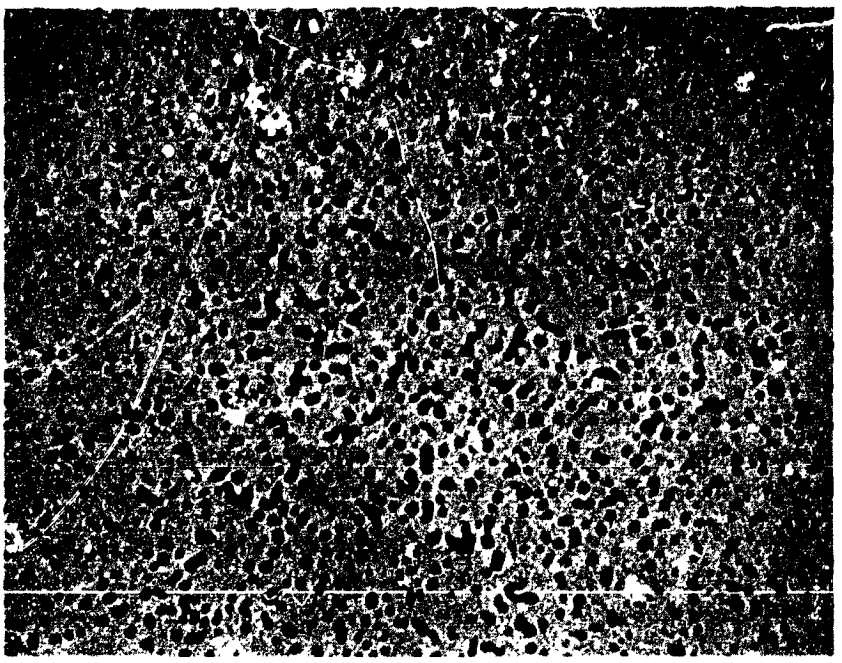

Neg. 1762 Tungsten Control

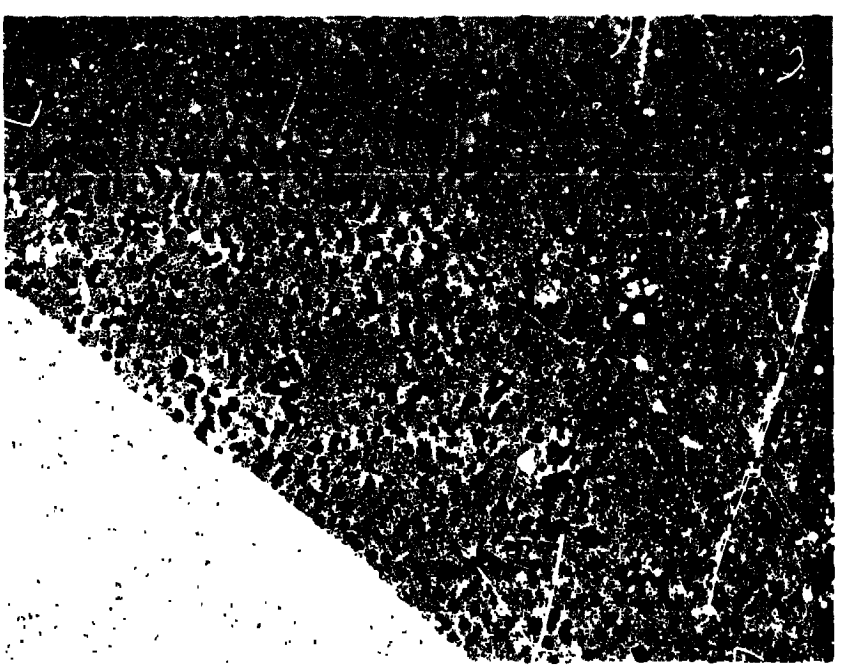

W-4.94A/oRe

-4.94A/oRe
NG AT

TABLE 5-I

PROPERTIES OF W-7A/oTa AND W-5A/oRe,

PREPARED BY CHEMICAL REDUCTION, COMPARED WITH

THOSE OF PURE TUNGSTEN

Composition,[a] atom %		Pure Tungsten	W-7Ta	W-5Re
Sintering Conditions[b]		2000°C,30 min	2000°C,60 min	2000°C,60 min
(c)	Density,% of max. theor.	79.22	77.76	81.69
	Tot.Pore Vol.,%of sample vol.	20.78	22.24	18.31
	Open Pore Vol.,%of sample vol.	19.69	17.08	16.59
	Occluded Pore Vol.,% of sample vol.	1.09	5.16	1.72
(d)	Av N_2 Permeability μP	0.31	0.09	0.28
	for av Den.,%of max.theor.	79.38	76.50	80.61
Av Pore Density, pores/cm^2		4.06×10^6	2.66×10^6	2.90×10^6
Av Pore Diameter, μ		2.48	2.86	2.70

(a) Lot L spherical powder base, with 92% by number of particles in 1.7-5μ range and average diameter of 3.23μ

(b) Sintered in 10^{-5} torr range

(c) Determined on porosimeter samples ≈ 3/4" long x 3/16" diameter

(d) Average values for ionizer buttons, 3/16" dia x 0.04" thick

the hydrogen-reduction and the vapor-plating methods yielded very nonuniform pore sizes with no increase in pore density. Thus, addition of tantalum as fine metallic particles yields ionizer structures superior to those made by the reduction and vapor-plating processes. Addition of 5A/oRe by hydrogen reduction had little effect on densification rate at 2000°C or on final permeability. However, its pore density of 2.90×10^6 pores/cm^2 was much higher than the 0.66×10^6 pores/cm^2 determined for the 2.77A/o (150Å) Re precoating, but lower than the 4.06×10^6 pores/cm^2 established for pure tungsten.

Typical pore structures of the W-7A/oTa and the W-5A/oRe compositions are shown in Fig. 5-4 at magnifications of 400X and 2000X. Pore size of the W-7A/oTa structure is at least as nonuniform as those of W-10Ta alloys made with tantalum particle additions. On the other hand, pore size of the W-5A/oRe structure is relatively uniform. Since suitably fine rhenium powder is not commercially available for discrete particle additions, and since vapor precoating with rhenium has proven unfeasible, the hydrogen-reduction method of rhenium addition remains promising and should be investigated further.

5.4 Addition of Rhenium and Osmium by Impregnation of Presintered Tungsten

Adding secondary elements by impregnation of presintered tungsten is not a reduction method. However, since it is experimental in nature, it is within the context of this report section.

Attempts were made to add rhenium and osmium by:

1. Superficial oxidation and hydrogen-reduction of the internal surfaces of presintered buttons, produced from 2-5μ powder, to roughen these surfaces. Buttons for infiltration with Re and Os were oxidized by heating to 450°C for 20 minutes in open air. The oxidized surface was subsequently reduced by heating in hydrogen for 30 minutes at 1000°C. Average pore diameter of buttons was 2.48μ. Average density was 79% of maximum theoretical.

Neg. 2176 400X

Neg. 2187 2000X

W+7 A/o Ta

Neg. 2178 400X

Neg. 2190 2000X

W+5 A/o Re

FIG. 5-4 PORE STRUCTURES OF IONIZERS, MADE FROM CHEMICALLY COATED SPHERICAL TUNGSTEN POWDER (Sintered at 2000°C for 1 hour)

2. Impregnation of the buttons with rhenium by immersion in a colloidal rhenium suspension, and osmium by immersion in Cu - 8.2 W/o Os alloy (1150°C for 30 minutes) with subsequent distillation of the copper. The Cu-Os alloy was designed to give an osmium addition equal to 1% of the button weight.
3. Resintering under vacuum.

Briefly, the weights of the buttons before impregnation were essentially the same after resintering, indicating that neither additive was retained. Therefore, no further experiments using this method were conducted.

6. ACCELERATED LIFE TESTING OF SELECTED IONIZER COMPOSITIONS

The objective of this phase of the program was to determine the useful life of the better ionizer compositions. It was desired, specifically, to learn how long the experimental materials could be heated (in the 1,100-1,300°C range) before their pore networks became so restricted through diffusion that their performance was limited. In order to perform life testing in a feasible length of time, it was necessary to accelerate diffusion by heating at higher temperatures (1,600°C and 1,800°C) and to extrapolate the data thus derived to the relatively low range of engine operation (1,100 to 1,300°C). An upper test-temperature limit of 1,800°C was decided upon, since it is reasonably certain that sintering at 1,800°C (and below) occurs by grain-boundary (or surface) diffusion. On the other hand, testing at 2,200°C, as initially specified, could induce transgranular diffusion. Thus, testing at 1,800°C and 2,200°C could result in a predominance of one diffusion mode at 1,800°C and another at 2,200°C. This would invalidate straight-line extrapolations of rate change data.

6.1 Selection of Compositions for Life Testing

Selections for life testing were limited to those compositions having retarded densification rates, as well as pore densities (after sintering) of greater than 2.6×10^6 pores/cm^2. Compositions recommended by EOS, and approved by NASA, are as follows:

Composition	Fabricated Under Phase
W-5A/oTa (1-3μ particles)	I
W-5A/oTa (1-5μ particles)	I
W-10A/oTa (1-3μ particles)	I

Composition	Fabricated Under Phase
W-10A/oTa (1-5μ particles)	I
W+102ÅTa (vapor precoating)	II
W+45ÅRe (vapor precoating)	II
W-7A/oTa (reduction)	III
W-5A/oRe (reduction)	III

6.2 Change of Density and Permeability with Heating Time at 1,600°C and 1,800°C

Ionizer buttons of the compositions listed above were heated at 1,600°C and 1,800°C under pressures in the 10^{-5} torr range. The density and N_2 permeability of each of the 32 buttons tested were determined after 0, 1, 2, 4, 6, and 8 hours of heating at 1,600°C, and after 0, 1, 2, 4 and 6 hours at 1,800°C. These data are listed in Table 6-I, where each density and permeability value (except for the 5A/oRe and 7A/oTa compositions) is the average for two buttons. Density data of Table 6-I are plotted in Fig. 6-1. It is interesting to note that densities of the 10A/oTa (particle) compositions decrease slightly at 1,600°C. Based on the slopes of the Fig. 6-1 curves, rates of densification were highest for tungsten and lowest for W-10A/oTa. The compositions are listed below in order of increasing dimensional stability:

Pure W
1.53A/oTa (vapor precoating)
0.85A/oRe (vapor precoating)
5A/oRe (reduction)
5A/oTa (1-5μ particles)
7A/oTa (reduction)
5A/oTa (1-3μ particles)
10A/oTa (particles)

Permeability data of Table 6-I are plotted in Fig. 6-2. Based on the slopes of the Fig. 6-2 curves, rates of permeability

TABLE 6-I

LIFETIME TEST DATA FOR SELECTED IONIZERS [a], SHOWING EFFECT OF HEATING [b] ON DENSITY AND NITROGEN PERMEABILITY

Ionizer Composition, atom %	Form or Method of Addition		1600°C, Hours at Temperature 0	1	2	4	6	8	Total Change, % increase or decrease	1800°C, Hours at Temperature 0	1	2	4	6	Total Change, % increase or decrease
Tungsten (control)		Density [c] →	79.33	79.67	79.95	80.65	81.43	82.31	2.98 inc.	79.28	81.82	83.45	86.03	87.60	8.32 inc.
		Perm. [d] →	.303	.262	.264	.227	.196	.159	47.52 dec.	.299	.199	.126	.038	<.021	92.98 dec.
W-5 Ta	1-3μ Ta particles	Density	79.45	79.45	79.66	79.63	79.61	79.76	0.31 inc.	79.45	80.05	80.83	81.59	82.24	2.79 inc.
		Perm.	.204	.190	.206	.202	.199	.202	0.98 dec.	.201	.190	.167	.132	.112	44.28 dec.
W-5 Ta	1-5μ Ta particles	Density	78.43	78.41	78.48	78.61	78.64	78.83	0.40 inc.	78.48	79.01	79.63	80.36	81.09	2.61 inc.
		Perm.	.206	.189	.205	.200	.197	.193	6.31 dec.	.205	.192	.173	.133	.116	43.41 dec.
W-10 Ta	1-3μ Ta particles	Density	81.35	81.11	81.32	81.22	81.24	81.16	0.19 dec.	81.35	81.30	81.37	81.56	81.85	0.50 inc.
		Perm.	.196	.191	.206	.203	.207	.198	1.02 inc.	.173	.202	.187	.166	.159	8.09 dec.
W-10 Ta	1-5μ Ta particles	Density	79.01	78.64	78.78	78.80	78.85	78.80	0.21 dec.	79.09	78.98	79.06	79.14	79.30	0.21 inc.
		Perm.	.195	.199	.216	.213	.210	.209	7.18 inc.	.195	.200	.208	.182	.168	13.65 dec.
W+1.52 Ta	Ta Vapor precoating	Density	78.84	79.08	79.57	80.01	80.58	80.84	2.00 inc.	78.87	81.44	83.16	85.18	86.94	8.07 inc.
		Perm.	.199	.177	.180	.163	.148	.148	25.63 dec.	.200	.140	.103	.039	<.021	>89.50 dec.
W+0.85 Re	Re Vapor precoating	Density	80.68	80.81	81.07	81.93	82.06	82.19	1.51 inc.	80.84	82.24	83.66	85.68	87.13	6.29 inc.
		Perm.	.337	.292	.301	.280	.241	.225	33.23 dec.	.340	.213	.189	.073	.029	91.47 dec.
W+5 Re	Oxidation -reduction	Density [e]	80.20	80.14	80.92	81.07	81.23	81.74	1.54 inc.	80.97	81.35	82.83	84.27	85.30	4.33 inc.
		Perm. [e]	.281	.204	.211	.200	.191	.183	34.88 dec.	.340	206	.133	.093	.044	87.06 dec.
W+7 Ta	Oxidation -reduction	Density [e]	76.50	76.61	76.92	77.08	77.18	77.29	0.79 inc.	76.50	76.98	77.60	78.02	78.70	2.20 inc.
		Perm. [e]	.069	.044	.050	.048	.045	.043	37.68 dec.	.075	.061	.049	.024	<.020	>73.33 dec.

(a) Ionizers of button size ≈ 0.187" dia. x 0.04" thick.

(b) Heating performed in 10^{-5} torr range

(c) Density expressed as % of max. theoretical

(d) Units of permeability are 10^{-6} $g \cdot cm^{-1} \cdot sec^{-1} \cdot torr^{-1}$

(e) Data on single buttons (All other values are averages of data on two buttons.)

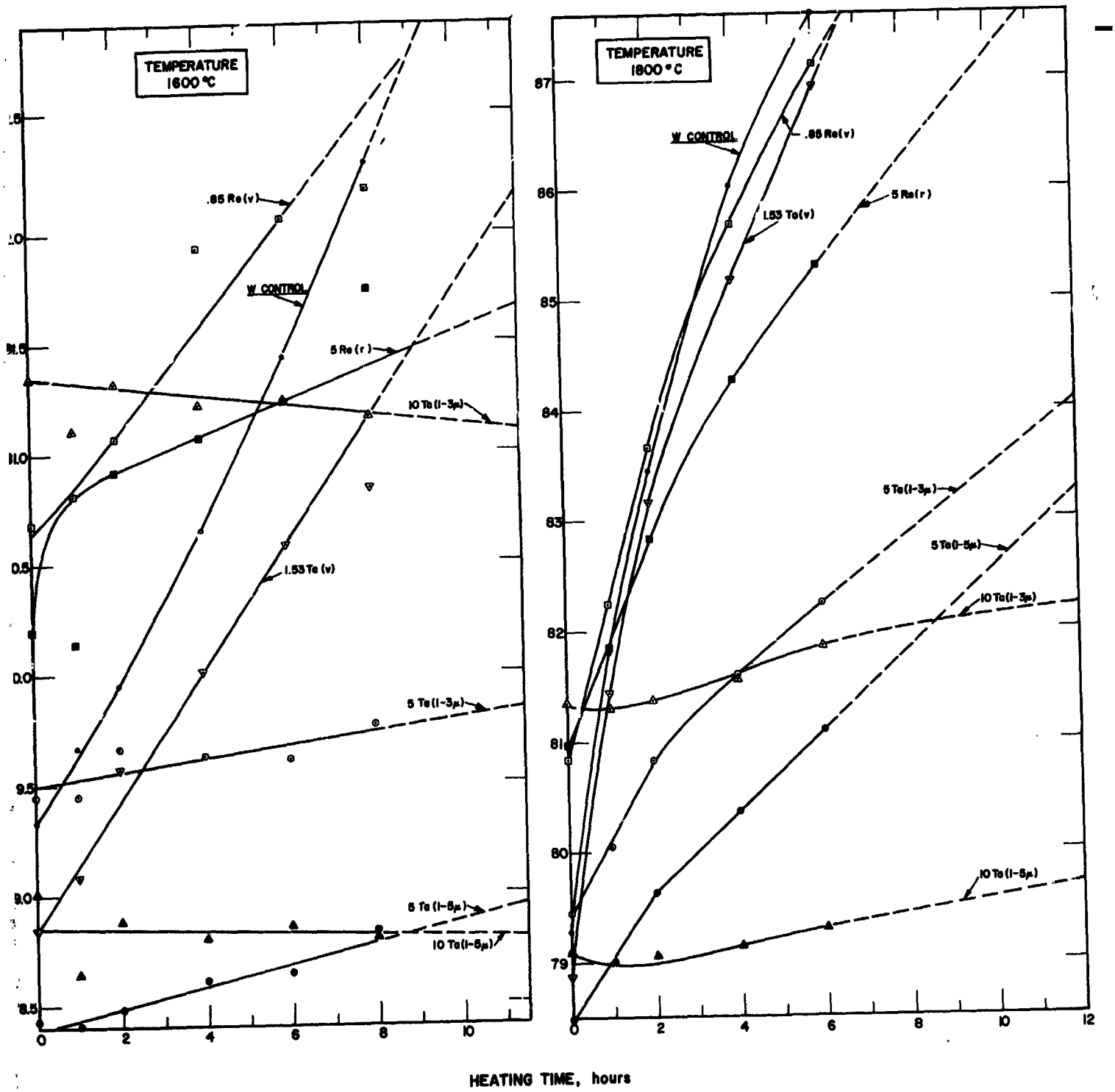

FIG. 6-1 EFFECT OF HEATING TIME AT 1600°C AND 1800°C ON DENSITY OF SELECTED IONIZER COMPOSITIONS (Heated in 10^{-5} torr range)

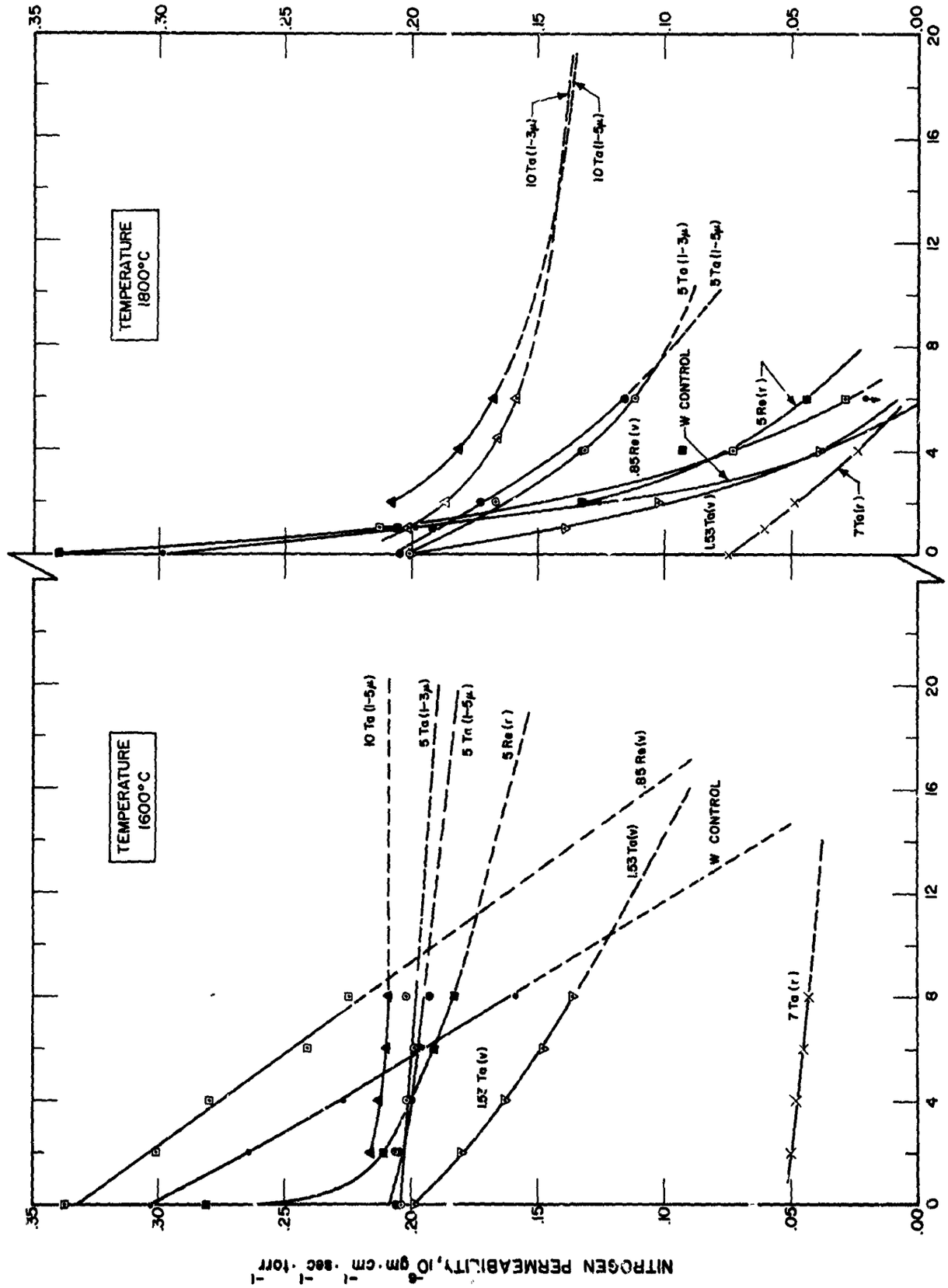

FIG. 6-2 EFFECT OF HEATING TIME AT 1600°C AND 1800°C ON NITROGEN PERMEABILITY OF SELECTED

change were also highest for tungsten and lowest for W-10A/oTa. The compositions are listed below in order of increasing structural stability:

Pure W
0.85A/oRe (vapor precoating)
1.53A/oTa (vapor precoating)
5A/oRe (reduction)
5A/oTa (1-5μ particles)
7A/oTa (reduction)
5A/oTa (1-3μ particles)
10A/oTa (particles)

Since the preceding lists are in general agreement, it may be concluded that compositions which increased most rapidly in density, simultaneously decreased most rapidly in permeability.

Extrapolation of the curves of Fig. 6-2 indicates that the compositions would reach a permeability level of 0.05 μP (the value that was taken to represent the end of useful life) in the following times:

Ionizer Composition, A/o[a]	Heating Time to Reach 0.05 μP 1,600°C	1,800°C
7 Ta (r)	2.0 hrs	1.9 hrs
W (control)	14.7	3.5
0.85 Re (v)	19.9	5.0
1.53 Ta (v)	24.0	3.5
5 Re (r)	57.4	5.6
5 Ta (1-5μ)	13.9	13.9
5 Ta (1-3μ)	215	18.5
10 Ta (1-5μ)	ind.[b]	83.8
10 Ta (1-3μ)	ind.	90.0

(a) Postscripts (r) and (v) indicate additions by reduction and vapor precoating, respectively

(b) Indeterminate, due to shallow slopes of "K vs t" curves

If selection of the most stable composition was based solely on the preceding tabulated data, the choice would undoubtedly be W-10A/oTa (1-3μ particles).

6.3 Determination of Useful Ionizer Lifetime

Since mass permeability coefficient K (in $gm \cdot cm^{-1} \cdot sec^{-1} \cdot torr^{-1}$) is related to specific permeability K_S (in cm^2) by a constant*, rate of permeability change may be expressed in the physical dimensions l^2/t. In order to determine the useful lifetime of an ionizer (at service temperatures of 1,100-1,300°C) from the 1,600°C and 1,800°C data, it is necessary to know the temperature dependence of the rate dK_S/dt. The temperature dependence of diffusion rate is given, in general, by the form $D = D_o e^{-Q/RT}$, where D_c, Q and R are constants. Thus, plots of log D versus 1/T yield straight lines at constant concentration and at temperatures of constant diffusion mechanism. If it is assumed that rate of permeability change dK_S/dt has the same temperature dependence as diffusion rate D (both having dimensions of l^2/t) then plots of log (dK/dt) versus 1/T will be straight lines. Obviously, extrapolation from two points down to ionizer service temperatures is not as reliable as extrapolation from three or more points.

Knowing the as-sintered permeability (K) of an ionizer, and assuming that the ionizer will remain functional until its permeability decreases to 0.05 μP, the permissible decrement of permeability becomes K-0.05. Dividing K-0.05 by the hourly K decrement (ΔK_{hr}) at a given temperature, yields the hours of life to be expected at that temperature. Using the experimentally derived slopes of Fig. 6-2 (i.e., ΔK_{hr} values for 1,800°C and 1,600°C) and plotting these as log ΔK_{hr} versus 1/T, straight line extrapolations were made to obtain ΔK_{hr} values at 1,300°C, 1200°C, and 1100°C (Appendix B, Figs. B-1, B-2, and B-3). Useful

*$(7.5)(10)^{-4} \nu K = K_S$, where ν is the coefficient of kinematic viscosity in cm^2/sec

lifetime expectations at the latter temperatures were then calculated as $(K-0.05)/\Delta K_{hr}$. The lifetimes thus determined, as well as the data used in the derivations, are listed in Table 6-II. Here, the lifetimes of the 10A/oTa compositions are not listed, since the slopes of their 1,600°C "K vs t" curves (i.e., their rates of permeability change) were too small to be measured. However, this very fact indicates that W-10A/oTa should have an even longer useful life than W-5A/oTa (1-3μ particles).

Straight-line plots of change in densification rate ($\log \Delta\rho_{hr}$) as a function of reciprocal temperature (T) were not drawn and are not included in this report. The technical justification for such plots is not apparent.

To summarize the data of Table 6-II, extrapolations of accelerated life-test data indicate that W-5A/oTa ionizers (made with tantalum particles) should have a minimum useful life of 34,000 hours at 1,200°C, while W-10A/oTa ionizers may be expected to function significantly longer. Useful lifetime at 1,200°C of unstabilized tungsten is indicated to be less than 100 hours, while lifetimes of other experimental ionizers are less than 10,000 hours. Despite the fairly good stability of W-7A/oTa, prepared by reduction of Ta_2O_5, its initial low permeability (even at relatively low density) would eliminate it from further consideration as an ionizer material.

TABLE 6-II

EXPERIMENTAL AND EXTRAPOLATED PERMEABILITY DATA FROM 1800°C and 1600°C LIFE TESTS,

WITH USEFUL IONIZER LIFETIMES DERIVED THEREFROM

Ionizer Composition, atom %	Form or Method of Addition	Average N_2 Permeability, μP (a) (K)	Total Permissible Decrement of K, μP ($K-.05=\Delta K_T$)(b)	Temperature, °C: 1800	1600	1300	1200	1100	1300	1200	1100
				Decrement of K per 1 Hour, μP (ΔK_{hr})					Useful Ionizer Life, hours ($\Delta K_T/\Delta K_{hr}$)		
				(c)	(c)	(d)	(d)	(d)			
Tungsten (control)	——	.309	.259	2.8×10^{-2}	1.7×10^{-2}	5.9×10^{-3}	3.8×10^{-3}	2.3×10^{-3}	44	68	113
W-0.85 Re	Vapor precoating	.291	.241	2.3×10^{-2}	1.4×10^{-2}	5.6×10^{-3}	3.8×10^{-3}	2.4×10^{-3}	43	63	100
W-1.53 Ta	Vapor precoating	.191	.141	2.5×10^{-2}	5.0×10^{-3}	2.1×10^{-4}	5.5×10^{-5}	1.2×10^{-5}	670	2600	12000
W-5 Re	Reduction	.281	.231	1.4×10^{-2}	2.7×10^{-3}	1.0×10^{-4}	2.7×10^{-5}	5.6×10^{-6}	2300	8600	41000
W-7 Ta	Reduction	.092	.041	1.3×10^{-2}	1.4×10^{-3}	2.0×10^{-5}	3.5×10^{-6}	4.1×10^{-7}	2100	12000	100000
W-5 Ta	1-5μ particles	.212	.162	8.0×10^{-3}	1.1×10^{-3}	2.4×10^{-5}	4.7×10^{-6}	7.2×10^{-7}	6800	34000	225000
W-5 Ta	1-3μ particles	.206	.156	4.6×10^{-3}	7.1×10^{-4}	1.8×10^{-5}	3.8×10^{-6}	6.5×10^{-7}	8700	41000	240000

(a) One microperm unit (μP) is defined as $10^{-6}\ g\cdot cm^{-1}\cdot sec^{-1}\cdot torr^{-1}$

(b) At $K = < .05\mu P$, the pores are assumed to be too restricted for efficient ionization

(c) Values were determined from experimental "K vs t" slopes.

(d) Values were determined by extrapolation of "log ΔK_{hr} vs 1/T" slopes.

7. IONIZATION PERFORMANCE TESTING OF SELECTED COMPOSITIONS

Ionizer performance characteristics of greatest importance are the neutral fraction and the critical temperature as a function of ion current density and ionizer structure (i.e., pore density and pore size). These parameters are representative of the ionization (propellant utilization) efficiency and ion generation efficiency, respectively, and are related to ion engine parameters. They are treated in detail by Kuskevics (Ref. 4).

7.1 Ion Current Density, Neutral Fraction and Critical Temperatures

The common measurements of surface ionization are the ion current density and neutral efflux as a function of ionizer temperature for various cesium flow rates. A typical set of curves for porous tungsten (with decreasing temperature) is shown in Fig. 7-1, in order to define the various regions of operation. As temperature is decreased, ion current density does not remain constant in the low cesium coverage region, because of a change in ionization efficiency and cesium permeation. The "critical temperature" lies on a portion of the curve denoted as the transition region (characterized by a rapid change of slope) leading to the high cesium-coverage region (characterized by low ionization efficiency and high neutral efflux). There are sometimes two "critical temperatures." One, T_{CI}, is defined as the temperature at which the ion current has declined by 5 percent (two times the minimum detectable current change). The other, T_C, is defined as the temperature corresponding to minimum neutral fraction. These definitions are discussed in much greater detail in Ref. 2. The optimum temperature for operation of ion thrusters lies in the relatively small range between the lower T_{CI} and the higher $T_{C\alpha}$. The sum of the ion and equivalent atom currents shows that the total flow rate decreases about 3.5 percent per 100°C.

A typical neutral fraction curve is shown in Fig. 7-1, while a set of such curves is shown in Fig. 7-2. These curves are theoretically described by the Saha-Langmuir equation, from which constant-work-function curves were calculated and also plotted (with dashed lines) in Fig. 7-2. The experimental curves (solid lines) show a decrease with decreasing temperature, similar to that of the constant-work-function curves, for porous ionizers having low neutral fractions (below 1 percent). At the transition region, the work function starts to decrease due to increasing cesium surface coverage, and the neutral fraction-vs-ionizer temperature curves exhibit a flat region. For some ionizers, this flat region extends over several hundred degrees. At higher cesium flow (yielding higher neutral fraction) the curves may have no minimum below 1400°C. Figure 7-3 displays a set of curves for solid tungsten. The superior performance of solid tungsten at high current densities is due to uniform cesium arrival and coverage from vapor condensation. For porous ionizers, the cesium spreads across the surface from the pores by surface diffusion, which involves surface coverage gradients; therefore, there is neither uniform arrival nor coverage. At lower ion current densities, emission from inside the pores may be more prevalent than emission from the surface, and performance can be superior to solid tungsten. This mechanism is discussed in detail in Ref. 5.

7.2 Ionization Test Equipment and Procedures

The test apparatus, instrumentation, and procedures are described in detail by LaChance et al (Ref. 1, 2, 6, 7). New modifications include a special chopper circuit and an isolation transformer, so that ionizer and cesium reservoir thermocouple outputs could be recorded at near ground potential. These components are recalibrated for each test. The reservoir is loaded with several grams of cesium in a special dry box containing a pure argon atmosphere. Upon removal of the ionizer assembly from the dry box, the cesium in the reservoir is under one atmosphere pressure of argon. The low permeability of

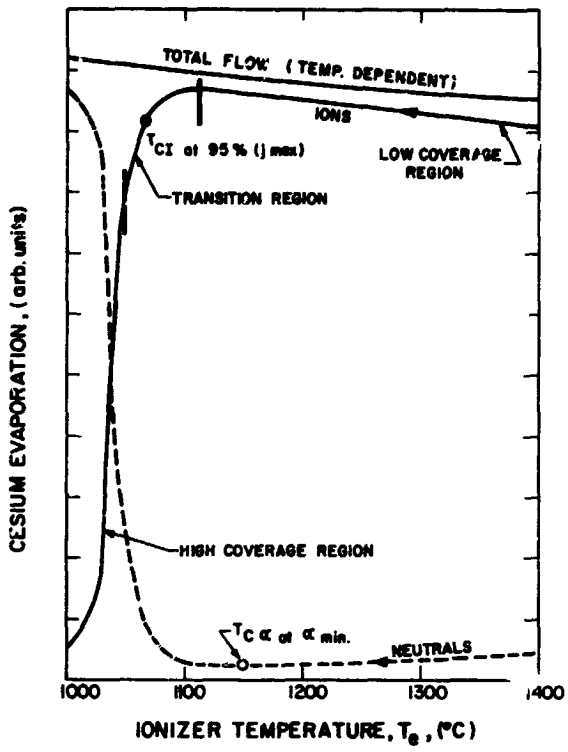

FIG. 7-1 ION CURRENT, NEUTRAL EFFLUX AND TOTAL FLOW VS IONIZER TEMPERATURE FOR POROUS TUNGSTEN

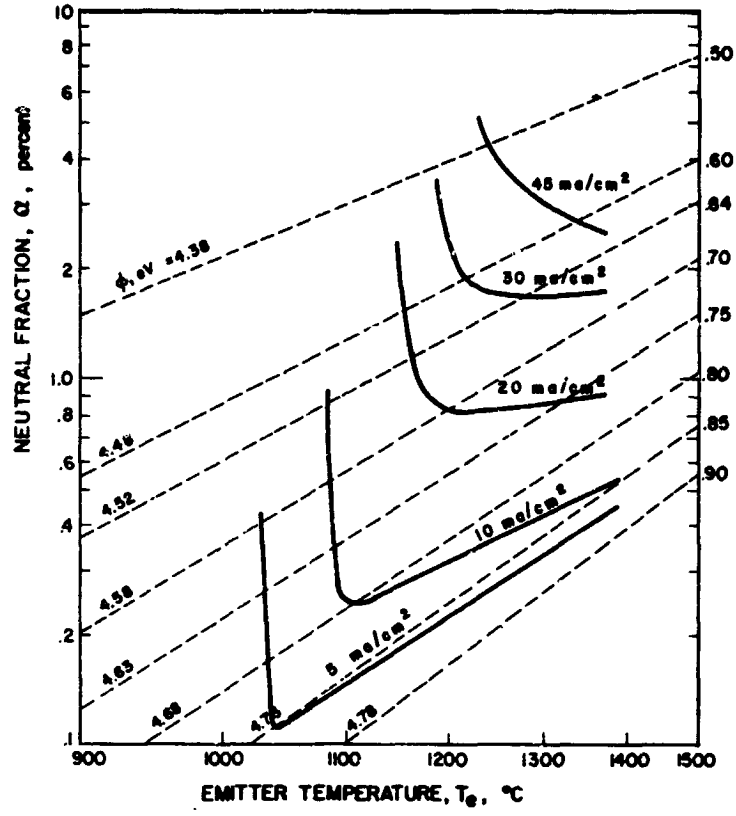

FIG. 7-2 NEUTRAL FRACTION VS IONIZER TEMPERATURE FOR A W-0.85A/oRe IONIZER

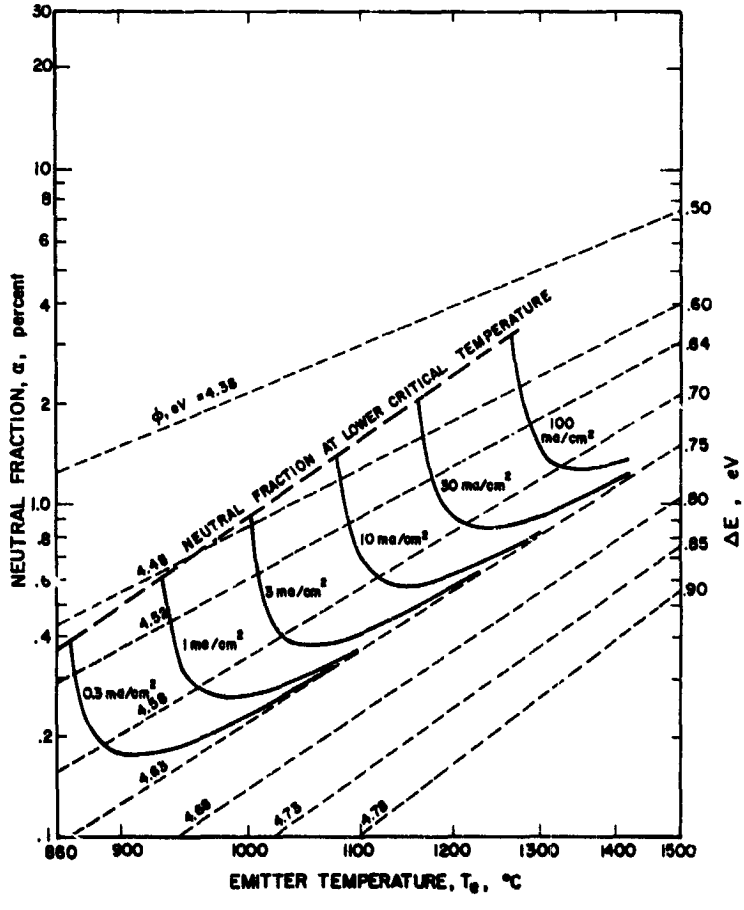

FIG. 7-3

NEUTRAL FRACTION VS IONIZER TEMPERATURE AS A FUNCTION OF ION CURRENT DENSITY FOR SOLID TUNGSTEN

the porous ionizer acts as the only barrier against the infustion of air while the assembly is being mounted into the accelerator and transferred into the vacuum test chamber. Reservoir heating and cooling coils are brazed to a hollow block which is pressed onto the reservoir. This block can be subsequently removed and used again.

The vacuum system, shown in Fig. 7-4 and used in these experiments, is capable of operating in the 10^{-8} torr range without load and in the low 10^{-6} torr range during the very high current operation periods. The 1-ft x 3-ft chamber has a flooded stainless steel LN_2 liner. The 10-in. oil-diffusion pump is connected to the vacuum chamber through a liquid nitrogen cooled elbow which serves as an antimigration trap. With the multihole liner in front of it and the single 45^{o} restriction, it is a two-bounce trap.

An E3(1-4μ) spherical tungsten powder ionizer was tested under Air Force contract to determine the effect of residual gases on performance. A Veeco GA-4 Residual Gas Analyzer was used to monitor the partial pressures in the chamber.

A typical spectrum for the pressures, before and during an ionizer test, is shown in Fig. 7-5. As noted here, the predominant gases are H_2, gases with mass number 28 (mostly N_2, C_2H_4, and some CO), and methane. There is no O_2 and little CO_2. There are large changes in gas content due to presence of the energetic ion beam, which breaks down heavier molecules and serves to outgas the system.

The pressure-vs-ion beam current behavior is typical for all tests reported below. At any beam current, the pressure decreases with time.

7.3 Performance of Ionizers Made From Tungsten Microspheres and Tantalum Particles

A series of ionizers made from tungsten microspheres with 10A/oTa particle additions were tested. The effects of the size ranges of various tantalum particle additions on pore structure were described in detail in Section 3. Significant parameters are summarized as follows:

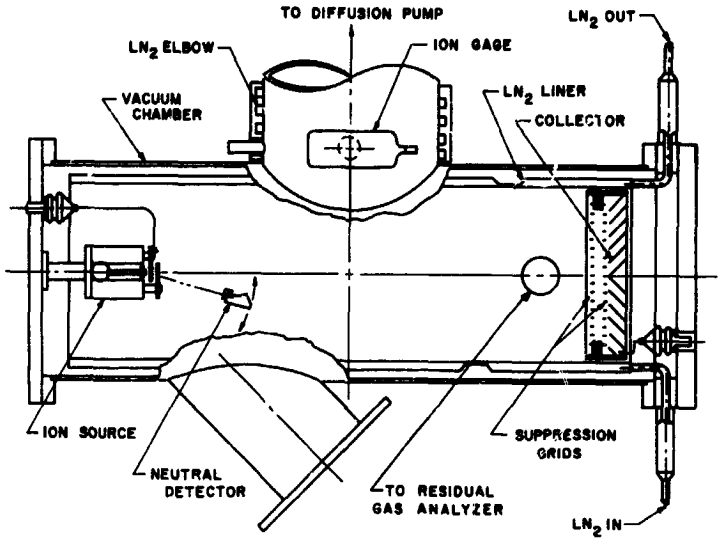

FIG. 7-4

SCHEMATIC OF VACUUM CHAMBER WITH ION SOURCE, NEUTRAL DETECTOR, ION COLLECTOR, AND RESIDUAL GAS ANALYZER

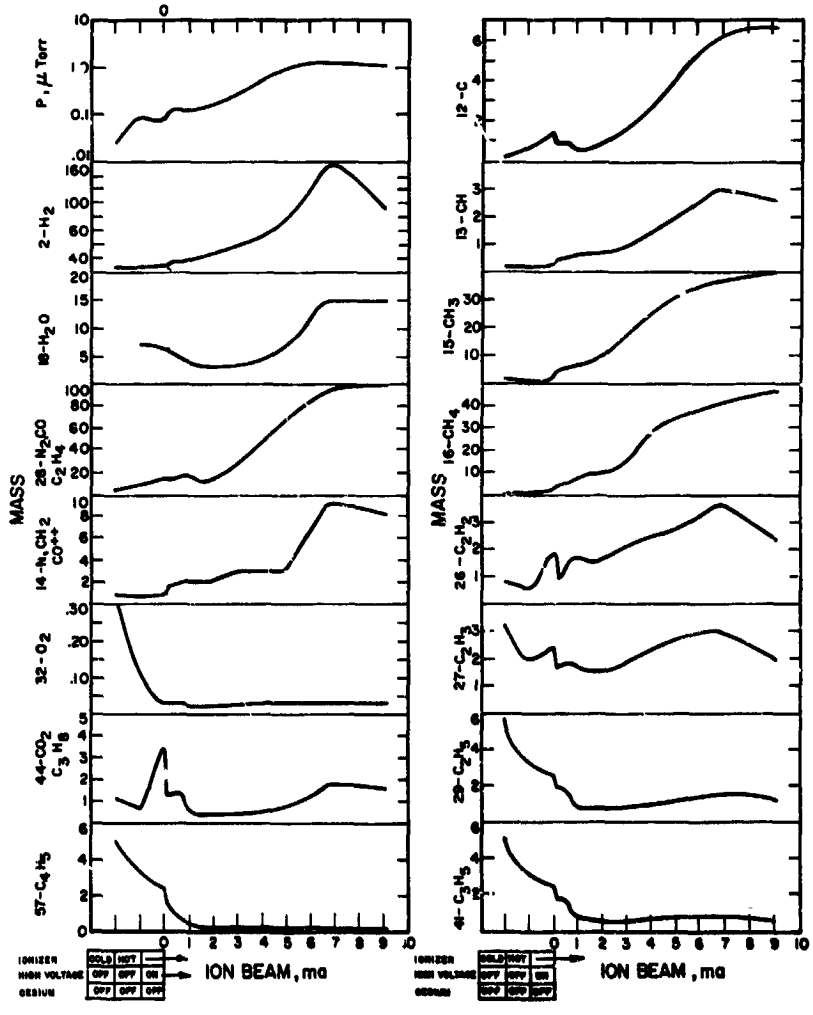

FIG. 7-5

RESIDUAL GAS ANALYSIS WITH INCREASING ION BEAM CURRENT IN DIFFUSION PUMPED SYSTEM WITH LIQUID NITROGEN LINER AND TRAP (All readings in scale divisions on a Veeco GA4 Residual Gas Analyzer)

Ionizer No.	W Particle Size Range, μ	Ta Particle Size Range, μ	Av Pore Density, Pores/cm^2	Av Pore Diameter, μ	N_2 Permeability, μP
LB-10Ta-4	1.7-5	1-3	3.40×10^6	2.37	0.21×10^{-6}
E4-10Ta-3	2-5	1-3	3.51×10^6	2.34	0.16×10^{-6}
LC-10Ta-13	1.7-5	1-5	3.15×10^6	2.62	0.19×10^{-6}

The ionization performance characteristics of these ionizers (Figs. 7-6 through 7-14) demonstrate the superior performance of refined pore structures.* The two-digit number on each curve indicates the day and sequence, respectively, in which the curves were determined. For example, curve 24 was determined on the second day of testing, and it was the fourth curve to be recorded. The temperature T_r denoted for the j-vs-T_e curves indicates the cesium reservoir temperature.

The average of the ion current density critical temperatures of the E4-10Ta-3 ionizer was about 50°C lower than that of the LB-10-Ta-4 ionizer, and 200°C lower than that of the coarsest ionizer, LC-10Ta-13. The three ionizers exhibited considerably larger differences between their corresponding neutral fraction critical temperatures. Those of the two finer-structured ionizers could be considered to be about 1000°C below that of the coarser LC-10Ta-13 ionizer. For all three ionizers, there was no pronounced minimum below 1400°C in the α-vs-T_e curves from which the ionizer work function could be accurately determined. The LC-10Ta-13 ionizer curves had a shallow minimum below 10 ma/cm^2, indicating a work function of 4.7-4.8 eV. The E4-10Ta-3 ionizer curves had a shallow minimum below 15 ma/cm^2, corresponding approximately to a work function of 4.6-4.7 eV. The LB-10Ta-4 ionizer curves had a shallow minimum below 20 ma/cm^2, which also relates to a

* The j-vs-T_e and α-vs-T_e curves, presented for each of the ionizer buttons, are typical of about 15 curves recorded over 2 to 5 days of testing. The α-vs-j data points are final values, recorded after thorough aging of the buttons; in several instances, the final values differ slightly from values of the α-vs-T_e curves.

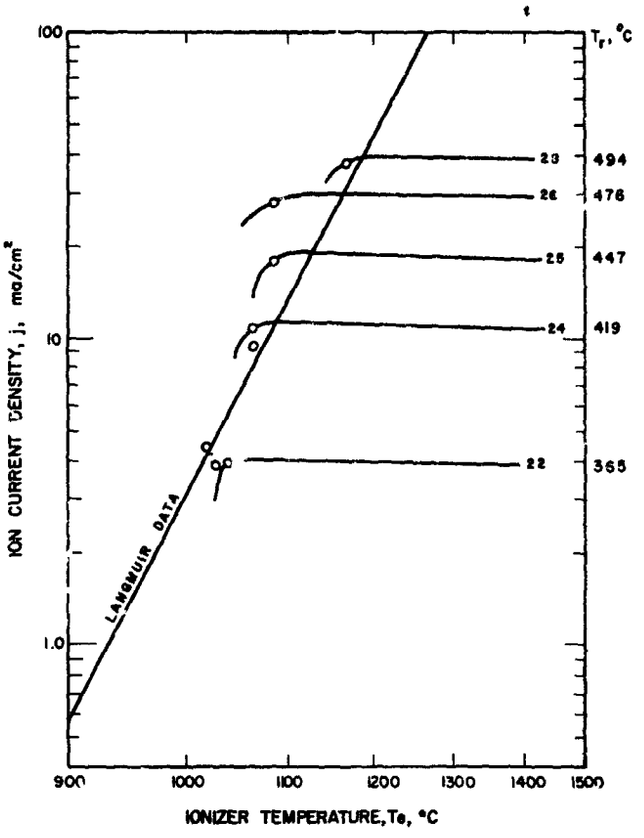

FIG. 7-6 ION CURRENT DENSITY VS IONIZER TEMPERATURE FOR A W-10A/oTa(1-3μ) IONIZER (LB-10Ta-4)

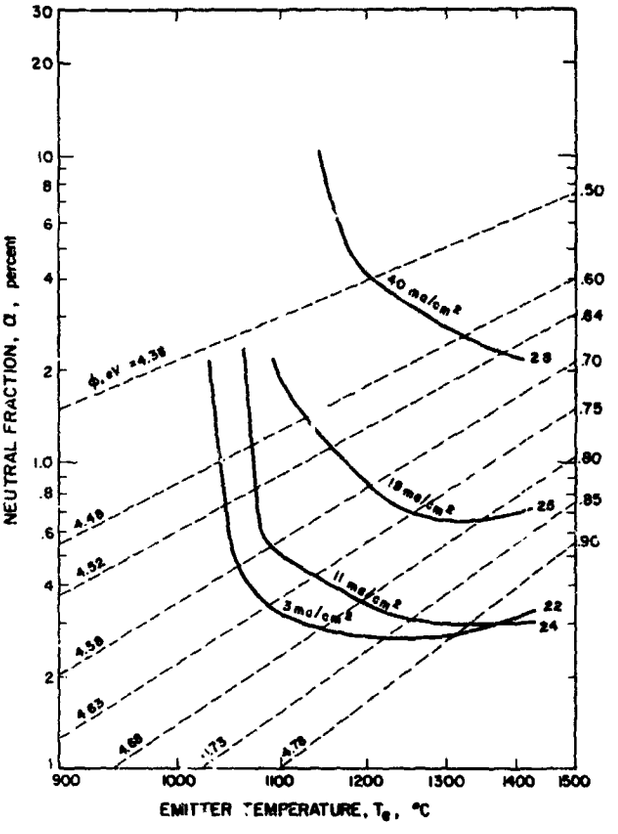

FIG. 7-7 NEUTRAL FRACTION VS IONIZER TEMPERATURE FOR A W-10A/oTa(1-3μ) IONIZER (LB-10Ta-4)

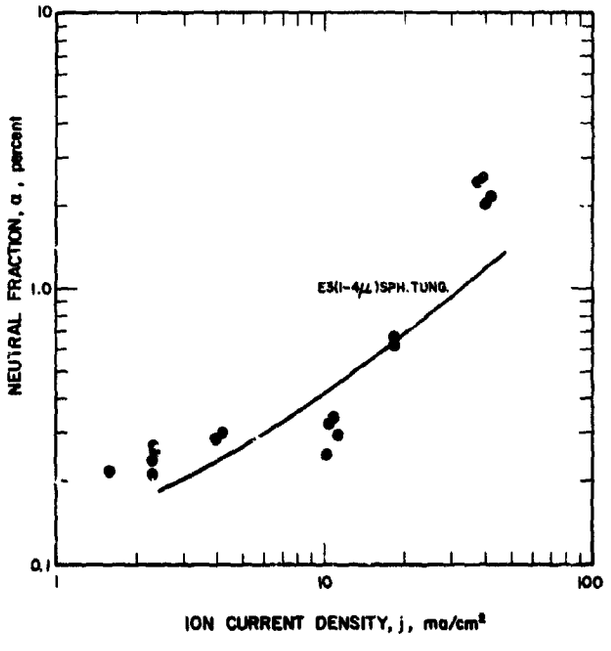

FIG. 7-8

NEUTRAL FRACTION VS ION CURRENT DENSITY FOR A W-10A/oTa(1-3μ) IONIZER (LB-10Ta-4) COMPARED WITH AN E3(1-4μ) SPHERICAL TUNGSTEN POWDER IONIZER

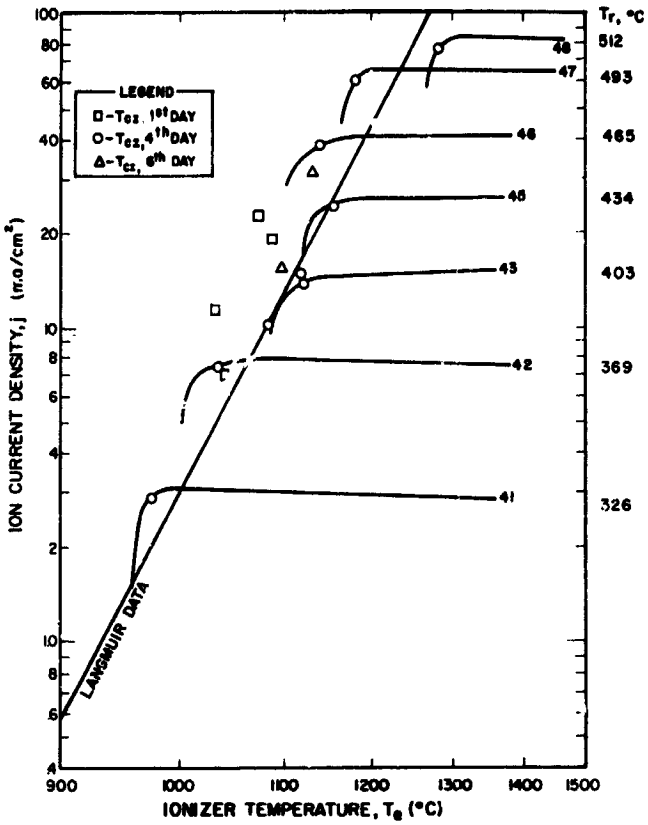

FIG. 7-9 ION CURRENT DENSITY VS IONIZER TEMPERATURE FOR W-10A/oTa IONIZER (E4-10Ta-3)

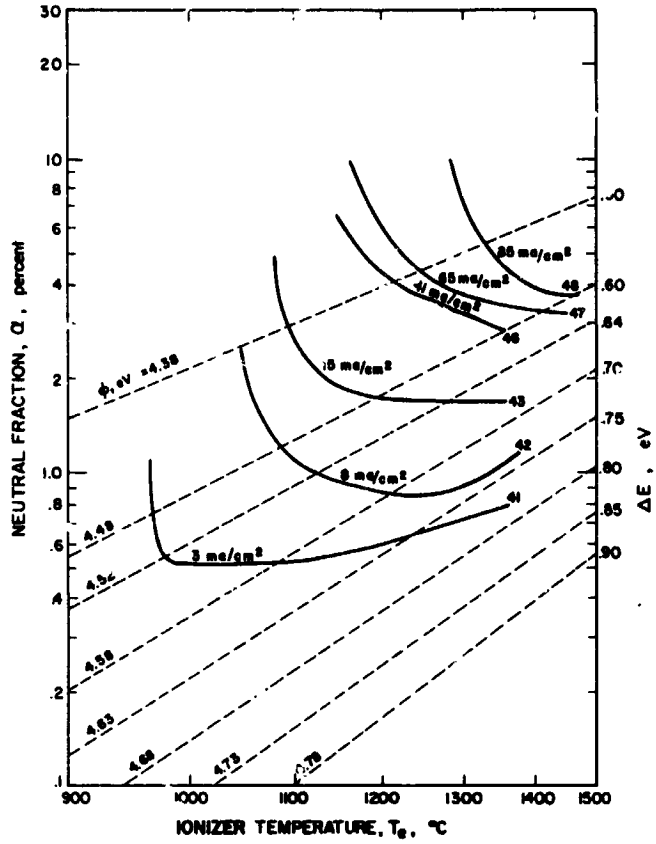

FIG. 7-10 NEUTRAL FRACTION VS IONIZER TEMPERATURE FOR W-10A/oTa IONIZER (E4-10Ta-3)

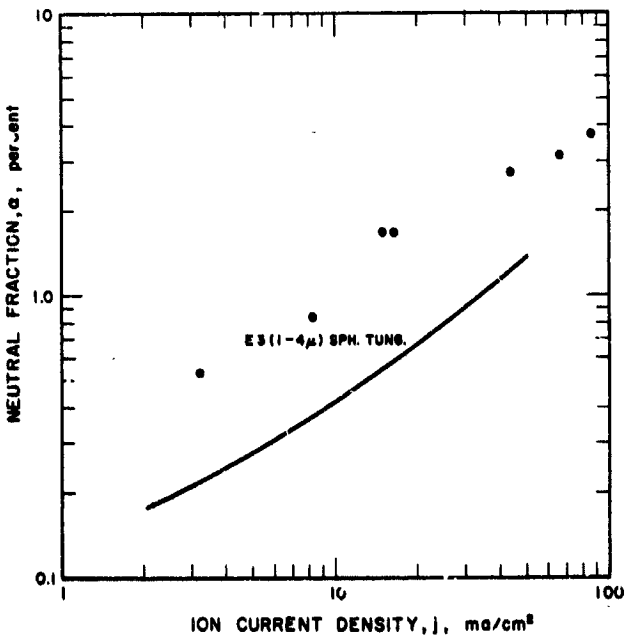

FIG. 7-11

NEUTRAL FRACTION VS ION CURRENT DENSITY FOR A W-10A/oTa(1-3μ) IONIZER (E4-10Ta-3) COMPARED WITH AN E3(1-4μ) SPHERICAL TUNGSTEN POWDER IONIZER

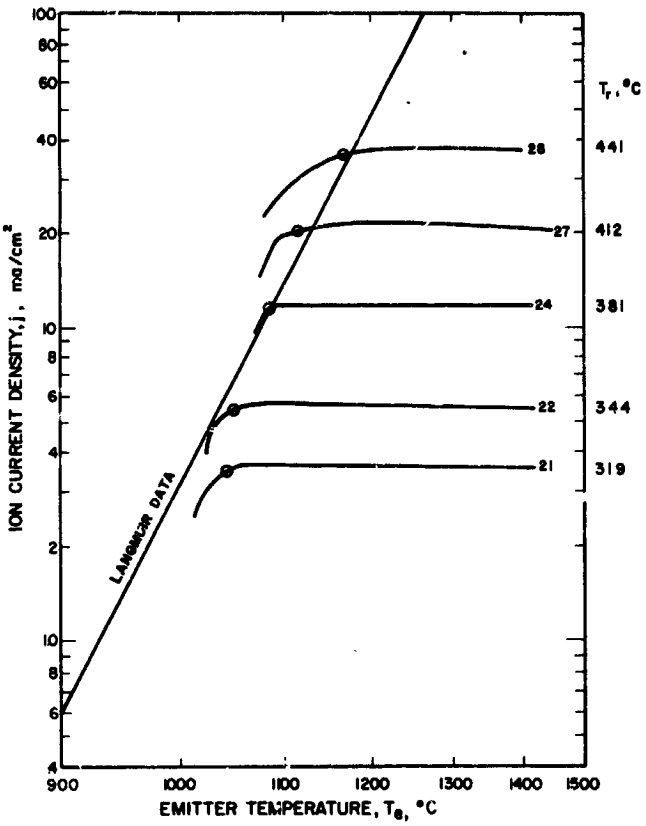

FIG. 7-12 ION CURRENT DENSITY VS IONIZER TEMPERATURE FOR A W-10A/oTa(1-5μ) IONIZER (LC10-Ta-13)

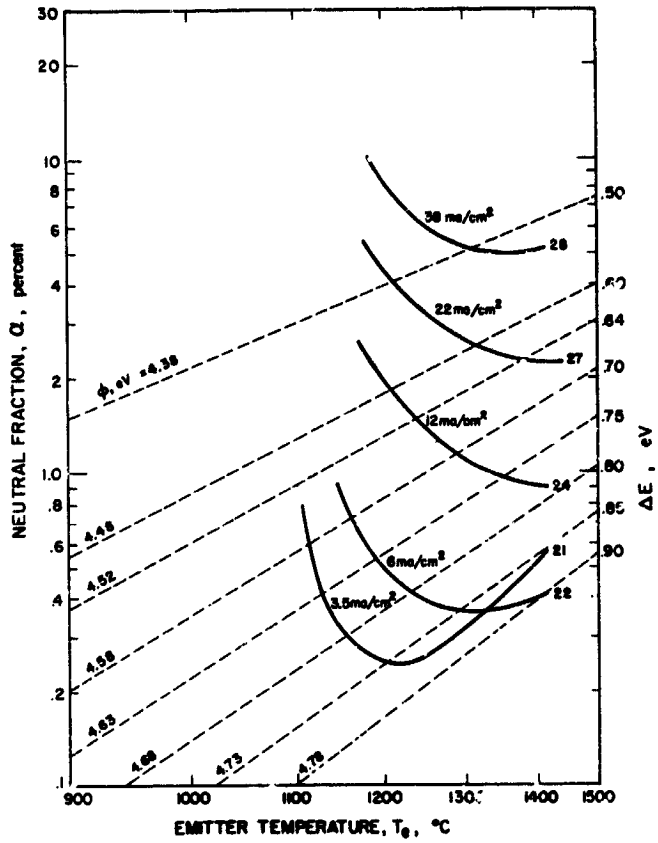

FIG. 7-13 NEUTRAL FRACTION VS IONIZER TEMPERATURE FOR A W-10A/oTa(1-5μ) IONIZER (LC10-Ta-13)

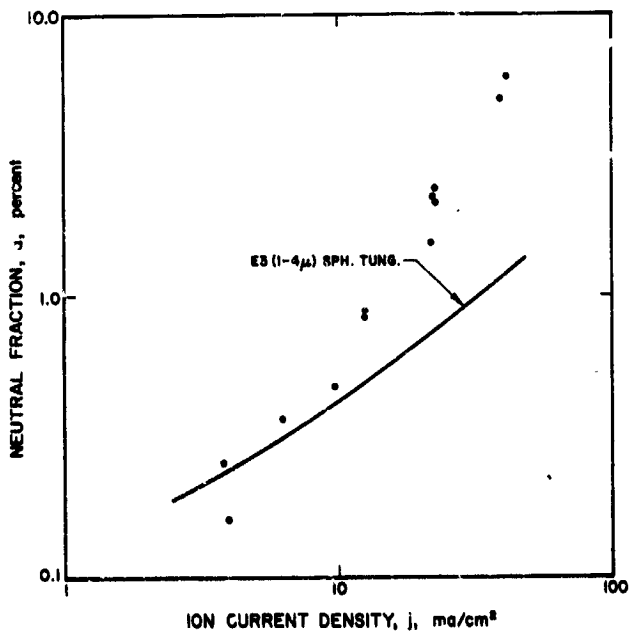

FIG. 7-14

NEUTRAI FRACTION VS ION CURRENT DENSITY FOR A W-10A/oTa(1-5μ) IONIZER (LC10-Ta-13) COMPARED WITH AN E3(1-4μ) SPHERICAL TUNGSTEN POWDER IONIZER

work function of 4.7-4.8 eV. At 40 ma/cm^2, the neutral fractions of the LB-10Ta-4, E4-10Ta-3, and LC-10Ta-13 ionizers were 2.3, 2.6, and 5.5 percent, respectively.

7.4 Performance of Ionizers Made From Tungsten Microspheres, Precoated by Vapor Deposition with Tantalum and Rhenium

Two ionizers made from 1.7-5μ tungsten microspheres precoated with either rhenium or tantalum showed good ionization characteristics. Significant parameters are summarized as follows:

Ionizer No.	Element	Coating Thick, Å	A/o	Av Pore Density, pores/cm^2	Av Pore Diameter, μ	Nitrogen Permeability, μP
aLRe-5	Re	45	0.85	4.01 x 10^6	2.45	0.30
aLTa-14	Ta	102	1.53	6.07 x 10^6	2.01	0.19

The W-0.85A/oRe ionizer (aLRe-5) had a very sharp critical temperature as compared with most of the other ionizers. While its ion current critical temperatures were, on the average, about 50C° below the Langmuir data for solid tungsten (Fig 7-15), its neutral fraction minimums averaged only 50C° higher (Fig. 7-16). Neutral fraction declined with ionizer temperature at fairly constant work function, until within 50C° of the minimum for ion current densities below 20 ma/cm^2; the work function was between 4.6 eV and 4.8 eV. Below 15 ma/cm^2, the neutral fraction for the aLRe-5 ionizer was lower than for the E3 (1-4μ) spherical tungsten powder ionizer and it increased to 2.2 percent at 40 ma/cm^2, as shown in Fig. 7-17.

The W-1.53A/oTa ionizer (aLTa-14) had the highest pore density of any ionizer material ever tested at EOS. Its ion current critical temperatures averaged 20C° below the Langmuir line for all data. Typical curves are shown in Fig. 7-18. The neutral fraction 100C° above the ion current critical temperature was equivalent to that of E3(1-4μ) spherical tungsten powder ionizers. Minimum neutral fractions (Fig. 7-19) were at least 200C° higher than the corresponding T_{CI} values (above 1300°C, except for low current densities).

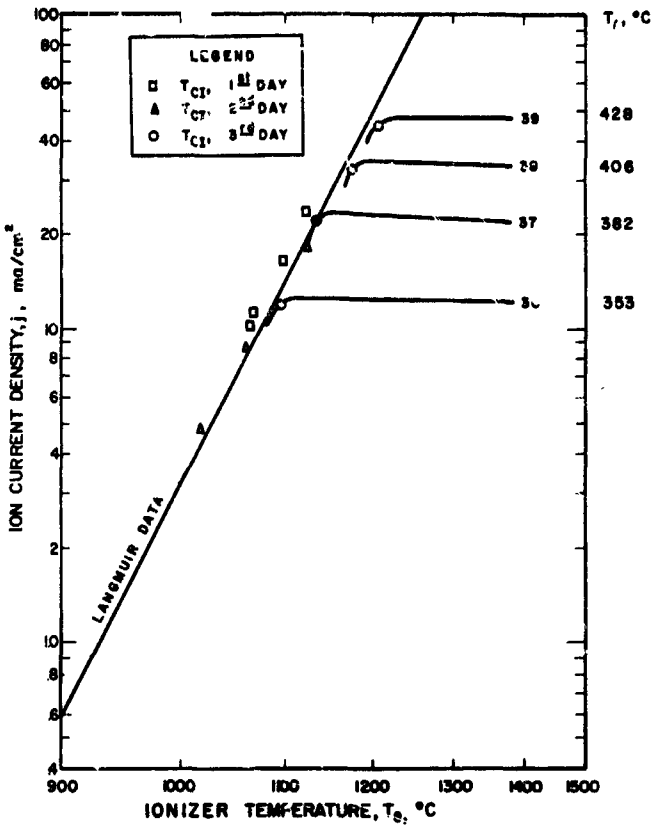

FIG. 7-15 ION CURRENT DENSITY VS IONIZER TEMPERATURE FOR A W-0.85A/oRe IONIZER (aLRe-5)

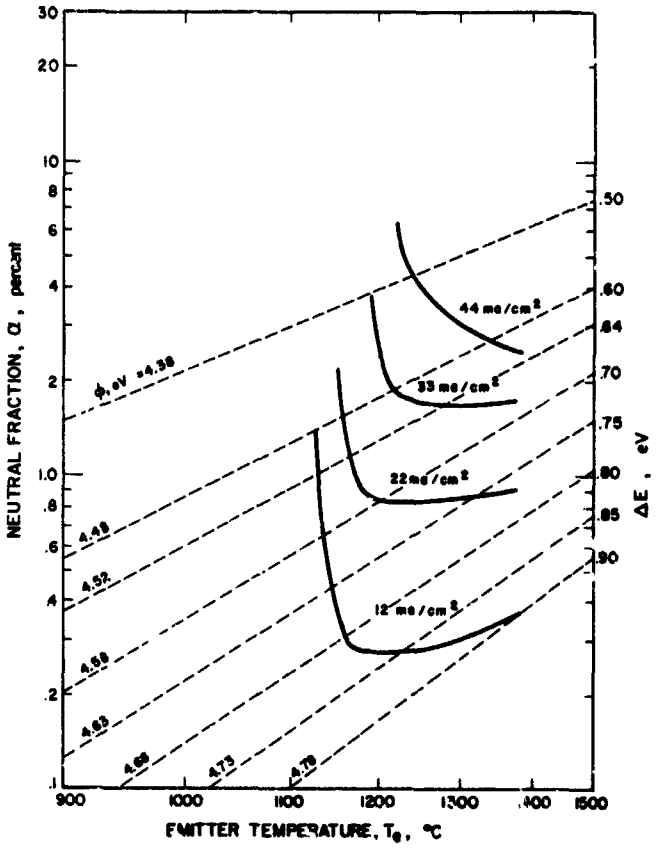

FIG. 7-16 NEUTRAL FRACTION VS IONIZER TEMPERATURE FOR A W-0.85A/oRe IONIZER (aLRe-5)

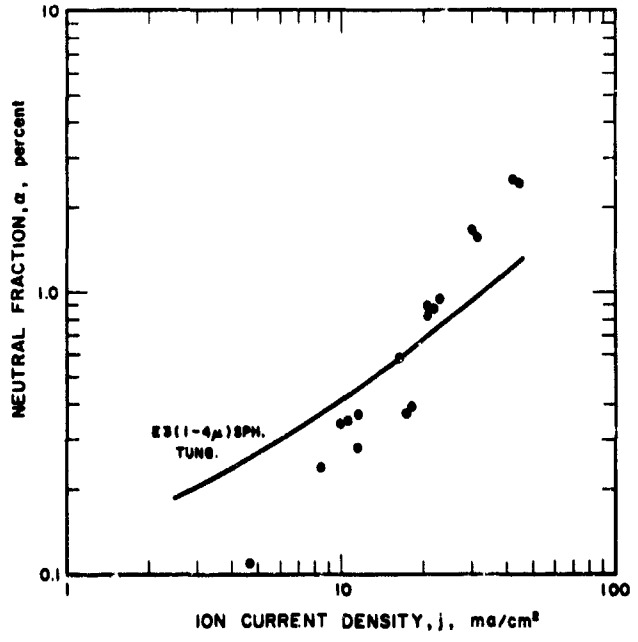

FIG. 7-17

NEUTRAL FRACTION VS ION CURRENT DENSITY FOR A W-0.85A/oRe IONIZER (aLRe-5) COMPARED WITH AN E3(1-4μ) SPHERICAL TUNGSTEN POWDER IONIZER

Further aging of the ionizer lowered the neutral fraction at high temperatures; the equilibrium values are shown in Fig. 7-20. At 40 ma/cm^2, the neutral fraction was 0.5 percent, which was lower than the neutral fraction of any ionizer material tested previously. From α-vs-T_e curves, a work function of 4.9-5.0 eV or higher was indicated at 1400°C.

At current densities below 10 ma/cm^2, the cesium flow rate through w-1.53 A/oTa had a marked dependence upon the rate of change of ionizer temperature. A temperature decline caused a 10-25 percent drop in flow which then rose to a lower equilibrium level than the initial value; a temperature increase brought fourth a burst of cesium before declining to an equilibrium level higher than the initial value. This effect was independent of any ion acceleration field. To a lesser extent, several other ionizers with fine pore structures have shown the same behavior at low current densities. A coarse-structured tantalum ionizer, tested under Air Force contract, was completely unusable because the temperature-dependent flow was several times greater than the equilibrium flow. Further study is required to explain this effect.

Somewhat similar behavior has been observed in ionizers which had cracked and, therefore, leaked cesium directly from the feed manifold. However, the cracks also caused very high neutral efflux readings. Since the W-1.5A/oTa ionizers have very low neutral fractions, and since the neutral fraction does not appear to change markedly during the temperature-change-induced cesium flow rate fluctuations, cracking of the ionizers is not considered to be the reason for the fluctuations.

7.5 Performance of Ionizers Made from Tungsten Microspheres, with Surface Conversion Layer

An ionizer made from 1-4μ tungsten microspheres (E3-G-4) was treated as follows to produce a surface conversion layer:

Atmosphere	Temperature, C°	Time, Minimum
Air	455	20
Hydrogen	1000	30

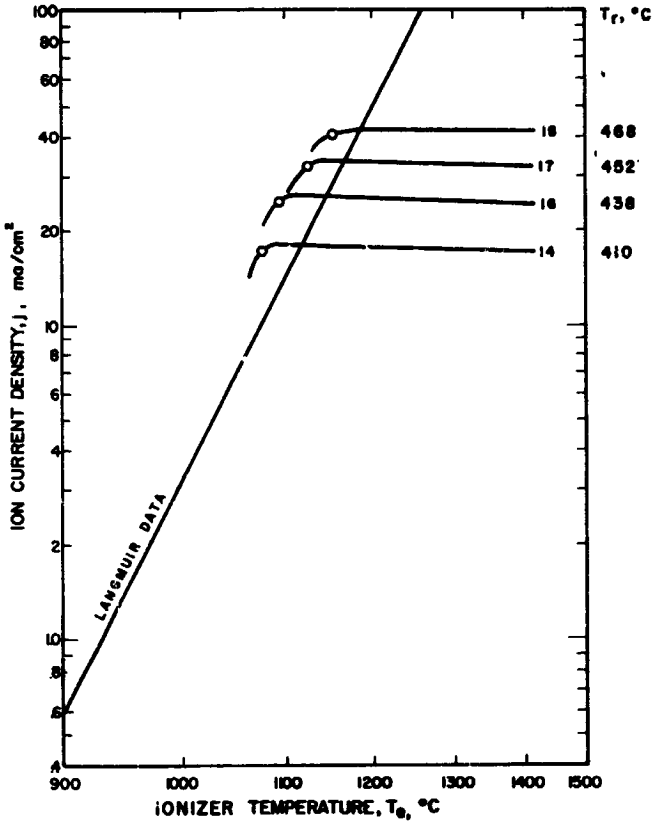

FIG. 7-18 ION CURRENT DENSITY VS IONIZER TEMPERATURE FOR A W-1.53A/oTa IONIZER (aLTa-14)

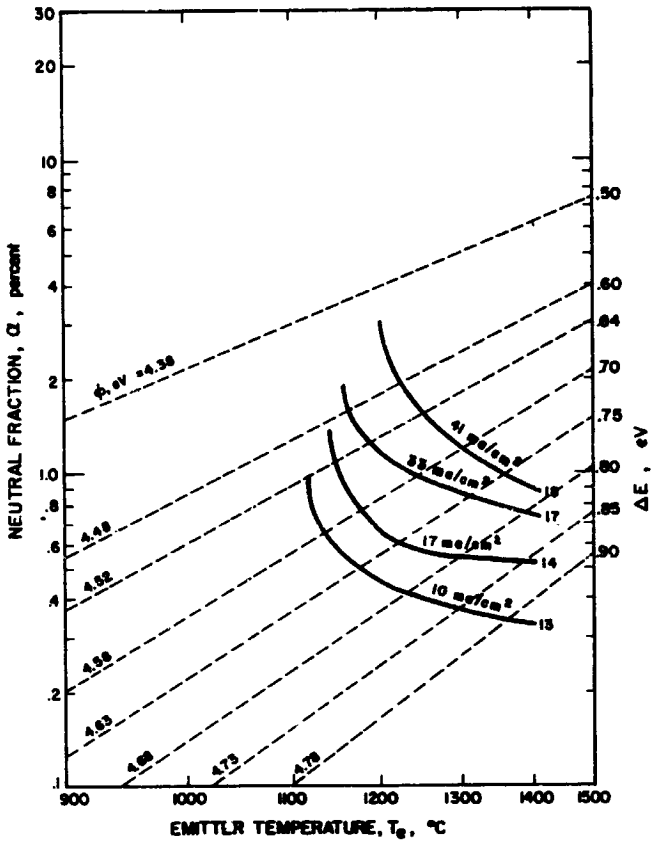

FIG. 7-19 NEUTRAL FRACTION VS IONIZER TEMPERATURE FOR A W-1.53A/oTa IONIZER (aLTa-14)

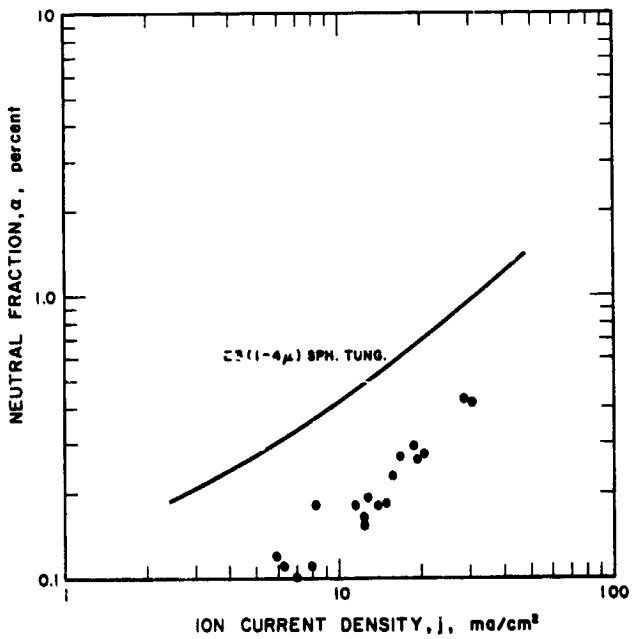

FIG. 7-20

NEUTRAL FRACTION VS ION CURRENT DENSITY FOR A W-1.53A/oTa IONIZER (aLTa-14) COMPARED WITH AN E3(1-4μ) SPHERICAL TUNGSTEN POWDER IONIZER

This oxidation-reduction cycle caused no change in button weight, a 2.0 percent increase in button volume, and a 5.6 percent increase (to 0.21μP) in nitrogen permeability. A pore density of 4.01×10^6 pores/cm^2 and an average pore diameter of 2.50μ were measured before surface conversion. The treated surfaces may have been very porous on an atomic scale, but this could not be ascertained from photomicrographs.

There appeared to be two ionization regions, as indicated by the ion current density-vs-ionizer temperature curves shown in Fig. 7-21. As the ionizer temperature was decreased, the neutral fraction first declined, reaching a minimum which was about 100° above the Langmuir data; then the neutral fraction increased discontinuously to 5-40 percent depending upon the current density (Fig. 7-22, curve 26.) The ionization mode then appeared to change character and the neutral fraction declined to 3-35 percent. As the temperature was decreased further, the ionization efficiency gradually decreased until the temperature reached a value of about 300° below the Langmuir line; at that point, ionization efficiency quickly dropped off. At higher current densities (greater than 25 ma/cm^2), there was only one increase in the neutral fraction beginning at about 100° above the Langmuir line, with a slope change at a temperature about 1000° lower. At high current densities, the increasing difference between these two transition points may be partly due to high accelerator drains between the two current declines. Upon increasing the ionizer temperature, there was no minimum in the ion current curves at any current density. While this behavior has been observed in other fine-structured ionizers, it usually has not been as significant as in this reduction-layer ionizer. Coarse-structured ionizers, previously treated by the oxidation-reduction process, have not shown definite abnormal ionization characteristics.

Ionization performance of the treated button was comparable generally to untreated E3(1-4μ) spherical tungsten powder ionizers. Neutral efflux, about 0.9 percent at 40 ma/cm^2 (Fig. 7-23) was slightly lower than for the untreated ionizers. The minimum of the neutral fraction-vs-ionizer temperature curves corresponded to a constant work function (for ion current densities below 20 ma/cm^2). At higher current densities (up to 50 ma/cm^2), the minimum was shallow below 1400°C. Work functions, as given by the Saha-Langmuir equation, ranged between 4.8 eV at 3 ma/cm^2 and 4.6 eV at 50 ma/cm^2.

7.6 Performance of Coarse (Commercial) Hydrogen-Reduced Tungsten Powder Ionizer

Ionization parameters of the Philips Mod. E tungsten ionizer were determined to be considerably better than the earlier Philips Mod. B, tested under the previous contract. These grades are designed to be dimensionally stable for use in large sastrugi-type ion engines. The early commercial ionizers, used and tested at EOS under Air Force contract, were also made by Philips, but were available only in small sizes. The latter ionizers showed a considerable spread in ionization characteristics from sample to sample. The Mod E. sample tested was equivalent to the best of the early samples tested. The ion current critical temperatures averaged about 25°C above the Langmuir data (Fig. 7-24) and the neutral fractions declined to low values only 40°C higher (Fig. 7-25). For ion current densities below 15 ma/cm^2, neutral fraction vs ionizer temperature curves exhibited a very shallow minimum below 1400°C. Surface work functions of between 4.6 eV and 4.7 eV were estimated. Extrapolated to 40 ma/cm^2, the neutral fraction was 6%, as shown in Fig. 7-26.

7.7 Comparison of Performance of Selected Compositions

The finer-structured ionizers continue to show the best ionization performance, confirming the trend discovered during the previous contract when ionizers were fabricated from three different size ranges of tungsten microspheres.

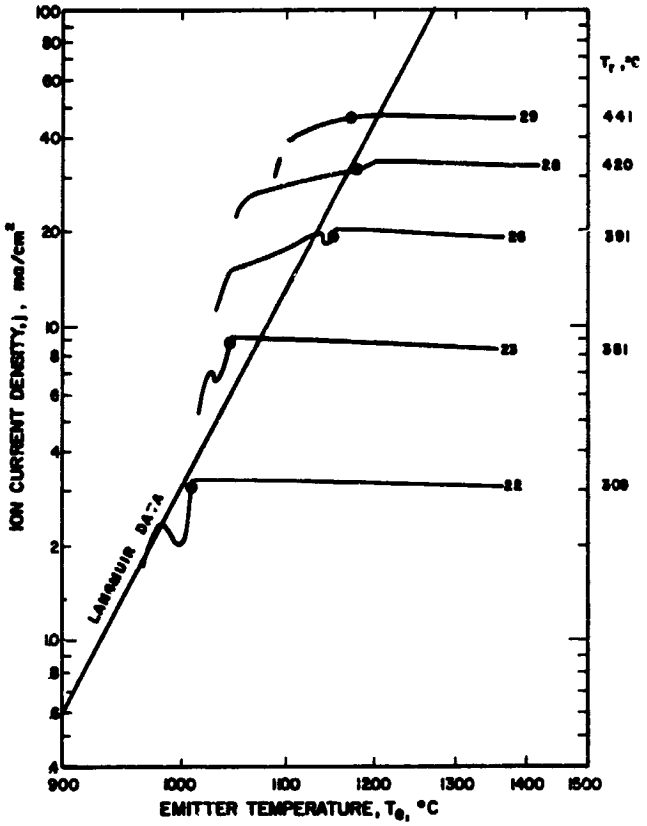

FIG. 7-21 ION CURRENT DENSITY VS IONIZER TEMPERATURE FOR E3(1-4μ) SPHERICAL TUNGSTEN POWDER IONIZER WITH REDUCTION-LAYER SURFACE TREATMENT

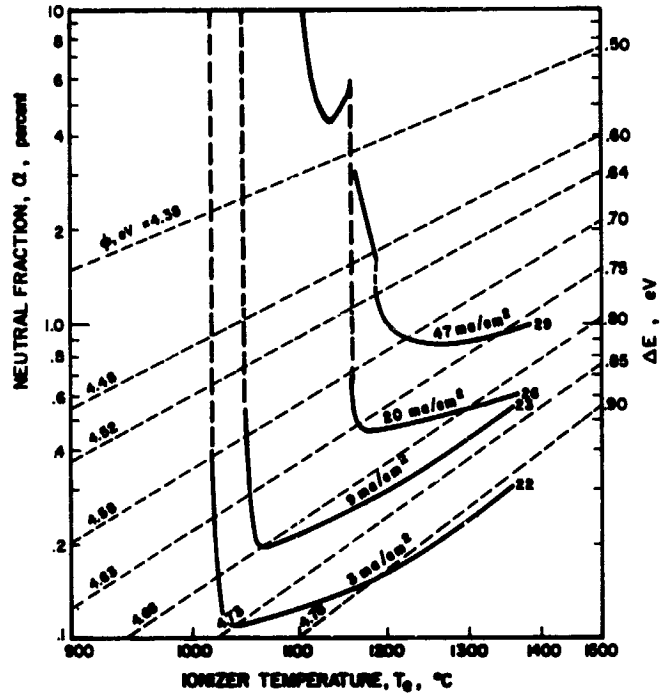

FIG. 7-22 NEUTRAL FRACTION VS IONIZER TEMPERATURE FOR E3(1-4μ) SPHERICAL TUNGSTEN POWDER IONIZER WITH REDUCTION-LAYER SURFACE TREATMENT

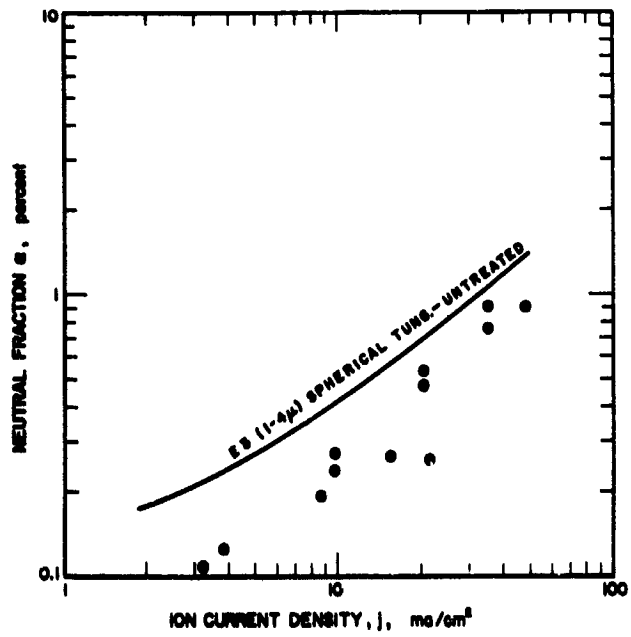

FIG. 7-23

NEUTRAL FRACTION VS ION CURRENT DENSITY FOR E3(1-4μ) SPHERICAL TUNGSTEN POWDER IONIZER WITH REDUCTION-LAYER SURFACE TREATMENT COMPARED WITH A SIMILAR UNTREATED IONIZER

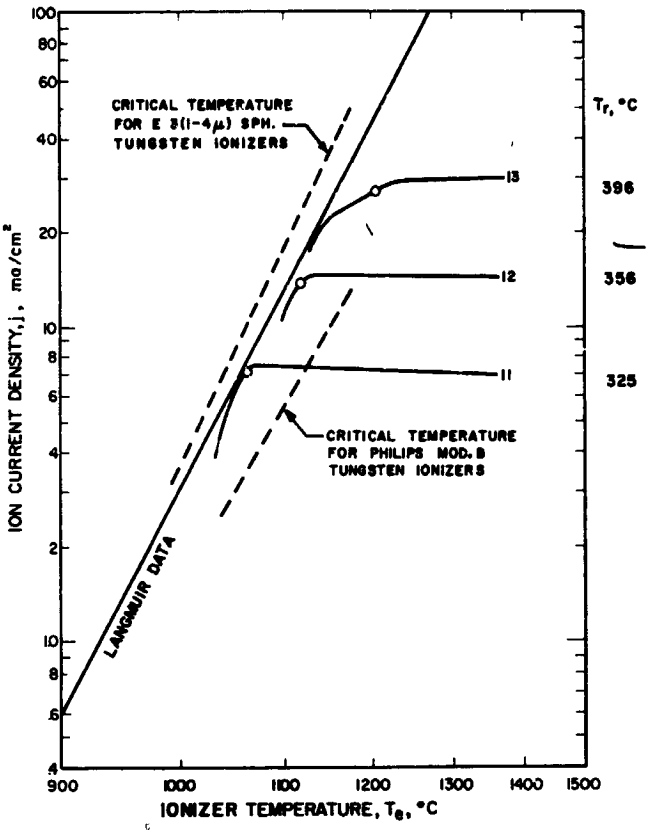

FIG. 7-24 ION CURRENT DENSITY VS IONIZER TEMPERATURE FOR PHILIPS MOD. E TUNGSTEN IONIZER COMPARED WITH PREVIOUS MOD. B AND E3(1-4μ) SPHERICAL TUNGSTEN POWDER IONIZERS

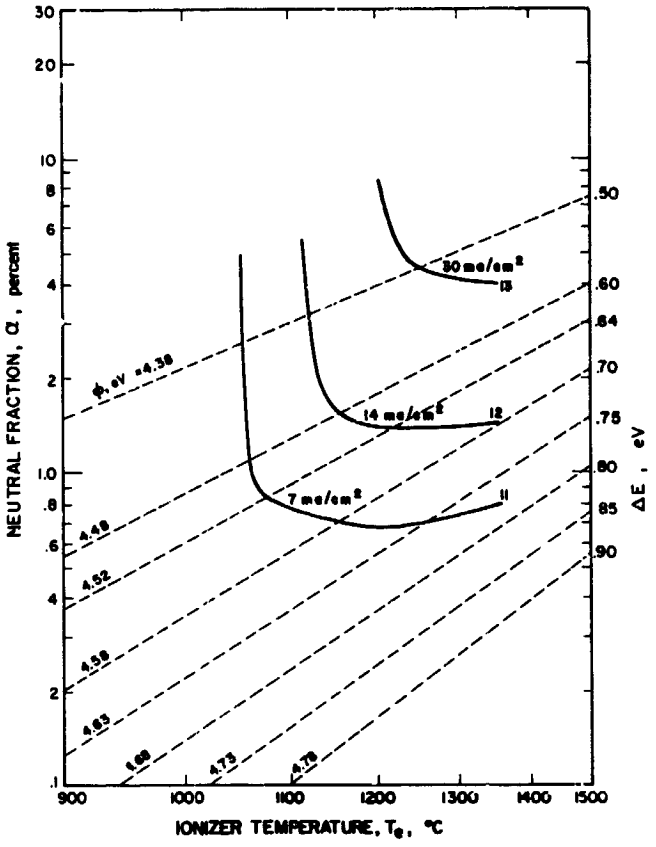

FIG. 7-25 NEUTRAL FRACTION VS IONIZER TEMPERATURE FOR PHILIPS MOD. E TUNGSTEN IONIZER

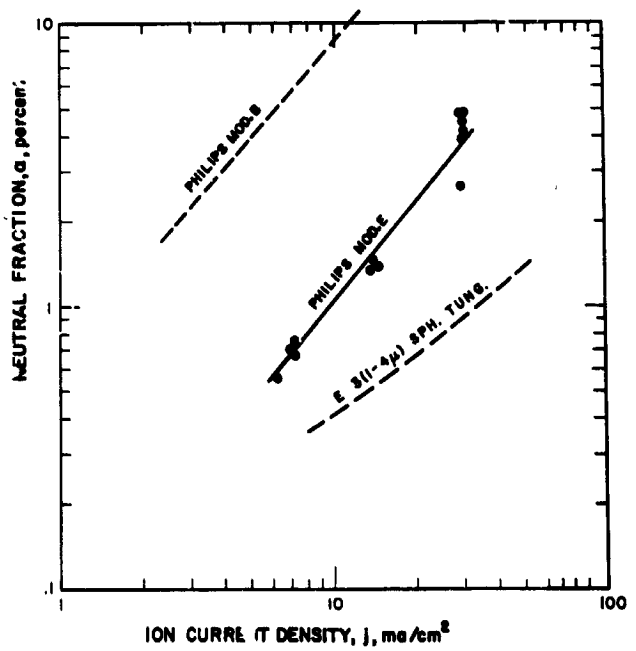

FIG. 7-26

NEUTRAL FRACTION VS ION CURRENT DENSITY FOR PHILIPS MOD. E TUNGSTEN COMPARED WITH PREVIOUS MOD. B AND E3(1-4μ) SPHERICAL TUNGSTEN POWDER IONIZERS

The 102Å tantalum-coated tungsten ionizer aLTa-14 had the lowest neutral fraction of any ionizer tested (Fig. 7-27). The E3 (1-4μ) spherical tungsten powder ionizer with the reduction layer, the 45Å rhenium-coated tungsten ionizer, and the W-10A/oTa mixed powder ionizer (LB-10Ta-4), also had very low neutral fractions. It is not known whether the slope differences exhibited by the ionizers are due to differences in pore structure or to the difficulties of performance testing at very high ion current densities. Future testing of additional samples should clarify this point.

Ion current critical temperatures of tantalum- and rhenium-coated tungsten ionizers and the two finer-structured W-10A/oTa mixed powder ionizers (E4-10Ta-3 and LB-10Ta-4) were as much as 20C° below the Langmuir data for solid tungsten.

An excellent property of the E3 (1-4μ) reduction-layer ionizer, the rhenium-coated tungsten ionizer, and the Philips Mod E. ionizer was that the minimum neutral fraction was within 50C° of the ion current critical temperature. The 102Å tantalum-coated tungsten ionizer did not reach its minimum neutral fraction until at least 200C° above the ion current critical temperature.

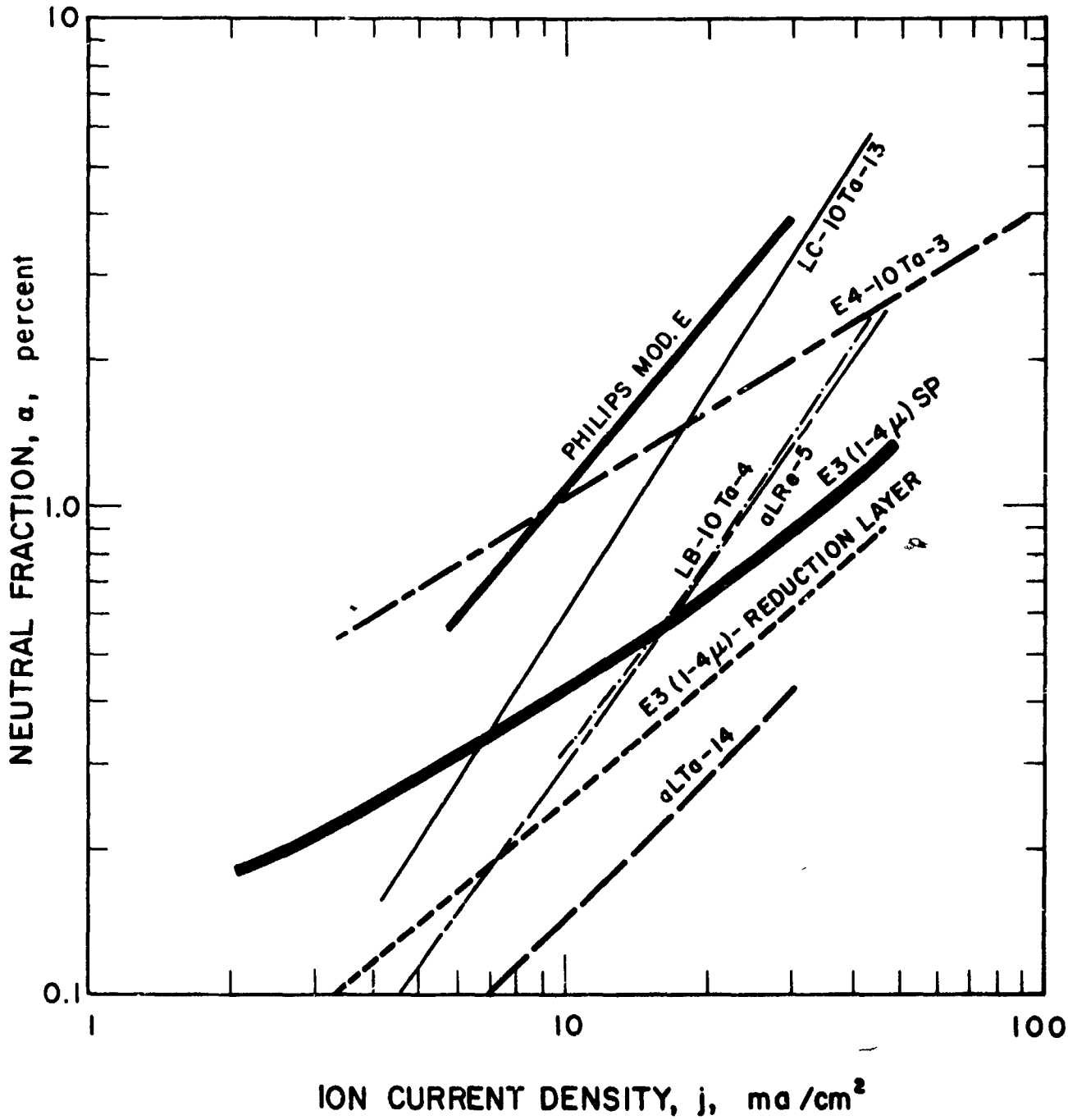

FIG. 7-27 COMPARISON OF NEUTRAL FRACTION VS ION CURRENT DENSITY FOR SELECTED COMPOSITIONS

8. NASA SAMPLE REQUIREMENTS AND MISCELLANEOUS WORK

The following sample selection was recommended by EOS, and approved by NASA, as required by this contract:

Number of Samples	Composition
3	Pure Tungsten
6	W-7A/oTa (1-3μ particles)
3	W+102Å Ta (vapor precoating)
3	W+45Å Re (vapor precoating)
1	W-7A/oTa (reduction)
1	W-5A/oRe (reduction)

The above samples were prepared from 1.7-5μ tungsten base microspheres (Lot L), pressed hydrostratically at 60,000 psi in the standard barrel shape*, vacuum sintered to a density of approximately 80 percent, and infiltrated with Cu-2Fe.

Miscellaneous work required under Phase VI (Change No. 2) of the contract was completed as follows:

1(a) Machining and submittal of four Phillips Mod. E ionizers to Space Technology Laboratories (STL);

1(b) Machining and performance testing of Phillips Mod. E ionizers,

2. Performance evaluation of Phillips Mod. E ionizer (as reported in Section 7);

3(a) Submittal to EOS type E-3 spherical tungsten ionizer material to STL (brazed into fixture); and

3(b) Submittal of EOS type E-4 (W-10A/oTa) ionizer material to STL.

*approximately 3/8-in. diameter by 3/4-in. long

9. CONCLUSIONS AND RECOMMENDATIONS

This work has indicated that the term "thermal stability" should not be applied indiscriminately to porous ionizers. Rather, it is more accurate to use the specific terms "dimensional stability" and "structural stability". Dimensional stability can be determined from density and heating - time data alone. However, determination of structural stability requires metallographic comparison of sintered pore structure with that of a standard baseline material, determination of permeability as a function of heating time, or both. Results have shown that ionizers can have excellent dimensional stability (shrinkage at very slow rates during sintering), and yet have very poor structural stability (markedly coarsened pore structures).

9.1 Ionizers from Tungsten Microspheres and Tantalum Particles (Phase I)

Early in the program, a preliminary series of W-10A/oTa ionizers were fabricated from 1.7-5μ tungsten microspheres and 1-3μ tantalum powder. Structural and performance evaluation indicated that this preliminary composition had very good pore stability and ionization performance. Therefore, it was agreed to proceed with Phase I of the program using tantalum particle additive, rather than "an alternate refractory powder additive" permitted by the scope of the work statement.

Two series of W-Ta mixtures were prepared, each containing 0.5, 2, 5, and 10A/o of discrete tantalum particles. Tantalum particles with diameters of 1-3μ were added to one series, and particles with diameters of 1-5μ to the other. Based on density versus sintering time at 2,000°C, densification rate was accelerated by 0.5A/oTa, affected very little by 2A/oTa, and retarded significantly by 5 and 10A/oTa. Thus, order of increasing dimensional stability

was indicated to be W-0.5A/oTa, W, W-5A/oTa, and W-10A/oTa. Accelerated densification (volume shrinkage) induced by 0.5A/oTa is attributed to the gettering of interstitial impurities (such as O, N, and H). Retarded densification induced by 5A/oTa and 10A/oTa is attributed to an opposing mechanism, which entails early and rapid diffusion of tantulum into the tungsten particles, with expansion of the latter.

Numerous ionizer buttons were prepared of tungsten with no Ta added and of the 8 Ta alloys. The severity of the sintering conditions necessary to bring these buttons to a target density of approximately 80 percent again indicated the order of increasing dimensional stability to be W-0.5A/oTa, W, W-5A/oTa, and W-10A/oTa. Very little variation in nitrogen permeability was noted among the W-Ta compositions (the range was 0.15-0.21 μP); however, their mean permeability was significantly lower than that of the tungsten control (0.31 μP), which indicates that the tantalum additions induced some restriction of the pore channels. Pore volume measurements (by mercury intrusion) showed that open pore volume decreased, and occluded pore volume increased, with increasing tantalum content. This, in turn, indicates that tantalum particle additions should be limited to the minimum percentage necessary to provide dimensional and structural stabilities. The 1-5μ Ta particles were found to yield larger volumes of occluded pores than 1-3μ particles. This indicates that the finer tantalum particles are better and also that even finer tantalum particles may be desirable.

Very important criteria governing selection of ionizers are pore density, pore size, and pore size uniformity. Pore density should be as high and pore size as small and as uniform as possible. Metallographic examination and pore counts indicated improved stability of pore structure for the sintered 0.5, 2, and 5A/oTa ionizers, since their pore densities were higher than that of unalloyed tungsten and their mean pore sizes were lower. On the other hand, the pore densities of 10A/oTa ionizers were lower than that of unalloyed tungsten. A

definite trend of decreasing pore density and increasing pore size was observed in 0.5, 2, 5, and 10A/oTa, in that order, with pore parameters of the unalloyed tungsten occurring between 5 and 10A/oTa. Thus, intermediate sintered mixtures of tungsten plus 6-8A/oTa show, in comparison with unalloyed tungsten, greater stability of pore structure, equivalent pore density and smaller mean pore size. Therefore, a W-7A/oTa mixture is recommended as being optimum.

Pore count data also indicated that sintered mixtures of tungsten plus 1-3μ Ta particles had somewhat higher pore densities and smaller mean pore sizes than did equivalent mixtures of tungsten plus 1-5μ Ta. Therefore, the finer 1-3μ Ta particles are recommended for future use, rather than the coarser 1-5μ particles.

Comparison of the pore structure of unalloyed tungsten with those of the W-Ta compositions indicates, in general, that tantalum particle additions entail some loss of pore uniformity. This was particularly true at the 10A/o Ta level for the coarser 1-5μ Ta addition. Reduction of tantalum content to 7 atom percent, and use of 1-3μ Ta additive as recommended, should reduce this undersirable effect.

9.2 Ionizers from Vapor Precoated Tungsten Microspheres (Phase II)

Fabrication of ionizers from vapor precoated tungsten microspheres was envisioned as a method of obtaining homogeneous dispersion of secondary elements, which would yield superior uniformity, stabilization and performance of the porous structures. Deposition of the relatively thick 500Å and 1,000Å coatings, initially established as the thickness goals, was not achieved. However, the thinner coatings of tantalum rhenium and osmium which were applied really provided more valuable information.

Sintering rate of the 102Å Ta (1.53A/o) precoated tungsten was more rapid than that of uncoated tungsten, indicating inferior dimensional stability. This correlates with the effect produced by 0.5A/oTa,

added as discrete particles. Sintering rates of 45Å Re (0.85A/o) and 17Å Os (0.34A/o) precoated powders were essentially the same as that of uncoated tungsten; thus, these additives had little influence on dimensional stability. Sintering rates of 837Å Ta (11.8A/o), 150Å Re (2.8A/o), and 133Å Os (2.6A/o) precoated tungsten were markedly lower than that of uncoated tungsten, indicating superior dimensional stability. (However, subsequent examination showed that the superior dimensional stability evidenced by 150Å Re and 133Å Os coatings did not provide improved structural stability). Thus, order of increasing dimensional stability was indicated to be W+102Å Ta, uncoated W, W+170Å Os, W+45Å Re, W+150Å Re, W+837Å Ta, and W+133Å Os.

Measurement of nitrogen permeabilities indicated that the osmium and rhenium coatings effected higher values of permeability, while tantalum coatings effected lower values. Such opposite trends indicate that the coating element can alter the mechanism of diffusion during sintering.

No correlation was found between nitrogen permeability and open pore volume, as might reasonably be expected, and as was noted for W-Ta particle mixtures.

Metallographic and pore count analyses indicated that, for the precoated alloys, pore densities decreased in the following order: W+102Å Ta, uncoated W, W+45Å Re, W+837Å Ta, W+17Å Os, W+150Å Re, and W+133Å Os. Thus, it is seen that 150Å Re and 133Å Os coatings markedly reduced structural stability while, at the same time, greatly increasing dimensional stability. Reasons for this apparent contradiction are summarized in Subsection 9.4.

Based on the preceding summary of results, the following conclusions can be drawn for the various precoated ionizers:

Coating	Advantages over W	Disadvantages
102Å Ta	Much higher pore density	Appreciably lower dimensional stability
837Å Ta	Much greater dimensional and structural stability	Markedly lower N_2 permeability (more pore restriction)
17Å Os	Practically none	Significantly lower pore density and larger pore diameter
133Å Os	Much greater dimensional stability	Markedly lower pore density and larger pore size
45Å Re	Practically none	Practically none, except high cost of coating
150Å Re	Much greater dimensional stability	Significantly lower pore densities and larger pore diameter

9.3 Ionizers from Hydrogen-Reduced Particle Mixtures (Phase III)

In an attempt to improve uniformity of additive dispersion without resorting to the expensive vapor-coating process, the reduction method of secondary addition was included in the program.

A W-5A/oTa ionizer was made by hydrogen-reduction of equivalent Ta_2O_2 plus superficially preoxidized (4-8μ) tungsten microspheres (with final vacuum sintering at 2,200°C). This material was observed to have significant nonuniformity of pore size; however, densification was greatly retarded by the tantalum addition. When finer (1.7-5μ) tungsten particles were incorporated (same technique, with sintering at 2,000°C) to produce a W-7A/oTa ionizer, pore structure was still observed to be very nonuniform.

A W-4.94A/o Re ionizer was made by hydrogen-reduction of equivalent NH_4ReO_4 plus superficially oxidized W (1.7-5μ). This material densified more slowly than the control sample which contained no rhenium, and had a higher pore density than the control. Additional W-5A/o Re ionizers were prepared by the same technique and sintered at a lower temperature of 2,000°C. Densification was again retarded and pore size was quite uniform; however, pore density was about 30 percent lower than that of untreated tungsten microspheres.

Attempts were made to inoculate presintered tungsten buttons with fine rhenium particles (in liquid suspension) and with osmium (by immersion in Cu-Os alloy with subsequent distillation of the copper). Only negligible amounts of rhenium and osmium were retained, which ruled out the feasibility of this method.

To summarize, results of this phase of the program indicated some promise for addition of rhenium by the hydrogen-reduction method. However, before this method can be completely evaluated, additional refinements in technique would be required. These might include dry ball milling of NH_4ReO_4 to insure extreme fineness, improved blending of NH_4ReO_4 and tungsten, and deagglomeration and reblending after hydrogen reduction.

No performance tests were conducted on materials inoculated by hydrogen reduction. However, ionization performance of pure tungsten that had been sintered and then subjected to an oxidation-reduction cycle is summarized in Section 7.

9.4 Correlation of Sintering Mechanisms with Experimental Results

As described previously, secondary additions can either accelerate or decelerate sintering rate, indicating decreased or increased dimensional stability respectively. Similarly, changes in pore structure can be either accelerated or decelerated, indicating decreased or increased structural stability, respectively. Since this report deals with two kinds of secondary additions, discrete particles and precoatings on tungsten, correlation of measured parameters with sintering mechanisms is not a simple matter.

One effect noted is that produced by tungsten particles of high surface energy on the sintering of tungsten microspheres of lower surface energy. Apparently, the high-energy particles diffuse rapidly into adjacent lower-energy particles, expanding the latter, reducing specific surface area, creating additional void spaces, and reducing the cumulative bridge width available for transgranular diffusion. The net effect of these events is a decrease in sintering rate (or increased dimensional stability), accompanied by accelerated coarsening of pore structure (or decreased structural stability). This is a simple demonstration of the way in which dimensional stability can be increased by a secondary addition, while, at the same time, structural stability is decreased.

Other additions which increased dimensional stability, but also decreased structural stability, were osmium and rhenium applied as vapor precoatings to the tungsten microspheres. However, since the coating form of these additions precluded particle-energy effects, another mechanism must have been responsible. Such a mechanism could be related to the classical Kirkendall effect, where atoms of adjacent

bimetal components diffuse at unbalanced rates. As this effect appears applicable to rhenium- and osmium-coated tungsten, diffusion of either element into the parent tungsten particles expands the tungsten lattice, countering normal shrinkage and retarding the resultant densification rates. Further, metallographic examination of sintered structures indicates that incorporation of both rhenium and osmium into the lattice promotes grain growth and pore coarsening. These effects, in turn, are almost certain indications of accelerated transgranular or volume diffusion.

Another sintering mechanism is indicated when tantalum is applied as a vapor coating on the tungsten base particles. It has been noted that the pore channels of sintered ionizers made from tantalum-coated tungsten were very restricted. The following analysis of the mechanism is based on the findings of this work as well as that of other investigators. After an initial period of rapid diffusion of tantalum atoms into the substrate particles, sintering occurs by grain boundary diffusion.* Grain boundary diffusion, in turn, promotes widening of interparticle diffusion bridges and acts to restrict the neck portions of the pore channels. Thus, when tantalum is applied as an intimate coating, diffusion by a single mode appears to predominate.

A complex combination of the above mechanisms occurs when mixtures of tungsten and tantalum particles are sintered at 2,000°C. The following sequence of events is theorized:

1. Early and rapid diffusion of tantalum into tungsten particles, due to chemical and surface energy differentials;
2. Subsequent diffusion by the grain boundary mechanism within tantalum-rich areas and by the transgranular mechanism within tantalum-deficient areas;

*The presence of tantalum in a tungsten lattice causes an increase in the threshold temperature of transgranular (volume) diffusion, thus allowing diffusion to proceed by the boundary mode.

3. Restriction of pore necks by bridging within tantulum-rich areas and opening of the pore necks within tantulum-deficient areas, with the net result that bulk permeability is not reduced seriously.

This explanation agrees with experimental data and indicates that mixtures of tungsten and tantalum particles sinter at 2,000°C by more than one diffusion mechanism.

9.5 Ionizer Performance (Phase IV)

As had been strongly indicated by results obtained under the previous contract (NAS3-2519), ionizers having finer sintered pore structures continue to show better ionization performance (Fig. 7-27). The ionizer having the finest sintered pore structure, aLTa-14, exhibited ionization performance equivalent to, or better than, the best ionizer previously tested. In addition, accelerated life tests indicated that the structural stability of this ionizer was appreciably better than that of pure tungsten. Somewhat lower performance was exhibited by W-10A/oTa ionizers, with pore structures that were somewhat less fine than that of pure tungsten; however, the structural stability of these ionizers was far superior to that of pure tungsten.

9.6 Accelerated Life Testing (Phase V)

Accelerated life testing at 1,800°C and 1,600°C under vacuum indicated the following trends:

Secondary Additive to 1.7-5μ Tungsten	Method or Form of Addition	Stability at 1,800°C and 1,600°C* Dimensional (based on $\Delta\rho/\Delta t$)	Structural (based on $-\Delta K/\Delta t$)	Useful Life at 1,200°C, hr (extrapolated)
None	—	1	1	68
0.85 Re	Vapor pre-coating	3	2	63
1.53 Ta	Vapor pre-coating	2	3	2,600
5 Re	H_2-reduction	4	4	8,600
7 Ta	H_2-reduction	6	6	12,000
5 Ta	1-5μ particles	5	5	34,000
5 Ta	1-3μ particles	7	7	41,000
10 Ta	1-5μ particles	8	8	> 41,000
10 Ta	1-3μ particles	9	9	> 41,000

*Stability increases from 1, least stable, to 9, most stable

Inspection of the above data confirms the recommendation that a W-7A/oTa ionizer, made with 1-3μ tantalum particles, should provide the best combination of properties. While ionizer testing has indicated that W-7A/oTa will have somewhat reduced performance, as compared with pure unstable tungsten, its very large increase in structural stability appears to overshadow this disadvantage. Therefore, W-7A/oTa is recommended as the best composition for long-time operation.

REFERENCES

1. Electro-Optical Systems, Inc., Ionizer Reservoir Development Studies, Final Report, by M. LaChance and G. Kuskevics, Contract NAS8-2547, Pasadena, Calif., May 1963

2. Electro-Optical Systems, Inc., Porous Ionizer Development and Testing, Final Report, by M. LaChance, G. Kuskevics, and B. Thompson, Contract NAS3-2519, Pasadena, Calif., May 1964

3. M. LaChance, G. Kuskevics, and B. Thompson, "High-Performance Cesium Ionizers Made from Sized Spherical Tungsten Powder" (paper presented at the AIAA 4th Elec. Prop. Conf., Sep 1964)

4. Electro-Optical Systems, Inc., Criteria and a Graphical Method for Optimization of Cesium Surface Ionizer Materials, by G. Kuskevics, RR 3, Jan 1962

5. Electro-Optical Systems, Inc., The Ionization of Cesium in Tungsten Capillaries, by A. Forrester, RR-20, Pasadena, Calif., Jul 1964

6. G. Kuskevics and B. Thompson, "Comparison of Commercial Spherical Powder and Wire Bundle Ionizers," AIAA J., Vol. 2, No. 2, 1964, pp. 284-294

7. Electro-Optical Systems, Inc., Surface Ion Source Phenomenon and Technology, by G. Kuskevics and J. Teem, RR-16, Pasadena, Calif., Sep 1963

APPENDIX A

TABLES A through Q

DATA FOR EXPERIMENTAL IONIZERS

TABLE A

PERMEABILITY AND DENSITY DATA FOR PURE TUNGSTEN

IONIZERS, MADE FROM 1.7-5μ SPHERICAL POWDER *

Ionizer No.	Weight, gm	Volume, cm^3	Density		δt, sec.	N_2 Permeability $gm\ cm^{-1}\ Sec^{-1}\ Torr^{-1}$
			gm/cm^3	% of Theor.		
			Tungsten Control			
L-1	.2819	.01817	15.51	80.36	14.13	$.180 \times 10^{-6}$
L-2	.2880	.01829	15.75	81.61	16.26	.180
L-3	.2820	.01797	15.69	81.30	14.21	.181
L-4	.2746	.01816	15.12	78.34	6.17	.417
L-5	.2841	.01810	15.70	81.35	16.46	.154
L-6	.2729	.01798	15.18	78.65	6.93	.368
L-7	.2748	.01820	15.10	78.24	7.83	.328
L-8	.2761	.01816	15.20	78.76	6.95	.369
L-9	.2768	.01818	15.23	78.91	6.96	.370
L-10	.2763	.01814	15.23	78.91	7.19	.357
L-11	.2714	.01798	15.09	78.19	6.38	.398
L-12	.2810	.01816	15.47	80.16	10.68	.241
L-13	.2774	.01807	15.35	79.53	9.46	.270
L-14	.2720	.01791	15.19	78.70	6.50	.390
L-15	.2780	.01825	15.23	78.91	6.73	.385
L-16	.2705	.01787	15.14	78.45	6.20	.408
L-17	.2735	.01791	15.27	79.12	7.86	.322
L-18	.2772	.01809	15.32	79.38	8.88	.288
L-19	.2797	.01831	15.28	79.17	8.72	$.296 \times 10^{-6}$
		Avgs.	15.32	79.38		$.309 \times 10^{-6}$

*Lot L Tung. microspheres with 92% of particles in 1.7-5μ range.

TABLE B

PERMEABILITY AND DENSITY DATA FOR W-0.5A/oTa

IONIZERS, MADE FROM W AND Ta POWDERS *

Ionizer No.	Weight, gm	Volume, cm^3	Density		δt, sec.	N_2 Permeability, $gm.cm^{-1}sec^{-1}\ torr^{-1}$
			gm/cm^3	% of Theor.		
			W-0.5A/o(1-3μ) Ta			
L.5BTa-1	.2774	.01790	15.49	80.30	17.71	$.143 \times 10^{-6}$
-2	.2752	.01776	15.50	80.35	15.31	.165
-3	.2796	.01780	15.71	81.44	19.34	.132
-4	.2758	.01768	15.60	80.87	17.66	.143
-5	.2708	.01763	15.36	79.63	14.40	.174
-6	.2775	.01783	15.56	80.66	15.64	.162
-7	.2805	.01775	15.80	81.91	20.25	.126
-8	.2782	.0177/	15.66	81.18	18.67	.136
-9	.2734	.01768	15.46	80.15	15.62	.162
-10	.2752	.01785	15.42	79.94	14.50	.175
-11	.2757	.01780	15.49	80.30	15.07	.169
-12	.2754	.01787	15.41	79.89	15.04	.169
-13	.2772	.01771	15.65	81.13	18.72	.136
-14	.2755	.01770	15.56	80.66	16.75	.151
-15	.2724	.01768	15.41	79.89	15.98	.158
-16	.2810	.01786	15.73	81.54	19.40	.132
-17	.2652	.01689	15.70	81.39	17.73	.137
-18	.2796	.01778	15.73	81.54	20.79	.123
-19	.2767	.01777	15.57	80.72	16.92	.150
-20	.2751	.01772	15.52	80.46	15.76	.160
-21	.2762	.01752	15.76	81.70	19.43	.130
-22	.2752	.01780	15.46	80.15	15.10	.167
-23	.2743	.01773	15.47	80.20	16.12	.157
-24	.2728	.01802	15.14	78.49	11.30	.223
-25	.2765	.01782	15.52	80.46	15.63	$.163 \times 10^{-6}$
		Avgs.	15.55	80.61		$.154 \times 10^{-6}$

* Lot L tung. microspheres with 92% of particles in 1.7-5μ range.
Lot BF high-purity Ta with 94% of particles in 1-3μ range.

TABLE C

PERMEABILITY AND DENSITY DATA FOR W-0.5A/oTa

IONIZERS, MADE FROM W AND Ta POWDERS *

Ionizer No.	Weight, gm	Volume, cm^3	Density		δt, sec.	N_2 Permeability, $gm.cm.^{-1} sec.^{-1} torr.^{-1}$
			gm/cm^3	% of Theor.		
			W-o.5A/o(1-5μ) Ta			
L.5CTa-1	.2733	.01783	15.33	79.47	13.65	$.188 \times 10^{-6}$
-2	.2705	.01763	15.34	79.52	13.37	.191
-3	.2734	.01774	15.41	79.89	14.14	.181
-4	.2733	.01774	15.41	79.89	13.56	.189
-5	.2745	.01784	15.39	79.78	14.42	.177
-6	.2739	.01775	15.43	79.99	15.26	.168
-7	.2731	.01778	15.36	79.63	13.73	.186
-8	.2716	.01770	15.34	79.52	13.46	.190
-9	.2731	.01778	15.36	79.63	14.06	.182
-10	.2682	.01757	15.26	79.11	14.41	.177
-11	.2728	.01776	15.36	79.63	13.71	.186
-12	.2742	.01784	15.37	79.68	14.22	.180
-13	.2732	.01780	15.35	79.57	13.52	.190
-14	.2745	.01787	15.36	79.63	13.71	.188
-15	.2735	.01780	15.37	79.68	14.32	.180
-16	.2761	.01782	15.49	80.30	15.70	.162
-17	.2724	.01772	15.37	79.68	13.61	.188
-18	.2742	.01773	15.47	80.20	14.85	.172
-19	.2735	.01781	15.35	79.57	14.14	.182
-20	.2714	.01774	15.30	79.32	12.97	.197
-21	.2754	.01784	15.44	80.04	15.44	.166
-22	.2734	.01776	15.39	79.78	14.25	.179
-23	.2743	.01777	15.44	80.04	15.19	$.167 \times 10^{-6}$
			15.38	79.94		$.181 \times 10^{-6}$

* Lot L tung. microspheres with 92% of particles in 1.7-5μ range.
Lot CF high-purity Ta with 93% of particles in 1-5μ range.

TABLE D

PERMEABILITY AND DENSITY DATA FOR W-2.0A/o Ta

IONIZERS, MADE FROM W AND Ta POWDERS *

Ionizers No.	Weight, gm	Volume, cm^3	Density		t, sec.	N_2 Permeability, $gm.cm^{-1}sec^{-1}\ torr^{-1}$
			gm/cm^3	% of Theor.		
			W-2A/o(1-3μ)Ta			
LB2Ta-1	.2804	.01810	15.49	80.47	16.06	$.158 \times 10^{-6}$
-2	.2807	.01815	15.47	80.36	15.34	.166
-3	.2794	.01793	15.53	80.94	16.95	.149
-4	.2786	.01810	15.39	79.95	14.72	.172
-5	.2785	.01795	15.52	80.62	15.76	.160
-6	.2791	.01808	15.44	80.21	15.55	.163
-7	.2784	.01782	15.62	81.14	17.12	.147
-8	.2788	.01799	15.50	80.52	16.01	.158
-9	.2773	.01793	15.47	80.36	14.39	.175
-10	.2824	.01809	15.61	81.09	17.46	.147
-11	.2786	.01804	15.44	80.21	14.77	.172
-12	.2806	.01804	15.55	80.78	16.53	.154
-13	.2802	.01804	15.53	80.68	17.36	.146
-14	.2801	.01802	15.54	80.73	16.59	.153
-15	.2782	.01791	15.53	80.68	16.74	.151
-16	.2800	.01806	15.50	80.52	14.93	.170
-17	.2787	.01795	15.53	80.68	16.51	.153
-18	.2752	.01782	15.44	80.21	14.99	.167
-19	.2767	.01783	15.52	80.62	14.18	.177
-20	.2796	.01799	15.54	80.73	17.07	.148
-21	.2813	.01814	15.51	80.57	16.35	.155
-22	.2772	.01786	15.52	80.62	16.71	.151
-23	.2785	.01791	15.55	80.78	16.62	.152
-24	.2802	.01795	15.61	81.09	17.59	$.144 \times 10^{-6}$
			15.52	80.62		$.158 \times 10^{-6}$

* Lot L tung. microspheres with 92% of particles in 1.7-5μ range.
Lot BF high-purity Ta with 94% of particles in 1-3μ range.

TABLE E

PERMEABILITY AND DENSITY DATA FOR W-2.0A/oTa

IONIZERS, MADE FROM W AND Ta POWDERS *

Ionizer No.	Weight, gm	Volume, cm^3	Density		δt, sec.	N_2 Permeability, $m.cm.^{-1} sec.^{-1} torr.^{-1}$
			gm/cm^3	% of Theor.		
			W-2A/o(1-5μ) Ta			
LC2Ta-1	.2758	.01787	15.43	80.16	17.42	$.145 \times 10^{-6}$
-2	.2778	.01826	15.21	79.01	12.80	.200
-3	.2777	.01800	15.43	80.16	16.89	.150
-4	.2793	.01809	15.44	80.21	17.15	.149
-5	.2771	.01813	15.28	79.38	14.76	.173
-6	.2780	.01806	15.39	79.95	15.41	.165
-7	.2749	.01819	15.11	78.49	13.20	.193
-8	.2782	.01798	15.47	80.36	16.03	.158
-9	.2766	.01812	15.26	79.27	14.64	.174
-10	.2784	.01809	15.39	79.95	16.16	.158
-11	.2758	.01800	15.32	79.58	15.73	.162
-12	.2751	.01806	15.23	79.12	13.18	.192
-13	.2782	.01813	15.34	79.69	16.46	.155
-14	.2676	.01774	15.08	78.34	12.48	.199
-15	.2773	.01810	15.32	79.58	15.41	.165
-16	.2756	.01804	15.28	79.38	14.35	$.177 \times 10^{-6}$
			15.31	79.53		$.170 \times 10^{-6}$

* Lot L tung. microspheres with 92% of particles in 1.7-5μ range.
Lot CF high-purity Ta with 93% of particles in 1-5μ range.

TABLE F

PERMEABILITY AND DENSITY DATA FOR W-5A/oTa

IONIZERS, MADE FROM W AND Ta POWDERS *

Ionizer No.	Weight, gm	Volume, cm^3	Density		δt., sec.	N_2 Permeability, $gm.cm.^{-1} sec.^{-1} torr.^{-1}$
			gm/cm^3	% of Theor.		
			W-5A/o(1-3μ)Ta **			
LB5Ta-1	.2758	.01808	15.25	79.55	13.05	$.194 \times 10^{-6}$
-2	.2741	.01814	15.11	78.82	14.73	.172
-3	.2744	.01833	14.97	78.09	12.67	.202
-4	.2731	.01815	15.05	78.51	13.60	.188
-5	.2685	.01774	15.14	78.98	11.24	.221
-6	.2690	.01803	14.92	77.83	11.31	.223
-7	.2698	.01809	14.91	77.78	11.26	.224
-8	.2736	.01821	15.02	78.35	12.39	.205
-9	.2731	.01804	15.14	78.98	11.44	.222
-10	.2723	.01794	15.23	79.45	12.79	.197
-11	.2743	.01804	15.21	79.34	12.39	.204
-12	.2723	.01823	14.94	77.93	11.68	.218
-13	.2702	.01802	14.99	78.20	11.82	.212
-14	.2751	.01814	15.17	79.13	11.94	.213
-15	.2768	.01815	15.23	79.45	13.08	$.195 \times 10^{-6}$
		Avgs.	15.06	78.56		$.206 \times 10^{-6}$
			W-5A/o(1-5μ)Ta ***			
LC5Ta-1	.2676	.01805	14.83	77.36	11.89	$.213 \times 10^{-6}$
-2	.2739	.01846	14.84	77.41	12.47	.207
-3	.2745	.01823	15.06	78.56	13.42	.190
-4	.2746	.01830	15.01	78.30	12.11	.211
-5	.2625	.01756	14.95	77.99	12.19	.202
-6	.2717	.01829	14.86	77.52	11.00	.231
-7	.2715	.01814	14.97	78.09	11.48	.220
-8	.2699	.01805	14.95	77.99	13.60	.186
-9	.2730	.01810	15.08	78.66	12.76	.199
-10	.2717	.01810	15.01	78.30	12.58	.201
-11	.2734	.01800	15.19	79.24	12.34	.210
-12	.2719	.01831	14.85	77.46	10.00	.254
-13	.2716	.01825	14.88	77.62	11.46	.221
-14	.2727	.01821	14.98	78.14	11.61	$.219 \times 10^{-6}$
		Avgs.	14.96	78.04		$.212 \times 10^{-6}$

* Lot L tung. microspheres with 92% of particles in 1.7-5μ range.

** Lot BF high-purity Ta with 94% of particles in 1-3μ range.

*** Lot CF high-purity Ta with 93% of particles in 1-5μ range.

TABLE G

PERMEABILITY AND DENSITY DATA FOR W-10A/oTa

IONIZERS, MADE FROM W AND Ta POWDERS *

Ionizer No.	Weight, gm	Volume, cm^3	Density		δt , sec.	N_2 Permeability, $gm.cm.^{-1} sec.^{-1} torr.^{-1}$
			gm/cm^3	% of Theor.		
			W-10A/o(1-3μ)Ta **			
LB10Ta-1	.2786	.01811	15.38	80.82	11.21	$.225 \times 10^{-6}$
-2	.2777	.01800	15.43	81.08	14.15	.177
-3	.2782	.01784	15.59	81.92	17.43	.142
-4	.2776	.01802	15.41	80.98	12.15	.206
-5	.2812	.01805	15.58	81.87	16.11	.157
-6	.2823	.01809	15.61	82.03	17.15	.147
-7	.2790	.01800	15.50	81.45	14.80	.170
-8	.2775	.01788	15.52	81.56	17.23	.144
-9	.2826	.01807	15.64	82.19	18.56	.135
-10	.2787	.01803	15.46	81.24	13.41	.188
-11	.2784	.01801	15.46	81.24	15.06	.167
-12	.2711	.01300	15.06	79.14	12.55	$.200 \times 10^{-6}$
		Avgs.	15.47	81.29		$.172 \times 10^{-6}$
			W-10A/o(1-5μ)Ta ***			
LC10Ta-1	.2729	.01816	15.03	78.98	12.75	$.198 \times 10^{-6}$
-2	.2747	.01842	14.91	78.35	11.23	.227
-3	.2729	.01823	14.97	78.67	16.02	.157
-4	.2731	.01827	14.95	78.56	11.89	.213
-5	.2728	.01833	14.88	78.19	10.56	.240
-6	.2734	.01837	14.88	78.19	10.55	.240
-7	.2747	.01834	14.98	78.72	12.50	.204
-8	.2766	.01840	15.03	78.98	12.77	.200
-9	.2710	.01806	15.01	78.88	11.45	.219
-10	.2700	.01817	14.86	78 09	9.28	.271
-11	.2717	.01860	14.61	76.77	10.05	.255
-12	.2715	.01804	15.05	79.09	11.73	.216
-13	.2744	.01822	15.06	79.14	13.46	.188
-14	.2743	.01814	15.12	79.45	14.50	.175
-15	.2748	.01818	15.12	79.45	15.31	$.166 \times 10^{-6}$
		Avgs.	14.96	78.61		$.211 \times 10^{-6}$

* Lot L tung. microspheres with 92% of particles in 1.7-5μ range.
** Lot BF high-purity Ta with 94% of particles in 1-3μ range.
*** Lot CF high-purity Ta with 93% of particles in 1-5μ range.

TABLE H

PERMEABILITY AND DENSITY DATA FOR IONIZERS

MADE FROM 1.7-5μ SPHERICAL TUNGSTEN PARTICLES, THINLY

COATED BY VACUUM DEPOSITION WITH 102Å OF TANTALUM (Phase IIa)

Ionizer No.	Weight, gm	Volume, cm^3	Density		δt, sec.	N_2 Permeability, $gm.cm.^{-1} sec.^{-1} torr.^{-1}$
			gm/cm^3	% of Theor.		
			W + 102Å Ta Coatings			
aLTa-1	.2719	.01792	15.17	78.60	12.91	$.200 \times 10^{-6}$
-2	.2752	.01805	15.25	79.02	13.90	.187
-3	.2731	.01803	15.15	78.50	13.06	.199
-4	.2716	.01792	15.16	78.55	12.85	.201
-5	.2739	.01807	15.16	78.55	13.30	.196
-6	.2720	.01798	15.13	78.39	13.04	.199
-7	.2750	.01805	15.24	78.96	13.74	.189
-8	.2737	.01800	15.21	78.81	13.28	.195
-9	.2755	.01814	15.19	78.70	13.83	.189
-10	.2744	.01801	15.24	78.96	13.62	.191
-11	.2732	.01798	15.19	78.70	12.97	.200
-12	.2753	.01801	15.29	79.22	14.43	.180
-13	.2742	.01801	15.22	78.86	13.63	.191
-14	.2745	.01807	15.19	78.70	13.48	.193
-15	.2750	.01809	15.20	78.76	13.93	.187
-16	.2766	.01805	15.32	79.38	15.26	.171
-17	.2758	.01812	15.22	78.86	13.52	.193
-18	.2760	.01810	15.25	79.02	14.96	.174
-19	.2731	.01800	15.17	78.60	13.14	$.197 \times 10^{-6}$
		Avgs.	15.21	78.81		$.191 \times 10^{-6}$

TABLE I

PERMEABILITY AND DENSITY DATA FOR IONIZERS
MADE FROM 1.7-5μ SPHERICAL TUNGSTEN PARTICLES*,
COATED BY VACUUM DEPOSITION WITH 837 Å OF TANTALUM (Phase II,

Ionizer No.	Weight, gm.	Volume, cm^3	Density		δt, Sec.	N_2 Permeability, $gm \cdot cm^{-1} sec^{-1} torr^{-1}$
			gm/cm^3	% of Theor.		
			W+ Å Ta Coatings			
bLTa-1	.2692	.01815	14.83	78.13	42.00	$.227 \times 10^{-6}$ **
-2	.2696	.01809	14.90	78.50	121.32	.078
-3	.2757	.01812	15.22	80.19	226.33	.042
-4	.2746	.01811	15.16	79.87	140.44	.067
-5	.2753	.01821	15.12	79.66	179.28	.053
-6	.2782	.01818	15.30	80.61	200.31	.047
-7	.2773	.01813	15.30	80.61	283.91	.034
-8	.2831	.01834	15.44	81.35	287.42	.033
-9	.2764	.01809	15.28	80.51	181.25	.052
-10	.2742	.01792	15.30	80.61	306.23	.032
-11	.2797	.01823	15.34	80.82	225.04	.042
-12	.2755	.01811	15.21	80.14	229.07	.041
-13	.2833	.01834	15.45	81.40	290.53	$.033 \times 10^{-6}$
	Averages =		15.25	80.35		$.046 \times 10^{-6}$

* Lot L tungsten microspheres with 92% of particles in 1.7-5μ range.

** High permeability value - not included in average.

TABLE J

PERMEABILITY AND DENSITY DATA FOR IONIZERS MADE FROM 1.7-5μ SPHERICAL TUNGSTEN PARTICLES, THINLY COATED BY VACUUM DEPOSITION WITH OSMIUM AND RHENIUM (Phase IIa)

Ionizer No.	Weight, gm	Volume, cm^3	Density gm/cm^3	Density % of Theor.	δt, sec.	N_2 Permeability $gm.cm.^{-1} sec.^{-1} torr.^{-1}$
			W+17Å Os Coating			
aLOs-1	.2604	.01719	15.15	78.50	5.20	$.508 \times 10^{-6}$
-2	.2630	.01706	15.42	79.90	7.22	.363
-3	.2600	.01699	15.30	79.27	6.45	.408
-4	.2515	.01663	15.12	78.34	4.96	.515
-5	.2591	.01710	15.15	78.50	5.60	.469
-6	.2575	.01718	14.99	77.67	5.02	.517
-7	.2696	.01706	15.80	81.87	14.87	.178
-8	.2587	.01712	15.11	78.29	5.09	.516
-9	.2591	.01709	15.16	78.55	5.40	.487
-10	.2608	.1719	15.17	78.60	5.68	.465
-11	.2578	.01709	15.08	78.13	4.96	.530
-12	.2571	.01702	15.11	78.29	5.07	$.518 \times 10^{-6}$
		Avgs.	15.21	78.81		$.456 \times 10^{-6}$
			W - 45Å Re Coating			
aLRe-1	.2805	.01722	16.29	84.40	28.71	$.092 \times 10^{-6}$
-2	.2666	.01711	15.58	80.73	8.97	.294
-3	.2592	.01678	15.45	80.05	7.54	.341
-4	.2668	.01713	15.58	80.73	7.29	.363
-5	.2675	.01705	15.69	81.30	8.67	.304
-6	.2658	.01708	15.56	80.62	7.77	.337
-7	.2657	.01717	15.47	80.16	7.43	.354
-8	.2689	.01712	15.71	81.40	9.03	.294
-9	.2717	.01705	15.94	82.15	12.91	.204
-10	.2677	.01709	15.66	81.14	8.10	.326
-11	.2686	.01711	15.70	81.35	9.59	.275
-12	.2684	.01709	15.71	81.40	8.66	.305
-13	.2667	.01697	15.72	81.45	8.82	$.299 \times 10^{-6}$
		Avgs.	15.70	81.35		$.291 \times 100^{-6}$

TABLE K

PERMEABILITY AND DENSITY DATA FOR IONIZERS MADE

FROM 1.7-5μ SPHERICAL TUNGSTEN PARTICLES*,

COATED BY VACUUM DEPOSITION WITH 133Å of OSMIUM (Phase II)

Ionizer No.	Weight, gm	Volume, cm^3	Density		δt, sec.	N_2 Permeability, $gm \cdot cm^{-1} sec^{-1} torr^{-1}$
			gm/cm^3	% of Theor.		
			W+133 Å Os Coating			
bLOs-1	.2835	.01801	15.74	81.22	12.40	0.744×10^{-6}
-2	.2762	.01788	15.45	79.72	5.60	1.644
-3	.2799	.01809	15.47	79.82	6.92	1.335
-4	.2669	.01764	15.13	78.07	5.61	1.612
-5	.2754	.01786	15.42	79.57	6.29	1.450
-6	.2814	.01833	15.35	79.21	6.65	1.413
-7	.2818	.01844	15.28	78.84	5.52	1.709
-8	.2778	.01799	15.44	79.67	6.73	1.394
-9	.2812	.01839	15.29	78.90	7.08	1.329
-10	.2754	.01790	15.39	79.41	6.70	1.379
-11	.2816	.01813	15.53	80.13	9.71	0.954
-12	.2799	.01821	15.37	79.31	6.50	1.433
-13	.2795	.01810	15.44	79.67	6.27	1.487
-14	.2762	.01804	15.31	79.00	5.54	1.663
-15	.2839	.01852	15.33	79.10	5.80	1.627
-16	.2815	.01830	15.38	79.36	8.15	1.149
-17	.2776	.01812	15.32	79.05	8.49	1.108
-18	.2780	.01810	15.36	79.26	7.37	1.259
-19	.2791	.01817	15.36	79.26	5.79	1.637
-20	.2783	.01817	15.32	79.05	6.17	1.513
-21	.2837	.01808	15.69	80.96	12.00	0.774
-22	.2720	.01783	15.26	78.74	5.62	1.617
-23	.2790	.01835	15.20	78.43	5.69	1.657×10^{-6}
	Averages =		15.38	79.36		1.386×10^{-6}

* Lot L tungsten microspheres with 92% of particles in 1.7-5μ range.

TABLE L

PERMEABILITY AND DENSITY DATA FOR IONIZERS MADE

FROM 1.7-5μ SPHERICAL TUNGSTEN PARTICLES*

COATED BY VACUUM DEPOSITION WITH 150 Å OF RHENIUM (Phase II)

Ionizer No.	Weight, gm	Volume, cm^3	Density		δt, Sec.	N_2 Permeability, $gm \cdot cm^{-1} sec^{-1} torr^{-1}$
			gm/cm^3	% of Theor.		
			W+150 Å Re Coating			
bLRe-1	.2864	.01798	15.93	82.33	15.24	0.622×10^{-6}
-2	.2808	.01807	15.54	80.31	4.24	2.214
-3	.2796	.01793	15.59	80.57	4.00	2.353
-4	.2874	.01814	15.84	81.86	16.50	0.572
-5	.2846	.01833	15.53	80.26	4.37	2.160
-6	.2877	.01822	15.79	81.60	7.30	1.288
-7	.2893	.01821	15.89	82.12	9.52	0.993
-8	.2847	.01815	15.69	81.09	5.15	1.842
-9	.2840	.01818	15.62	80.72	4.79	1.937
-10	.2821	.01830	15.42	79.69	4.49	2.116
-11	.2853	.01826	15.62	80.72	5.08	1.847
-12	.2943	.01828	16.05	82.95	20.36	0.460
-13	.2879	.01832	15.72	81.24	8.76	1.068×10^{-6}
	Averages =		15.71	81.19		1.502×10^{-6}

* Lot L tungsten microspheres with 92% of particles in 1.7-5μ range.

TABLE M

DENSITY, PORE VOLUME, AND MERCURY INTRUSION DATA

SHOWING EFFECT OF THIN COATINGS, VAPOR-DEPOSITED ON TUNGSTEN POWDER BASE

Composition, Atom % Equiv. Coating Thickness, Å	Pure Tungsten None		W-1.53 Ta 102		W-0.85 Re 45		W-0.34 Os 17	
Tungsten Particle Dia., μ *	1.7-5		1.7-5		1.7-5		1.7-5	
Sintering Parameters (10^{-5} torr range)	2000°C-30 min.		1800°C-45 min.		1800°C-45 min. 1900°C-70 min.		1800°C-45 min. 1900°C-85 min.	
Vol. of Sample, V_s, cm^3	.34125		.31720		.32041		.31355	
Density, % of Max. Theor.	79.22		78.96		80.47		78.45	
Total Pore Vol., % of V_s	20.78		21.04		19.53		21.55	
Open Pore Vol., % of V_s	19.69		19.20		18.94		20.73	
Occluded Pore Vol., % of V_s	1.09		1.84		0.59		0.82	
Mercury Pressure Range, psi	Mercury Intruded Over Respective Pressure Ranges							
	$\Delta V, cm^3$	% of V_s	$\Delta V, cm^3$	% of V_s	$\Delta V, cm^3$	% of V_s	$\Delta V, cm^3$	% of V_s
73-102	.0002	0.06	.0001	0.03	nil	nil	.0001	nil
102-160	.0560	16.41	.0001	0.03	.0353	11.02	.0509	16.23
160-235	.0100	2.93	.0489	15.42	.0047	1.47	.0126	4.02
235-335	.0003	0.09	.0100	3.15	.0198	6.18	.0005	0.16
335-568	.0002	0.06	.0011	0.35	.0002	0.06	.0003	0.10
568-1735	.0003	0.09	.0002	0.06	.0002	0.06	.0003	0.10
1735-3485	.0002	0.06	.0004	0.13	.0003	0.09	.0002	0.06
3485-4360	nil	nil	.0001	0.03	.0001	0.03	.0001	0.03
4360-4985	nil	nil	nil	nil	.0001	0.03	nil	nil
Totals	.0672	19.69	.0609	19.20	.0607	18.94	.0650	20.73

* Tungsten spherical powder from Lot L, with 92% by number of particles in 1.7-5μ range and average particle diameter of 3.23μ.

TABLE N

DENSITY, PORE VOLUME, AND MERCURY INTRUSION DATA

SHOWING EFFECT OF THICK COATINGS, VAPOR-DEPOSITED ON TUNGSTEN BASE POWDER*

Composition, Atom % / Equiv. Coating Thickness, Å	Pure Tungsten None		W-11.82 Ta 837		W-2.77 Re 150		W-2.57 Os 133	
Tungsten Particle Dia., μ*	1.7-5		1.7-5		1.7-5		1.7-5	
Sintering Parameters (10^{-5} torr range)	2000°C-30 min.		2100°C-145 min.		2000°C-120 min.		2200°C-210 min.	
Vol. of Sample, V_s, cm^3	.34125		.29115		.34171		.34588	
Density, % of Max. Theor.	79.22		81.24		82.33		80.65	
Total Pore Vol., % of V_s	20.78		18.76		17.67		19.35	
Open Pore Vol., % of V_s	19.69		15.70		14.46		18.27	
Occluded Pore Vol., % of V_s	1.09		3.06		3.21		1.08	
Mercury Pressure Range, psi	Mercury Intruded Over Respective Pressure Ranges							
	$\Delta V, cm^3$	% of V_s	$\Delta V, cm^3$	% of V_s	$\Delta V, cm^3$	% of V_s	$\Delta V, cm^3$	% of V_s
18.1-20	nil	nil	nil	nil	.0020	0.59	nil	nil
20-29	"	"	"	"	.0024	0.70	"	"
29-43	"	"	"	"	.0036	1.05	"	"
43-55	"	"	"	"	.0028	0.82	.0003	0.09
55-73	"	"	"	"	.0040	1.17	.0442	12.78
73-102	.0002	0.06	.0016	0.55	.0058	1.70	.0161	4.65
102-160	.0560	16.41	nil	nil	.0185	5.41	.0024	0.69
160-235	.0100	2.93	.0414	14.22	.0086	2.52	.0001	0.03
235-335	.0003	0.09	.0021	0.72	.0015	0.44	.0001	0.03
335-568	.0002	0.06	.0006	0.21	.0002	0.06	nil	nil
568-1735	.0003	0.09	nil	nil	nil	nil	"	"
1735-3485	.0002	0.06	"	"	"	"	"	"
Totals	.0672	19.69	.0457	15.70	.0494	14.46	.0632	18.27

* Tungsten spherical powder from Lot L, with 92% by number of particles in 1.7-5μ range and average particle diameter of 3.23μ.

TABLE O

DIMENSIONS, WEIGHTS, DENSITIES, AND PERMEABILITIES FOR W + 7% Ta AND W + 5% Re, SINTERED FOR 60 MIN. AT 2000°C

Button Number	Dia., inch	Area, cm^2	Thick., inch	Thick., cm	Thick, cm / Area, cm^2	Volume, cm^3	Weight, gram	Density, gm/cm^2	Max.Theor. Density, gm/cm^2	% of Max Theor. Density	δt, seconds	Permeability, gm/cm·sec·mm Hg
W + 5Re-1	.1853	.17400	.0445	.11303	.64960	.01967	.3089	15.70	19.39	80.97	31.51	$.340 \times 10^{-6}$
W + 5Re-2	.1851	.17360	.0453	.11506	.66279	.01997	.3105	15.55	19.39	80.20	39.00	$.281 \times 10^{-6}$
W + 5Re-3	.1851	.17360	.0453	.11506	.66279	.01997	.3113	15.59	19.39	80.40	43.97	$.249 \times 10^{-6}$
W + 5Re-4	.1853	.17400	.0455	.11557	.66420	.02011	.3151	15.67	19.39	80.81	43.06	$.255 \times 10^{-6}$
							Average =	15.63		80.61		$.281 \times 10^{-6}$
W + 5Re-Porosimeter	.1856	.17456	.7179	1.82347		.31830	5.0422	15.84		81.69		
W + 7Ta-1	.1858	.17491	.0403	.10236	.58522	.01790	.2617	14.62	19.11	76.50	129.45	$.075 \times 10^{-6}$
W + 7Ta-2	.1858	.17491	.0402	.10211	.58379	.01786	.2612	14.62	19.11	76.50	139.02	$.069 \times 10^{-6}$
W + 7Ta-3	.1859	.17511	.0404	.10262	.58603	.01797	.2615	14.55	19.11	76.14	51.61	$.188 \times 10^{-6}$
W + 7Ta-4	.1854	.17415	.0405	.10287	.59070	.01791	.2632	14.70	19.11	76.92	263.24	$.037 \times 10^{-6}$
							Average =	14.62		76.50		$.092 \times 10^{-6}$
W + 7Ta-Porosimeter	.1854	.17415	.4051	1.02895		.17919	2.6621	14.86		77.76		

TABLE P

EFFECT OF TANTALUM AND RHENIUM ADDITIVES
ON DENSITY AND OCCLUDED PORE VOLUME

Composition, atom %	W + 7A/o Ta		W + 5A/o Re	
Sample Identity	L7Ta - 2		L5Re - 1	
Tungsten Particle Size	1.7-5μ		1.7-5μ	
Sintering Temperature, °C	2000		2000	
Sintering Time, minutes	60		60	
Vol. of Sample, V_s, cm^3	.17919		.31830	
Density, % of max. theor.	77.76		81.69	
Total Pore Vol., % of V_s	22.24		18.31	
Open Pore Vol., % of V_s	17.08		16.59	
Occluded Pore Vol., % of V_s	5.16		1.72	
Mercury Pressure Range, psi	Mercury Intruded Over Respective Pressure Ranges			
	$\Delta V, cm^3$	% of V_s	$\Delta V, cm^3$	% of V_s
43-55	nil	nil	.0001	0.03
55-73	.0001	0.06	.0002	0.06
73-102	.0001	0.06	.0001	0.03
102-160	.0009	0.50	.0451	14.17
160-235	.0274	15.29	.0059	1.85
235-325	.0012	0.67	.0008	0.25
335-568	.0004	0.22	.0004	0.13
568-1735	.0001	0.06	.0002	0.06
1735-3485	.0002	0.11	nil	nil
3485-4360	.0001	0.06	nil	nil
4360-4985	.0001	0.06	nil	nil
Totals	.0306	17.08	.0528	16.59

TABLE Q

EFFECT OF TANTALUM AND RHENIUM ADDITIVES ON PORE DENSITY

Sample Identity	Density, % of Theor.	Negative No.	Pores Counted at 2000X in 80 cm^2 Half Pores	Whole Pores	Total Pores
		W + 7A/o Ta			
L7Ta-2	77.76	2186	17	43	51.5
		2187	14	40	47
		2188	20	50	60
		2189	14	47	54
				Avg. =	53.1
Pores/cm^2 at 1X = 2.66×10^6 (a)					
Vol. % of Open Pores = 17.08 (b)					
Avg. Pore Diameter = 2.86μ (c)					
		W + 5A/o Re			
L5Re-1	81.69	2190	18	47	56
		2191	14	54	61
		2192	16	55	63
		2193	15	44	51.5
				Avg. =	57.9
Pores/cm^2 at 1X = 2.90×10^6 (a)					
Vol. % of Open Pores = 16.59 (b)					
Avg. Pore Diameter = 2.70μ (c)					

(a) Pores/cm^2 at 1X = (Total pores at 2000X)$(2000)^2$/80 cm^2

(b) Vol. % of Open Pores = (100)(Vol. of Hg Intruded)/Vol. of Sample

(c) Avg. Pore Dia., $\mu = 1128\sqrt{\frac{\text{(Vol. \% of Open Pores)}}{\text{(Pores/cm}^2\text{ at 1X)}}}$

APPENDIX B

FIGURES B-1, B-2, AND B-3

DATA FOR EXPERIMENTAL IONIZERS

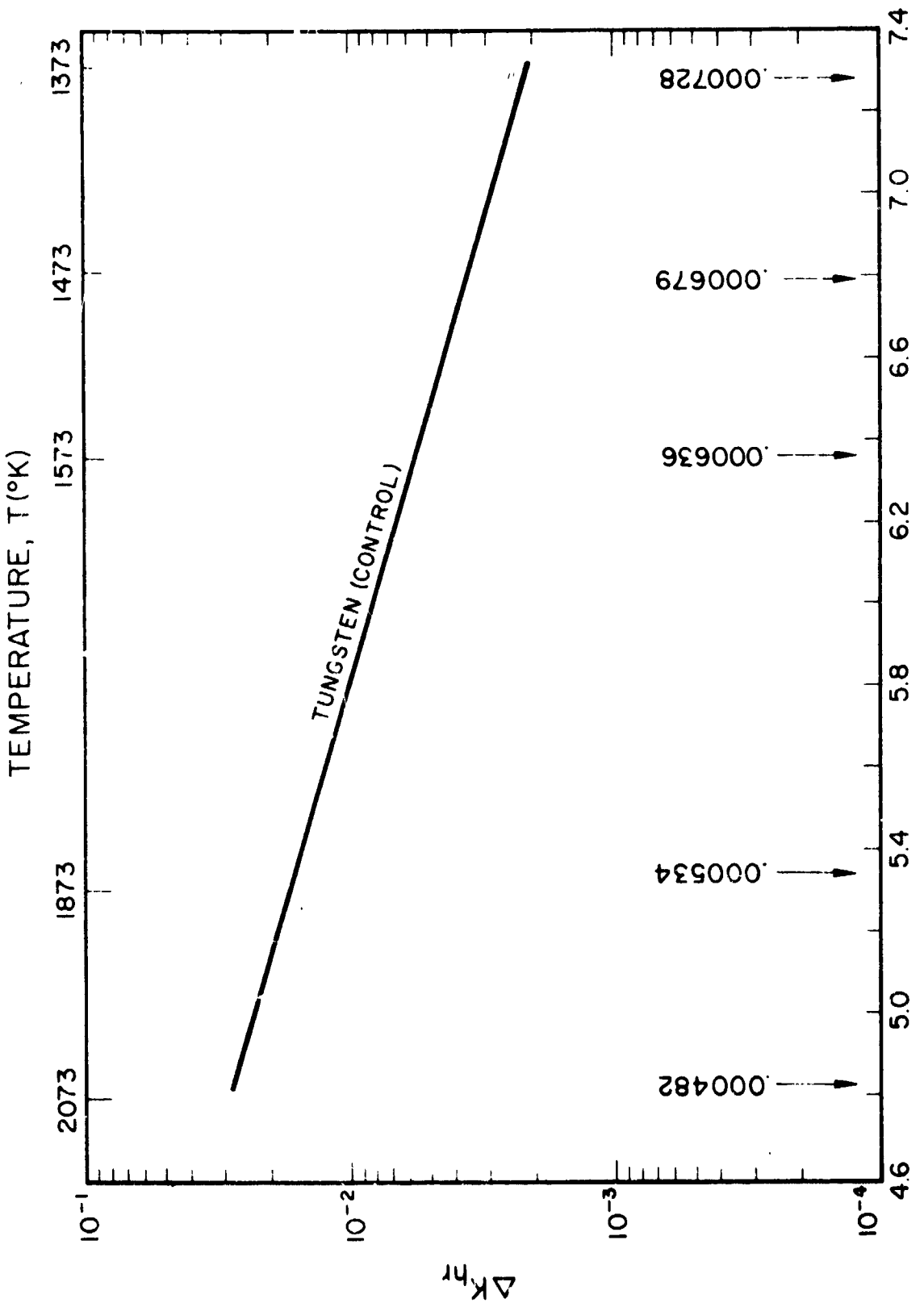

FIG. B-1 CHANGE IN ΔK_{hr} AS A FUNCTION OF RECIPROCAL TEMPERATURE

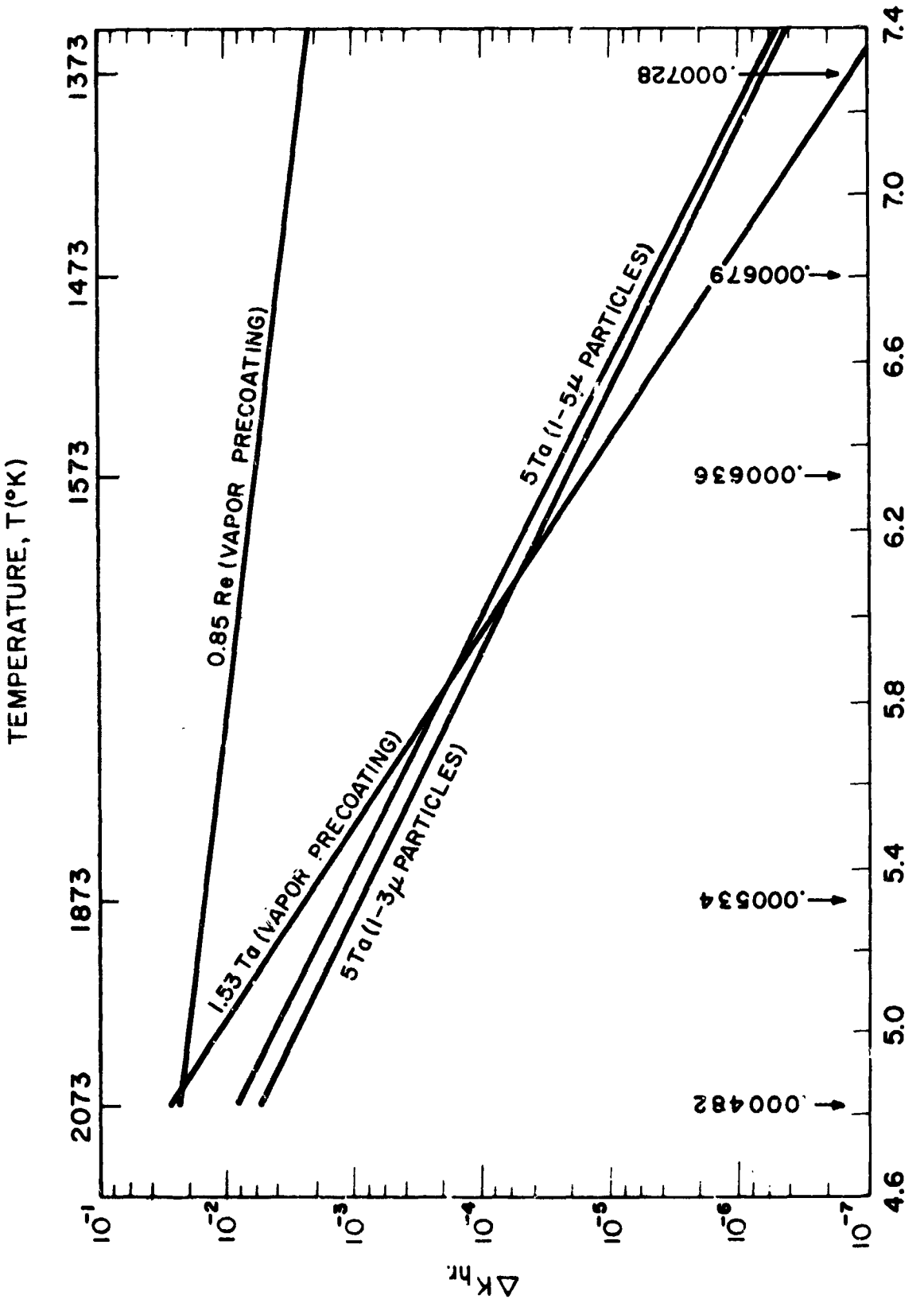

FIG. B-2 CHANGE IN ΔK_{hr} AS A FUNCTION OF RECIPROCAL TEMPERATURE

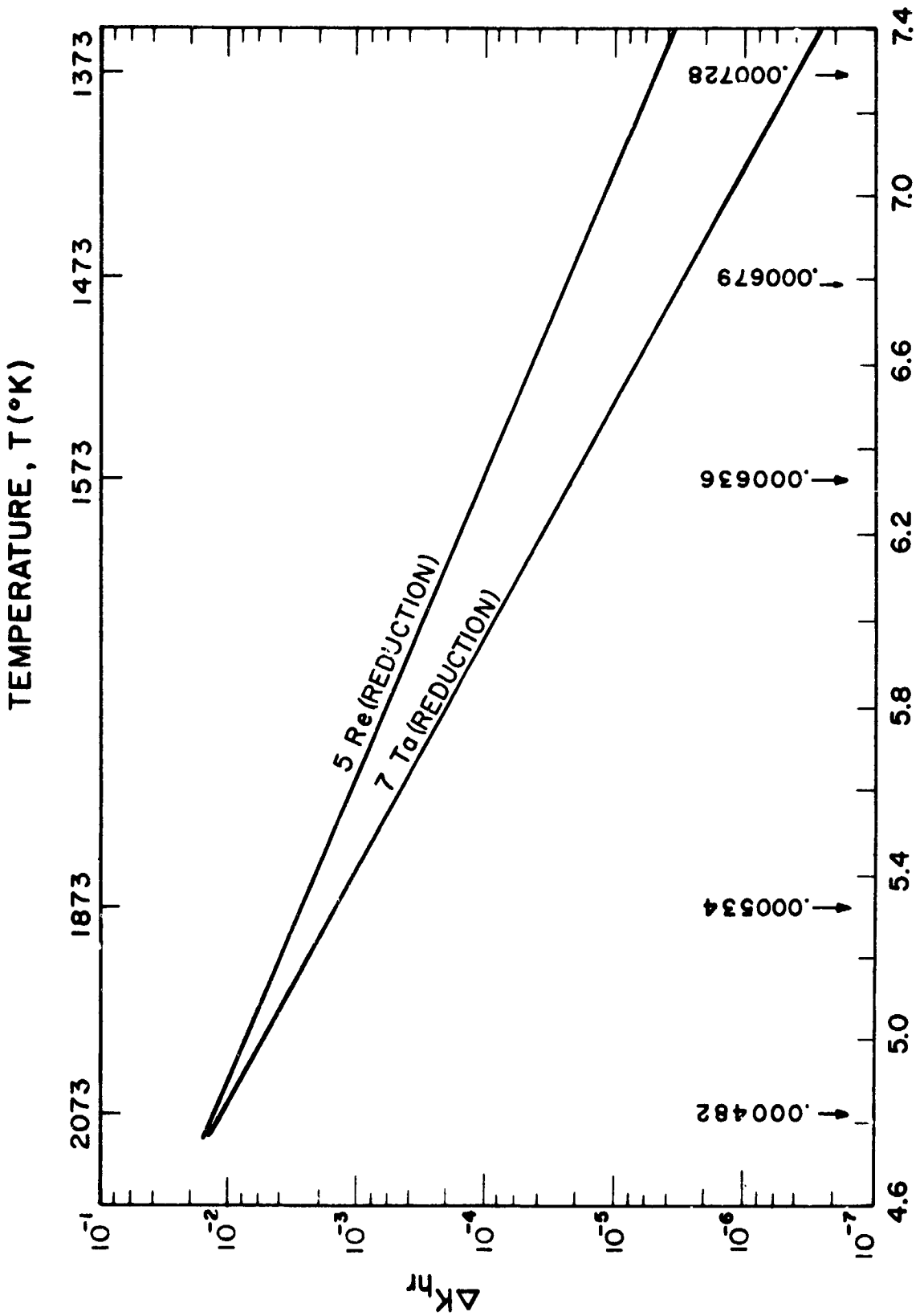

FIG. B-3 CHANGE IN ΔK_{hr} AS A FUNCTION OF RECIPROCAL TEMPERATURE